II. RESULTADOS

ARTÍCULO 1

Orbital forcing of dust supply to the North Canary Basin over the last 250 kyrs

Ana Moreno[1], Jordi Targarona[1], Jorijntje Henderiks[2], Miquel Canals[1*], Tim Freudenthal[3] and Helge Meggers[3]

[1]*Grup de Recerca Consolidat en Geociències Marines, Departament d'Estratigrafia i Paleontologia, Universitat de Barcelona, Campus de Pedralbes, E-08071 Barcelona, Spain*

[2]*Swiss Federal Institute of Technology, Geological Institute, CH-8092 Zürich, Switzerland*

[3]*Universität Bremen, FB Geowissenschaften, Postfach 33 04 40, D-28359 Bremen, Germany*

Publicado en:

Quaternary Science Reviews, 20, 1327-1339 (2001)

0277-3791/01/$

PII: SO277-3791 (00)00184-0

Abstract

The Canary Basin lies in a region of strong interaction between the atmospheric and ocean circulation systems: Trade winds drive seasonal coastal upwelling and dust storm outbreaks from the neighbouring Sahara desert are the major source of terrigenous sediment. To investigate the forcing mechanisms for dust input and wind strength in the North Canary Basin, the temporal pattern of variability of sedimentological and geochemical proxy records has been analysed in two sediment cores between latitudes 30?30'N and 31?40'N.

Spectral analysis of the dust proxy records indicates that insolation changes related to eccentricity and precession are the main periods of temporal variation in the record. Si/Al and grain-size of the terrigenous fraction show an increase in glacial-interglacial transitions while Al concentration and Fe/Al ratio are both in phase with minima in the precessional index. Hence, the results obtained show that the wind strength was intensified at Terminations. At times of maxima of Northern Hemisphere seasonal insolation, when the African monsoon was enhanced, the North Canary Basin also received higher dust input. This result suggests that the moisture brought by the monsoon may have increased the availability of dust in the source region.

1.1. Introduction

Eolian sediment generated in the world's arid and semiarid regions with persistent dry winds is transported over large distances and contributes to sediment in the ocean basins (Prospero, 1996). Indeed, the Saharan region has been revealed as the major source of dust particles to the deep-sea sediments of the North Atlantic Ocean (Schütz *et al*., 1981). Sedimentological and geochemical analyses of sediments from deep sea cores may help to identify variations in continental aridity and wind strength, thus helping to understand mechanisms involved in climate change (see for example Sarnthein *et al*., 1982; Stein, 1985). Changes in eolian grain-size have been used to investigate paleowind pathways off Northwest Africa (Parkin and Shackleton, 1973). Pollen assemblages (Hooghiemstra *et al*., 1992; Marret and Turon, 1994) and freshwater diatoms (Pokras and Mix, 1985; Pokras and Mix, 1987) in marine cores have also been used as proxies for wind strength. Mass accumulation rates (MAR) of marine sediments free from biogenic and authigenic components, can be used to study eolian sedimentation (Clemens and Prell, 1990). In addition, mineral and geochemical composition, such as aluminium concentration (Matthewson *et al*., 1995) or Fe/Al ratio (Bergametti *et al*., 1989), are useful proxies to monitor changes in aridity of the source areas. Therefore, sedimentological and geochemical studies of deep-sea sediments may provide useful information about paleowind directions and strength and continental climate.

In the study of marine sediments, Kolla *et al*., (1979) pioneered the use of quartz as an indicator of eolian transport to the Atlantic Ocean. They concluded that the increase of wind strength and aridity were both higher during the Last Glacial Maximum (LGM). Sarnthein *et al*., (1981) and Hooghiemstra (1989) interpreted that wind strength was enhanced during eccentricity-controlled glacial periods on the basis of grain-size and palynological studies. In addition, Ruddiman (1997) proposed that the high glacial influxes of dust to the tropical Atlantic are mainly due to changes in transport by winter winds, rather than to glacial hyper-aridity. Recently, several authors have highlighted the importance of the local oceanographical conditions in the

sedimentological record (Bertrand *et al.*, 1996). In some Northwest African records the higher dust input has been recognised at the Stage 2-1 transition (Lézine and Denèfle, 1997; Martinez *et al.*, 1999) thus questioning the assumption that glacial stages were characterised by stronger winds.

Several studies have linked dust input to climate variation in the source areas, thus providing a low-latitude climate response to solar radiation. Matthewson *et al*., (1995) and Tiedemann *et al*., (1989) interpret increments in dust supply to an increase in aridity at the source. This hypothesis is based in the relation between the humidity/aridity cycles and the low-latitude insolation forcing of the African monsoon. Therefore, in times of minima in the precessional index, a higher seasonality leads to more intense monsoons (McIntyre et al., 1989). Wet intervals in Northwestern Africa are recorded in lakes concomitantly with intensifications in the monsoonal regime (Kutzbach and Street-Perrott, 1985; Gasse *et al*., 1989; Lamb *et al*., 1995). However, after mapping sand-dune extent on North Africa, aridity has been related with Northern Hemisphere glaciations instead of the precessional insolation timing (Sarnthein, 1978). In addition, results from General Circulation Models (GCM) suggest that ice sheets can affect African climate via changes in sea surface temperatures over the North Atlantic Ocean (deMenocal and Rind, 1993a; deMenocal *et al*., 1993b). In conclusion, the tempo of aridity in Northwestern Africa during the Late Pleistocene is still a matter of debate (Ruddiman, 1997).

In summary, the deep-sea sediment record under the influence of Saharan dust plumes can provide the key to test the previous hypotheses. The aim of this study is to evaluate to which extent orbital forcing plays a key role driving changes in dust input to the North Canary Basin (NCB). Our wind strength proxies show a variation mainly controlled by the 100-kyr cycle while the dust input record is modified by the seasonality implied by the precessional insolation timing. Finally, the interpretation of these results leads us to propose a conceptual model to explain the variation of dust supply to the NCB over the last 250 kyrs.

1.2. Oceanographic and climatic setting

The Canary Basin lies in the recirculation regime linking the Gulf Stream with the North Equatorial Current via the Azores and Canary Currents (Klein and Siedler, 1989). At this latitude coastal upwelling is driven by the interaction between the Trade winds and the Canary Current. Along the Northwestern African margin, the Trade winds show a pattern of seasonal variations. Thus, dividing the Northwestern African margin into regions of permanent and seasonal upwelling (Fütterer, 1983; Wooster *et al*., 1976). North of latitude 25?N, the upwelling has a seasonal character, being more active in spring and summer, because of the seasonal shift in the location of the subtropical high-pressure cell, which drives the trades (Mittelstaedt, 1983). Although the upwelling zone is restricted to the coast, satellite imagery has shown that large upwelling filaments develop at specific coastal positions such as Cape Ghir, Cape Blanc or Cape Yubi (Van Camp *et al*., 1991; Gabric *et al*., 1993; Davenport *et al*., 1999). As a result, the upwelling signal can be transported far offshore.

The NCB is located in the path of long-range atmospheric dust transport offshore the Northwestern Africa (Prospero, 1996). Dust input into this area is controlled by the Northeast Trade winds and the Saharan Air Layer (SAL) wind systems (Sarnthein and Koopmann, 1980).

At present, major dust outbreaks that carry dust to the NCB are linked with the northern branch of the SAL wind system (Torres-Padrón *et al.*, 2002). These observations were also confirmed from modelling results (Tetzlaff and Wolter, 1980) and by calculations of isentropic back-trajectories after satellite data (Bustos *et al*., 1998). These Saharan winds transport particles from the rim of the South Sahara and Sahel regions. There the widespread lateritic soils and ferruginous crusts give characteristic high Fe content to the dust (Sarnthein *et al*., 1981).

The current dust input to the NCB was studied by Torres-Padrón *et al.* (2002). These authors have found that the highest occurrence of dust outbreaks take place in winter and summer related to two dominant meteorological scenarios. In winter, dust events occur favoured by the weakening of the Azores High and the Intertropical Convergence Zone (ITCZ) is located southwards. Bergametti *et al.* (1989) observed dust transport from the Sahelian regions when the incursion of a polar depression cuts the Azores High into two anticyclonic cells, an oceanic and a continental one. In contrast, dust outbreaks appear in summer when the high pressure is centred around the Azores combined with a low-pressure cell over Northern Africa, which favours dust transport from a northern source (Torres-Padrón *et al.* 2002).

Up to now, the Sahelian origin of the dust was the most accepted in the literature. However, Chiapello *et al*., (1997) showed that the low level summer Trade winds transport mineral aerosol from northeastern Morocco to the Canary region. This conclusion opens the possibility that indeed the sediment composition of the North Canary Basin may represent two different sources. The predominance of one source over the other may be related to the prevailing meteorological scenario.

1.3. Material and methods

The two cores studied, GeoB 4216-1 and GeoB 5559-2, were retrieved during R/V METEOR cruises M37/1 and M42/4b in years 1996 and 1998 respectively (Wefer *et al*., 1997; Wefer *et al*., 1998) (Table 1). The core sites were selected because they are located in the path of present day dust plumes originating in the Sahara and hence the cores are expected to monitor changes in dust supply (Figure 1). Furthermore, Core GeoB 5559-2 has been recovered from a seamount slope as far offshore as to avoid the effects of sediment transported by coastal currents, thus holding the best potential to record a purer eolian signal (Grousset *et al*., 1998; Rea, 1994).

Table 1. Core data

Tabla 1.*- Datos de los testigos*

Gravity core	Cruise	Longitude (N)	Latitude (W)	Depth (m)	Core length (cm)
GeoB 4216	M 37/1	30?37’8	12?23’7	2,324	1,117
GeoB 5559	M 42/4b	31?38’7	13?11’2	3,178	585

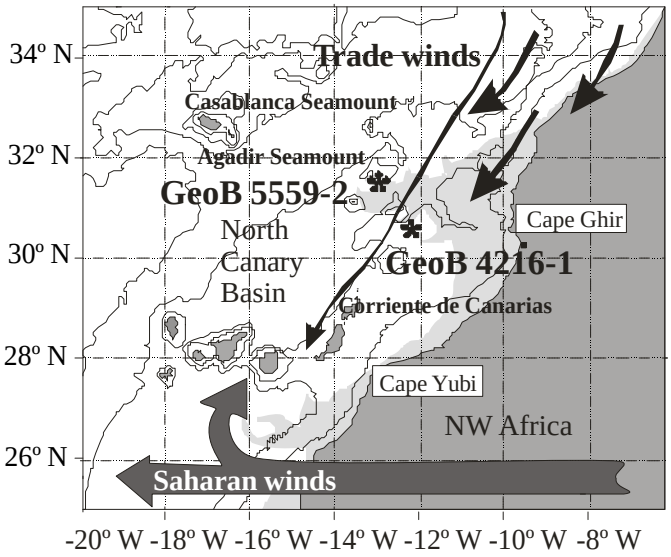

Figure 1.- Map of Northwest Africa showing the location of cores GeoB 5559-2 and GeoB 4216-1. Seasonal upwelling and filaments are outlined (light-shaded area) based in Van Camp *et al*., (1991), Hagen *et al*., (1996) and Davenport *et al*., (1999). Arrows indicate the average position of the present-day dominant wind systems and the Canary Current.

Figura 1.- *Mapa del noroeste de África, mostrando la localización de los testigos GeoB 5559-2 y GeoB 4216-1. Se han marcado (área sombreada) el upwelling estacional y los filamentos, basándose en Van Camp et al., (1991), Hagen et al., (1996) y Davenport et al., (1999). Las flechas indican la posición media de los vientos dominantes actualmente y la situación de la Corriente de Canarias.*

Both cores were sampled on board with a resolution of 5 cm using syringes. Water content, porosity and density were measured on each sample by weighing a known volume of sediment (ranging between 8 and 10 ml) before and after drying at 80?C.

Grain-size distribution was measured after leaching the carbonate fraction with a pH ammonium acetate solution buffered at a pH of 4.0 and after oxidation of the organic matter with 10% H_2O_2. This carbonate-organic matter free fraction was analysed with a Coulter LS 100 laser particle size analyser (CLS), which is able to measure a wide range of particles (between 0.4 and 800 ?m.). CLS precision and accuracy were tested running several analyses with latex micro spheres of a known diameter and through replicate analyses that gave a coefficient of variation of 0.44%. The calculated parameters are the median and the ratio between the particles coarser than 2 ?m and the total of particles.

Sediment samples for X-ray fluorescence analyses were ground and homogenised in an agate mortar. Glass discs were prepared for major element determination by fusing about 0.3 g of ground bulk sediment with a Li tetra borate flux. Pressing about 5 g of ground bulk sediment into a briquet, with boric acid backing, produced the discs for trace element analysis. Bulk sediment geochemistry of the samples was determined in a Philips PW 2,400 sequential wavelength disperse X-ray spectrometer. The following major elements, Al, P, K, Ca, Si, Mn, Ti, Fe, Mg and Na, were calculated as oxides while the trace elements, Ba, Mo, Nb, Zr, Y, Sr, Th, Pb, Sn, Ce,

Ga, Zn, W, Cu, Co, Ni, V were measured in ppm. After calibration with international standards (GSS-1 to GSS-7), the analytical precision was checked by replicate analyses of samples. This was found to be lower than 0.8% for major elements and about 4% for trace elements. All analyses were corrected for the contribution and dilution effect of the sea-salt content of the dried sediment. Results are presented after normalising the data to Al in order to account for the metal variations in respect to the variations of the aluminosilicate mineral fraction (Loring and Rantala, 1992).

1.4. Isotopic analyses and age model

Stable oxygen isotope measurements on fine fraction carbonate (<38 ?m) of Core GeoB 5559-2 were made on a Micromass PRISM (IRMS) mass spectrometer at the Geological Institute, ETH Zürich. Samples were homogenised by crushing before analysis. The analytical error of the internal lab standard was maximally ±0.10‰ for $?^{18}O$. All data are reported relative to the PDB standard.

Compositional variations within the fine fraction can significantly influence the stable isotopic stratigraphy measured on the nannofossil fraction. For example, Paull and Thierstein (1987) showed that oxygen and carbon isotopic ratios of individual splits of the <38 ?m fraction of deep-sea carbonate particles vary systematically with size over a range of 1.25-4.0 ‰. Low-diversity coccolith assemblage and other types of particles dominate most of these splits. However, empirical evidence from many cores suggests that the glacial-interglacial variability of the oxygen isotope signal dominates over possible compositional effects, and therefore raw fine fraction isotope data produce consistent isotope stratigraphy from which general paleoceanographic inferences can be made (Anderson and Steinmetz, 1981; Steinmetz and Anderson, 1984).

GeoB 5559-2			
Depth (cm)	Age (kyr)	Event	LSR (cm/kyr)
48	17.85	2.2	2.39
158	64.09	4.2	2.50
193	79.25	5.1	2.19
228	99.38	5.3	1.84
268	123.82	5.5	1.82
313	135.10	6.2	3.21
418	183.3	6.6	1.38
443	196.06	7.1	1.92
493	215.54	7.3	2.73
538	240.19	7.5	0.91

Table 2.- Age control points based in the stacked record of Martinson *et al*., (1987) for GeoB 5559-2. The corresponding isotopic events and linear accumulation rates are also represented. Stratigraphy from Core GeoB 4216-1 has been elaborated in Freudenthal, *et al.,* (2002).

Tabla 2.- *Puntos de control temporal basados en el registro de Martinson et al., (1987) para el testigo GeoB 5559-2. Los correspondientes eventos isotópicos y las tasas de acumulación están también representadas. La estratigrafía para el testigo GeoB 4216-1 ha sido elaborada por Freudenthal et al., (2002).*

The age model of Core GeoB 5559-2 has been obtained from correlation between the measured ?^{18}O values and the well-dated SPECMAP ?^{18}O chronology (Figure 2) (Imbrie *et al*., 1984; Martinson *et al*., 1987; Pisias *et al*., 1984). Ages of individual samples have been calculated by linear interpolation between the isotopic events shown in Table 2 and Figure 2. Final correlation index between SPECMAP and GeoB 5559-2 is 0.807. It results, then, that a sampling resolution of 5 cm corresponds in average to 2,150 years.

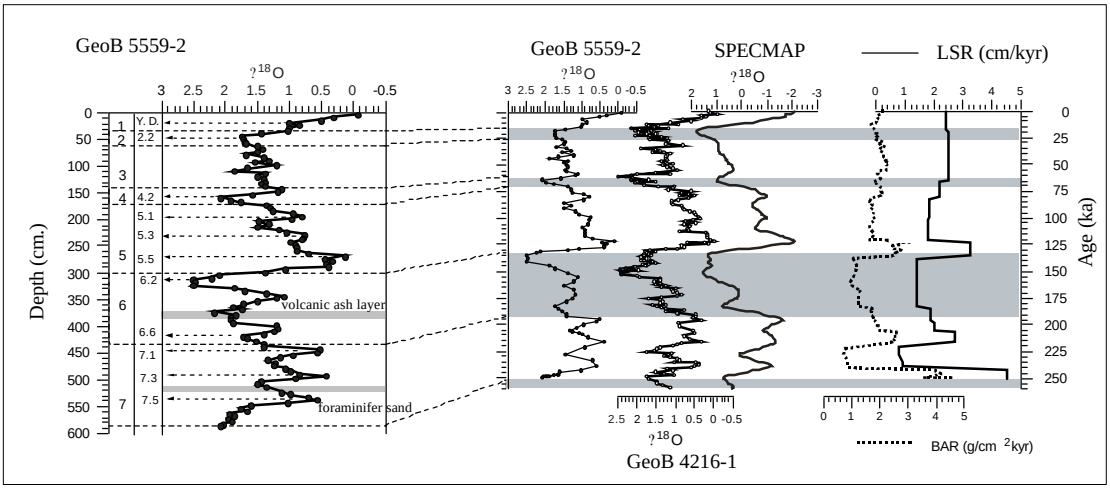

Figure 2.- Oxygen isotope records of GeoB 5559-2 plotted along coredepth (cm) and age (kyr) axes. Age control points based in the stacked record of Martinson *et al.*, (1987) are indicated (arrows). The small plateau in the ?^{18}O GeoB 5559-2 curve during the last deglaciation could correspond to the Younger Dryas (Y.D.). The two intervals shaded (a volcanic ash layer and a foraminifera sand) were excluded before obtaining the age model to avoid interpretative errors. SPECMAP curve (Martinson *et al*., 1987) and *G. bulloides* ?^{18}O curve from GeoB 4216-1 (Freudenthal *et al*., 2002) are shown to comparison. Linear sedimentation rates (cm/kyr) and bulk accumulation rates (g/cm^{2}kyr) from GeoB 5559-2 are also represented.

Figura 2.- *Perfiles de los registros de isótopos de oxígeno del testigo GeoB 5559-2 respecto a la profundidad (cm) y a la edad (miles de años). Los puntos de control temporal basados en el registro de Martinson et al., (1987) están indicados mediante flechas. Un pequeño "plateau" en la curva de ?^{18}O del testigo GeoB 5559-2 durante la deglaciación podría corresponder con el Younger Dryas (Y.D.). Los dos intervalos sombreados (una capa de cenizas volcánicas y una capa formada por arena de foraminíferos) se excluyeron antes de la construcción del modelo de edad para evitar errores interpretativos. La curva SPECMAP (Martinson et al., 1987) y el registro de ?^{18}O del testigo GeoB 4216-1 (Freudenthal et al, 2002) se muestran por comparación. Las tasas de sedimentación (cm/1000 años) y las tasas totales de acumulación (g/cm^2*1000 años) del testigo GeoB 5559-2 también se representan.*

The sedimentary record spans the last 250 kyrs, from oxygen isotope stages (OISs) 1 to 8. The age model of Core GeoB 4216-1, derived by correlating the ?^{18}O record measured on shells of planktic foraminifer *Globigerina bulloides* with the SPECMAP record, was taken from Freudenthal *et al.* (2002).

1.5. Results

1.5.1. Sedimentological description and grain-size distribution

The lithology in cores GeoB 4216-1 and GeoB 5559-2 consists of nannofossil mud with foraminifer-rich and terrigenous-rich intervals (see core description chapters in Wefer *et al.*, 1997 and Wefer *et al*., 1998). Visual examination evidenced a continuous sedimentation in Core GeoB 4216-1, except for an ash layer at 775 cm. The record in Core GeoB 5559-2 is interrupted in two intervals: a volcanic ash layer (between 380-390 cm) and a foraminifera sand (between 510-520 cm) (Figure 2). In the area, this volcanic ash layer has also been found in several cores (Wefer *et al*., 1997). Since these intervals are sedimentological events with no climatic significance, samples from these layers were excluded from our results.

In order to study the wind strength variation, grain-size analyses were carried out in the lithogenic fraction (Rea, 1994; Sarnthein *et al*., 1981). After the statistical analysis (k-means clustering) samples can be grouped into two main families according to their grain-size distribution although other statiscally non-relevant sample tipologies also exist (Figure 3). Samples that belong to the 1st Family are the most abundant (63.5%) and they are characterised by showing a unimodal distribution. In most of the samples, the mode is centred at 8 ?m and a few samples present about 5% of particles over 63 ?m diameter (Figure 3a). The 2nd Family constitutes 30% of the samples and displays a bi-modal distribution dominated by the finest fraction, with the mode centred at 5 ?m. Sand content in this family is always less than 10% (Figure 3b). The rest of the samples (6.5%) have a bi-modal distribution dominated by the coarsest fraction and belong to the 3rd family. As they correspond with the excluded intervals (the volcanic ash layer and the foraminifera sand) we haven't used them in our study.

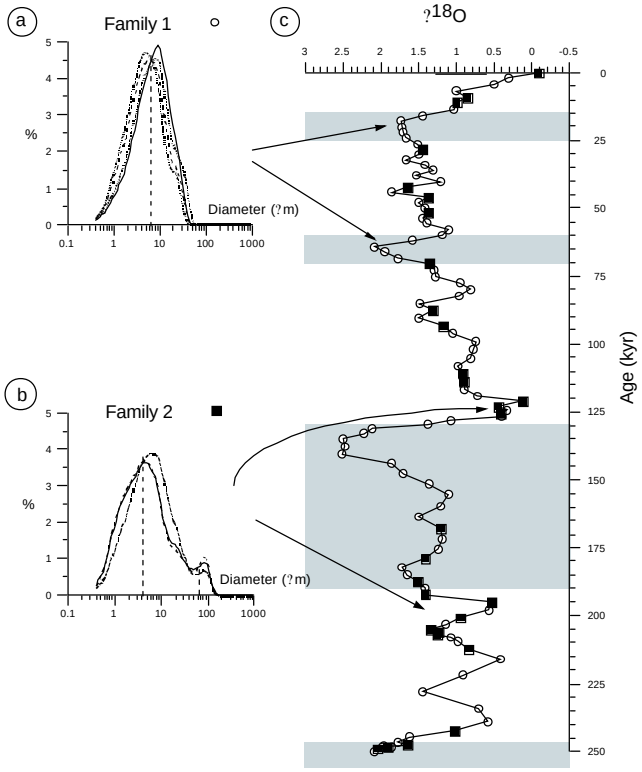

Figure 3.- Grain-size distribution of the carbonate-free fraction of samples from family 1 and 2 (Figures a and b) from core GeoB 5559-2. Modes (also the secondary mode in the bi-modal distribution) are indicated with a vertical dashed line. c) Temporal distribution of grain-size families. White dots: family 1 and black squares: family 2.

***Figura 3.**- Distribución granulométrica de las fracciones sin carbonato de las muestras pertenecientes a las familias 1 y 2 (figuras a y b) del testigo GeoB 5559-2. Las modas (incluyendo a las modas secundarias en las distribuciones bimodales) se indican con una línea vertical punteada. c) Distribución temporal de las familias granulométricas. Familia 1 con puntos y familia 2 con cuadrados negros.*

Grain-size families show a different distribution downcore (Figure 3c). The most homogeneous intervals, formed only by the 1st Family, correspond to full glacial conditions (OISs 2, 4 and 6), while interglacial periods (OISs 1 and 5) and also OIS 3 present samples from Family 2 occur within intervals where samples from the 1st Family dominate. Therefore, a clear glacial-interglacial control over the grain-size distribution can be observed in Core GeoB 5559-2.

Furthermore, grain-size distribution has been represented with a ratio that illustrates these glacial-interglacial variations. In this way, the coarse carbonate-free fraction, expressed here as *(silt+sand)/total* ratio, is significantly higher during full glacial conditions (OISs 2, 4 and 6) than during interglacials or OIS 3 (Figure 4a). This parameter displays an increase during colder periods in within interglacial substages, as 5b, 5d, 7b and 7d. Events with coarser lithogenic particles coincide with glacial-interglacial transitions. Furthermore, the same pattern of variation is recorded by the median of this lithogenic fraction (Figure 4b). Its values range between 6-12 ?m during full glacial periods and Terminations and between 4-6 ?m the rest of the record. Therefore, both parameters show the same glacial-interglacial variations with the coarser values at Terminations (I, II and maybe III) recorded in the core.

1.5.2. Geochemical markers

Geochemical parameters have been used successfully to evaluate the wind strength and the variations in dust input (Matthewson *et al*., 1995; Reichart *et al*., 1997). Here we use the Si/Al ratio as an indicator of terrigenous quartz input since in this region opal concentrations are very low (Neuer *et al*., 1997). Quartz from Northwest African sediments is mainly contained in the eolian lithogenic coarse fraction (Beltagy *et al*., 1972). Furthermore, Si concentration in the Saharan aerosol end-member is also higher in the coarser particles (Guieu and Thomas, 1996). Thus, Si/Al variations can be related to wind strength fluctuations (Boyle, 1983; Martinez *et al*., 1999).

Si/Al records in both cores have the same trend; however, Si/Al ratio in Core 4216-1 presents higher values (Figure 4c). The results show that the pattern of the Si/Al curve in cores GeoB 5559-2 and GeoB 4216-1 (Figure 4c) is very similar that the previously described for the grain-size parameters (Figure 4a,b). Higher values are recorded during cold periods and lower values during warm stages (ranging from 2.5 in interglacial stages and OIS 3 to 3.2 at Terminations I, II and maybe III). This pattern is found also during colder periods in within interglacial stages (see OISs 5 and 7 in Figure 4c) but the signal is weaker than during full glacial conditions. Maximum values of Si/Al ratio are reached at Terminations (I, II and maybe III) in the two studied cores. Since lithogenic coarse particles can be related to wind strength (Clemens, 1998), this implies that the wind strength in the NCB was increased at Terminations.

As reported by Matthewson *et al*., (1995), aluminium concentration is taken as useful proxy of dust input in NW African margin because it is incorporated into fine-grained, wind-borne clays. In the studied cores, the Al concentration presents a similar range of variation but they show somewhat higher values in Core GeoB 4216-1 (Figure 4d). Although aluminium concentrations are higher during full glacial periods, the general pattern does not show the same glacial-interglacial signal that Si/Al and grain-size proxies. On the contrary, the smaller increments recorded appear with a cyclicity of 23 kyr (Figure 4d). This result leads us to propose

that the dust input in the NCB is related to the precessional insolation timing.

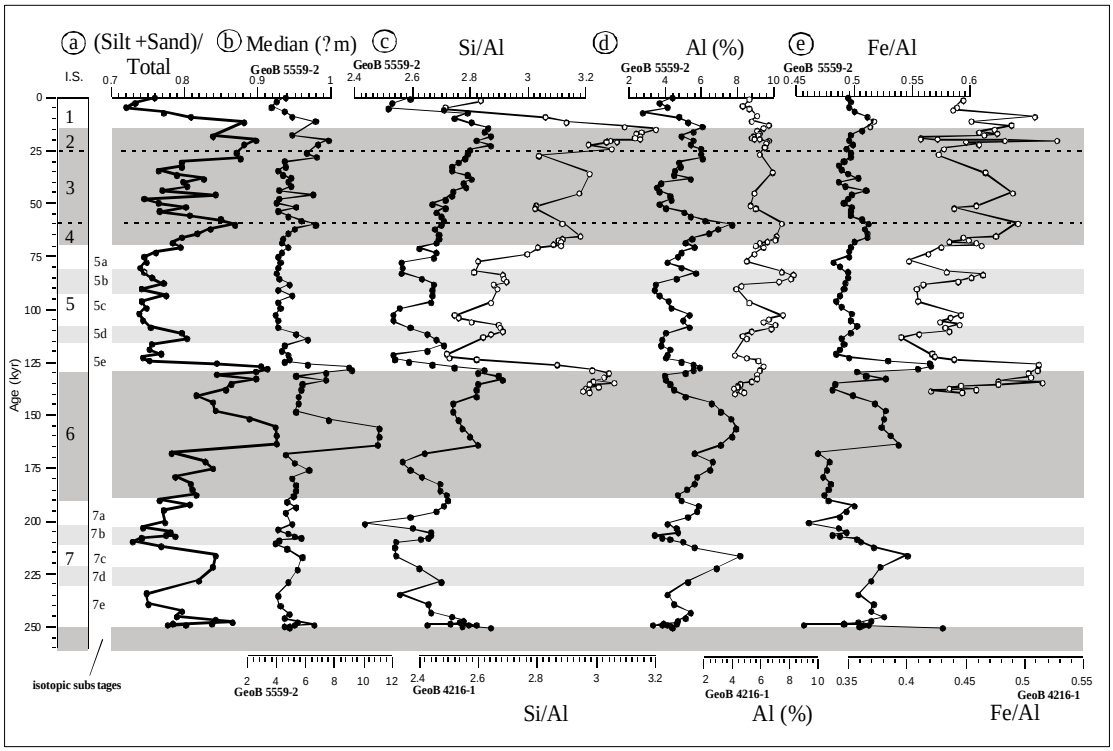

Figure 4.-Downcore profiles of (a) a grain-size parameter represented as *(silt+sand)/total*, (b) the median of the terrigenous fraction, (c) Si/Al ratio, as proxy indicators of wind stress, (d) the aluminium content (%) and (e) the Fe/Al ratio as proxy indicators of dust input to the North Canary Basin in GeoB 5559-2 (black dotted curves) and GeoB 4216-1 (white dotted curves). Geochemical study of Core GeoB 4216-1 has been carry out in the first 6 m. Glacial isotopic stages and substages are shaded.

***Figura 4.**- Perfiles de (a) un parámetro granulométrico representado como (limo+arena)/total, (b) la mediana de la fracción terrígena, (c) la relación Si/Al, como proxies de intensidad de vientos, (d) el contenido en aluminio (%) y (e) la relación Fe/Al como indicadores de aportes eólicos a la Cuenca del Norte de Canarias en el testigo GeoB 5559-2 (curvas con puntos negros) y GeoB 4216-1 (curvas con puntos blancos). El estudio geoquímico del testigo GeoB 4216-1 se ha llevado a cabo en los primeros 6 m. Los estadios isotópicos glaciares y sub-estadios están sombreados.*

Since eolian dust from the Sahel region has a high content of iron oxides such as hematite and goethite (Balsam *et al*., 1995), the Fe/Al ratio may be used as a proxy for eolian particles (Bergametti *et al*., 1989). On the contrary, dust transported by the low level Trade winds is expected to have low Fe/Al values, since lateritic soils are lacking in the dust source. In Saharan aerosols collected in Barbados the Fe/Al ratio oscillates between summer and winter with a mean value of 0,58 (Arimoto *et al*., 1995). The Fe/Al ratio from an observed dustfall at 25?N of latitude is 0.54 (Game, 1962). The values in the records range from 0.45 in warm periods and up to 0.55 in the cold ones (Figure 4e). The Fe/Al ratio and the aluminium both display a similar pattern coherent with a 23-kyr cyclity. In both cores, GeoB 5559-2 and 4216-1, the Fe/Al ratio shows the same range of values (Figure 4e). However, in Core 4216-1 the amplitude of variation is large. The aluminium concentration and the Si/Al ratio (Figure 4c,d) follow the same trend. Therefore, the Core GeoB 4216-1 record appears to be more sensitive to oscillations in dust input. This is probably due to its position along the path of the wind.

1.5.3. Spectral analyses

Spectral analyses of the records were carried with the Analyseries software package developed by Paillard *et al*., (1996) using the Blackman-Tuckey method. The results show the presence of the 100 kyr (eccentricity) and 23 kyr (precession) periods as the main cycles of temporal variability in the dust input to the North Canary Basin (Figure 5). The two 100 kyr cycles present in the record can be identified by the strong peaks of *(silt + sand)/total*, the median and the Si/Al records at the end of glacial stages (Figure 4a,b,c). On the other hand, Al concentration and Fe/Al ratio records vary with a 23-kyr cyclicity (Figure 4d,e). The wind strength proxies (Si/Al ratio and grain-size parameters) also display a 23-kyr cycle but it is not the dominant frequency in those records.

Cross-spectral analysis on the dust proxies was carried out against the Eccentricity-Tilt-Precession combination curve (ETP) (Imbrie *et al*., 1984). This curve is a normalised combination of the three orbital parameters and can thus be used to compare variations in proxy records with orbitally induced changes in the amount of insolation (Matthewson *et al*., 1995). The cross-spectra of dust proxies (Al, Fe/Al, Si/Al and grain-size) also shows maximum coherency at the 100 and 23 kyr periods (Figure 5). Coherency and phase angle of these proxies with the ETP curve are represented in Table 3.

1.6. Discussion

Two issues should be considered to explain which was the forcing mechanism behind supply Saharan dust to the North Canary Basin: (i) the increase of Fe-and-Al-rich dust input at minima in the precessional index and (ii) the response of wind strength to the 100-kyr cycle. Both are discussed separately.

1.6.1. Increase of Fe-and-Al-rich dust input at minima in the precessional index

Aluminium concentration and Fe/Al ratio are good indicators of dust input from the Northwest African margin, as they reflect Sahelian clays and laterites, respectively (Balsam *et al*., 1995; Bergametti *et al*., 1989; Matthewson *et al*., 1995). These proxies together with grain-size and Si/Al ratio, which are indicators of wind strength, vary with precession (Figure 5).

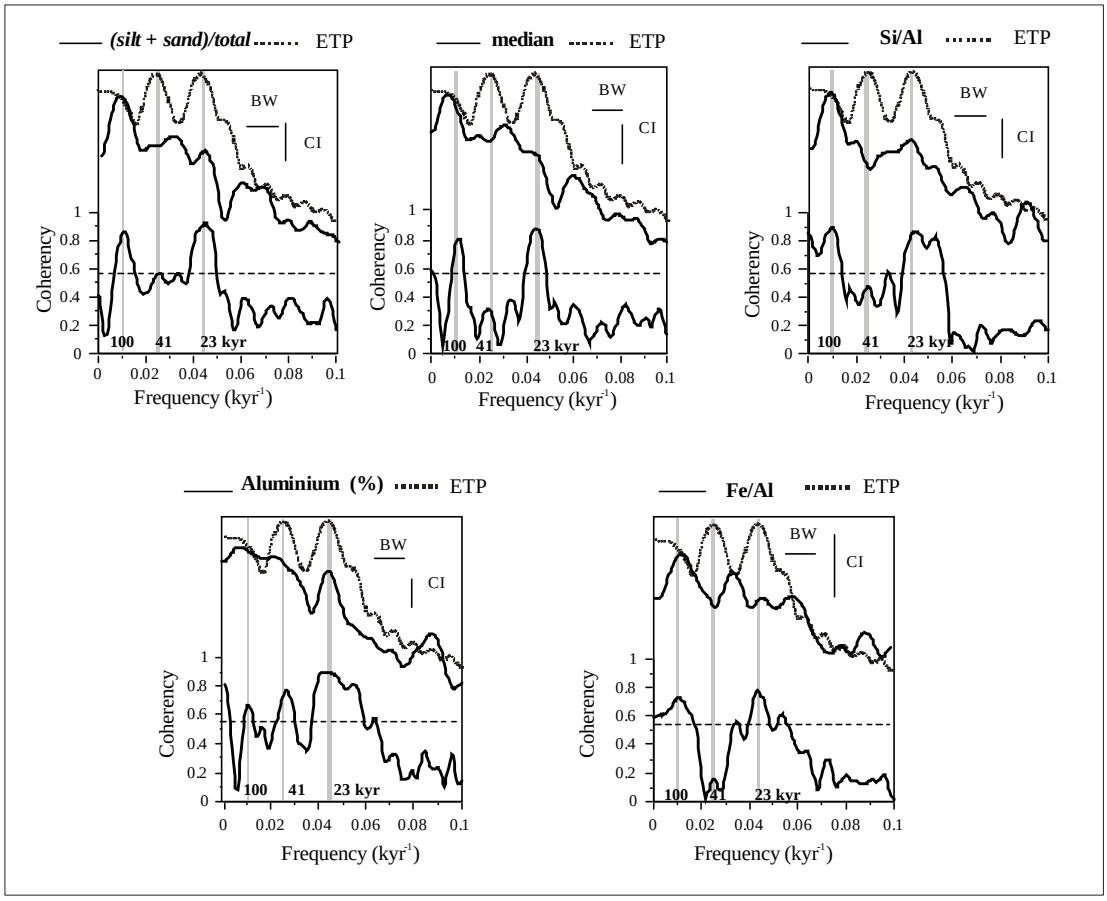

Figure 5..-Variance spectra of the core profiles shown in Figure 4 (expressed as the logarithm of spectral power density versus frequency in cycles kyr^{-1} using the Blackman-Tuckey method) compared with the spectrum of ETP. The three main orbital periods of eccentricity (100 kyr), obliquity (41 kyr) and precession (23 kyr) are marked as vertical grey bands. The coherency plot indicates what frequency components are shared between the proxies and the ETP curve. An 80% confidence level is set, above which statistical significance in the coherency relationship is considered to exist (this level correspond in this case with a coherency of 0.056). Bandwidth (BW) and 80% confidence interval (CI) are indicated with short horizontal and vertical segments, respectively.

Figura 5.- *Espectro de la varianza de los perfiles mostrados en la Figura 4 (expresados como el logaritmo de la densidad del poder espectral en relación a la frecuencia en ciclos cada 1.000 años, usando el método Blackman-Tuckey) comparado con el espectro de la curva ETP. Los tres principales periodos orbitales de excentricidad (100.000 años), oblicuidad (41.000 años) y precesión (23.000 años) están marcados con bandas grises verticales. El gráfico de coherencia indica qué frecuencias son comunes entre las proxies y la curva ETP. El nivel de confianza del 80% está indicado, por encima se considera que existe una relación de coherencia estadísticamente significante (en este caso, dicho nivel corresponde con una coherencia de 0,056). La anchura de banda (BW) y el intervalo de 80% de confianza (CI) se indican con un segmento horizontal y vertical, respectivamente.*

Maximum coherence with ETP for Al and Fe/Al is obtained at 23-kyr periods while for grain-size and Si/Al this is at 100 kyr (Figure 5). Therefore, the variation of dust supply into the NCB over the last 250 kyrs is related to the precession insolation cycle while the wind strength is linked to the glacial-interglacial time scales.

Table 3.- Correlation and phase angle of the proxy records of dust in Core GeoB 5559-2 and TOC in Core GeoB 4216-1 with respect to ETP (Imbrie *et al*., 1984). Maximum Ice Volume (?^{18}O) is based on the SPECMAP curve. ?^{18}O values refer to measurements in Core GeoB 5559-2. Phase angle is shown for selected proxies (coherency with ETP higher than 0.6 at the 80% of confidence). (Si+Sa)/T is abbreviation for (Silt + Sand) /Total.

Tabla 3.- *Correlación y ángulo de fase entre los registros de polvo en el testigo GeoB 5559-2 y el registro de Carbono Orgánico Total (TOC) en el testigo GeoB 4216-1 respecto a la curva ETP (Imbrie et al., 1984). El Volumen Máximo de Hielo (?^{18}O) está basado en la curva de SPECMAP. Los valores de ?^{18}O corresponden con las medidas realizadas en el testigo GeoB 5559-2. Los ángulos de fase están indicados para algunas proxies (aquellas en las que la coherencia con la curva ETP es mayor de 0,6 para una confianza del 80%). (Si+Sa)/T es la abreviatura de (Silt+Sand)/Total.*

Period (kyr)	SPECMAP	?^{18}O	Al (%)	Fe/Al	Si/Al	Median	(Si+Sa)/T	TOC
Correlation								
100	0.92	0.85	0.65	0.72	0.89	0.75	0.84	0.89
41	0.86	0.78	0.67	0.13	0.46	0.31	0.54	0.75
23	0.92	0.94	0.89	0.77	0.85	0.87	0.90	0.91
Phase angle								
100	-173?10?	177?15?	169?30?	-108?24?	-150?13?	-163?22?	-154?16?	-145?12?
41	-104?13?	-87?18?	-129?26?	-	-	-	-	-80?23?
23	-89?10?	-119?9?	14?13?	13?21?	-113?15?	-87?14?	-64?12?	-40?11?

Previous studies revealed a close relation between the increase in dust input in the tropical North Atlantic and the increase in aridity in the Sahara (see for example Tiedemann *et al*., 1989). These studies linked a higher dust input into the basin with enhanced aridity during glacial periods (Sarnthein, 1978; Kolla *et al*., 1979). In addition, deMenocal *et al*., (1993b) suggest that glacial-interglacial variations in the North Atlantic SST field influence both dust source area aridity and the intensity of the dust-transporting Trade winds. However, detailed studies showed that dust proxies vary with a 23 kyr periodicity (Pokras and Mix, 1985; Matthewson *et al*., 1995). These authors interpreted this periodicity to reflect aridity associated to the monsoon cycle. They further proposed that in periods with stronger monsoon, maxima of Northern Hemisphere seasonal insolation, extending to south Sahara and Sahel, the source area of dust was less dry and hence less of dust was available. In contrast, when monsoons were weaker at times of maxima in the precessional index, aridity increased together with dust availability.

In order to investigate the relation between dust input proxies and precession we calculated phase angles (Figure 6 and Table 3). Aluminium and Fe/Al ratio, which are indicating a Sahelian origin, appear in times of maxima Northern Hemisphere seasonal insolation, which means in phase with minima in the precessional index. As Figure 7 shows, aluminium concentration and boreal summer insolation correlate peak to peak. However, these two signals are not highly coherent: the magnitude of the aluminium variation is greater during glacial periods concomitantly with lower amplitude of summer insolation fluctuation. This result may indicate that, although the 23-kyr cycle is driving dust supply to the NCB, a glacial-interglacial signal is also evident, as we discuss below.

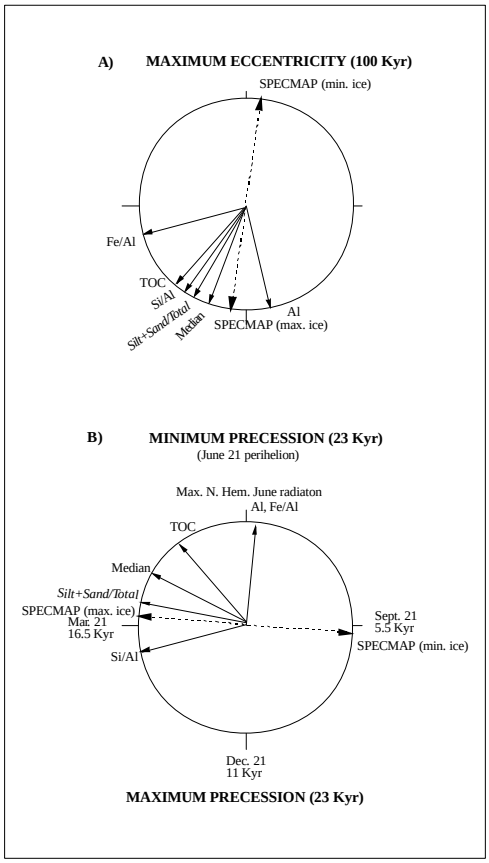

Figure 6.- Phase wheel summaries of insolation (represented as ETP variation), global ice volume (represented as the SPECMAP curve of Martinson *et al*., 1987) and proxy records of dust from GeoB 5559-2 and TOC from GeoB 4216-1. A) Phase relationships at the eccentricity band. B) Phase relationships at the precessional band. The obliquity parameter is not shown since none of the proxy records presents high coherence with that period. See table 3 for the accurate phase angles.

Figura 6.- *Ruedas que representan los ángulos de fase entre la insolación, representada como la variación de ETP, el volumen global de hielo, representado como la curva de SPECMAP de Martinson et al. (1987) y los registros de polvo del testigo GeoB 5559-2 y el TOC del testigo GeoB 4216-1. A) Relaciones de fase en la banda de la excentricidad. B) Relaciones de fase en la banda de la precesión. No se han tenido en cuenta las relaciones en la banda de la oblicuidad porque ninguno de los registros muestra alta coherencia en ese periodo (cf. Tabla 3 para los ángulos exactos).*

As outlined in the introduction, two wind systems transport dust into the NCB, the Trade winds and the SAL. The Trade wind system is also driving and controlling the intensity of the summer upwelling in the NCB. Hence, if Trade winds are related to dust supply and upwelling, the precession signal should also be expected in the basin's productivity records. Freudenthal *et al*., (2002) in their study of Core GeoB 4216-1 showed that indeed the TOC record varies with precession (Figure 7 and Table 3). The phase angles between TOC (taken as a productivity proxy) and ETP show that maximum productivity occurs in phase with minima in the precessional index (Figure 6). This is the same relationship we found for the dust supply (Figure 7).

A minimum in the precessional index implies high seasonality; this means warmer summers and colder winters (Kutzbach, 1981). Therefore, during warmer summers, with the ocean colder than land because of its higher thermal capacity, a strong thermal land-ocean contrast takes place. This leads to an intensification of the Azores high-pressure over the ocean (H) (Figure 8a). On the other hand, the higher insolation on the Sahara induces the development of a stronger low-pressure over the continent (L). The strong pressure gradient between the high and the low is then expected to increase the strength of Trade winds. Therefore, such scenario explains both the records of dust and productivity in terms of changes in Trade wind intensity.

The problem with this interpretation is that it assumes all the dust derived from a northern source. However, the fact that dust from the equatorial latitude records also displays the same precession-related-variations (Matthewson *et al*., 1995; Tiedemann *et al*., 1989; Flores *et al.,* 2000), means that it is difficult to explain these records simply in terms of Trade wind variations.

Furthermore, cores at these latitudes also show precession-related-variations in the fresh-water diatom record (Pokras and Mix, 1985; Pokras and Mix, 1987). Clearly, the source of fresh-water diatoms is the dry lake beds from the Sahel region (Gasse and Fontes, 1992; Pokras, 1991). Therefore, their presence in the records can not be related to the Trade wind system.

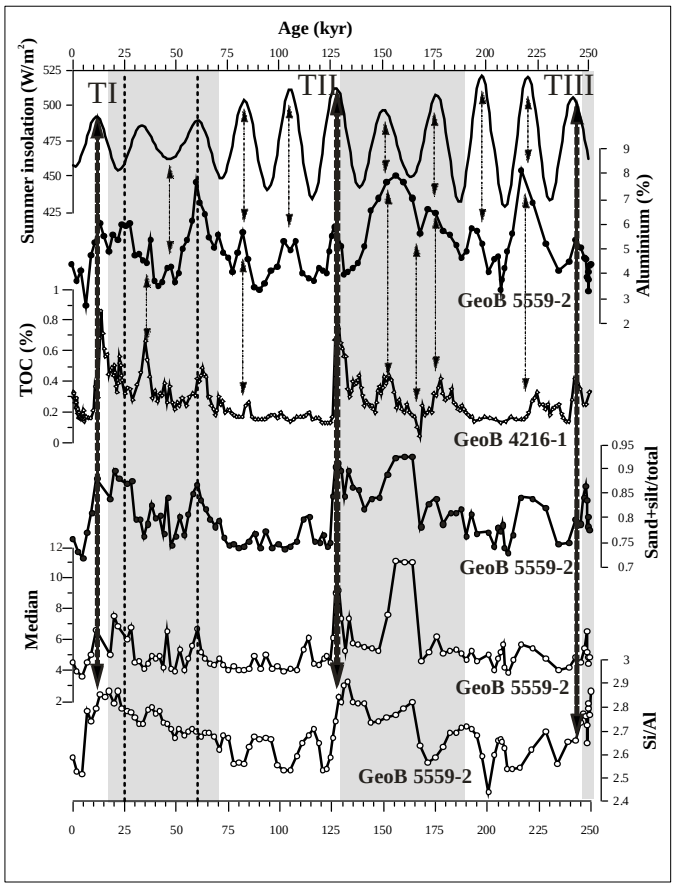

Figure 7.- Comparison among Al content, TOC percentages and proxies for wind strength (Si/Al and grain-size parameters) with the boreal summer insolation variation at 30ºN (Berger, 1978). Glacial stages are shaded.

***Figura 7.**- Comparación entre el contenido en Al, porcentajes de carbono orgánico total y proxies de intensidad de vientos (Si/Al y parámetros granulométricos) con la variación de la insolación de verano a 30ºN (Berger, 1978). Los estadios glaciares están sombreados.*

During a minimum in the precessional index, the monsoonal system is enhanced owing to the maxima of Northern Hemisphere seasonal insolation (Kutzbach and Gallimore, 1988). The intensification of monsoonal winds weakens the Northern Hemisphere Trade winds at the equatorial latitudes (McIntyre *et al*., 1989). So that the Northern Trade winds can not supply dust from the Sahel region to Equatorial latitudes. Such consideration opens another interpretation for the dust record of the NCB, which also can explain the records of Matthewson *et al*., (1995).

In maxima of Northern Hemisphere seasonal insolation, the winter scenario is reverse with respect to the summer one. At this case, due to the ocean's higher thermal capacity than land, the summer Azores high, is shifted southwards and becomes very weak. Meanwhile, on the cooler continent a very strong high pressure develops (Figure 8b). In this meteorological context, the SAL, and specially its northern branch, should be well developed, and thus may account for enhanced dust transport to the NCB.

Apparently, this model may be in contradiction with the fact that during a precession-minimum-summer, the monsoon regime is enhanced bringing rainfall to the Sahel region

(Kutzbach, 1981; McIntyre *et al*., 1989). This increase is well documented in African lake level records (Gasse *et al*., 1990; Kutzbach and Street-Perrott, 1985; Street-Perrot and Perrot, 1990). Subsequently, the increased moisture would have reduced dust availability. Nevertheless, it is evident that an increase in moisture also implies a change in the weathering patterns. Rea (1994) concluded that in hyper-arid conditions (< 100 mm annual rainfall) dust generation falls off because the lack of moisture prevents the break down of the large minerals into clays of a size suitable for long-distance transport. In this case, an enhanced monsoon, which probably extended to the Sahel area, may have provided enough moisture to increase significantly dust generation, and therefore dust availability. The dust would then be transported by the Saharan winds to the NCB. Furthermore, a grass Savannah vegetation type such as it is today in the Sahel area (White, 1983) allows for dust generation. Since pollen studies from the region show the presence of this vegetation type over the last 250 kyrs (Hooghiemstra, 1996), it is suggested that monsoon rainfall, because of its seasonality, may be insufficient to develop a more permanent type of vegetation cover. This is inferred from the fact that grass Savannah spread northwards into the Sahara reacting to moisture, while the Guinean rain forest belt did not shift beyond 15?N latitude (Hooghiemstra, 1996). According to the data set recopilated by Hoelzmann *et al.*, (1998) the boundary between steppe and savanna vegetation at 6,000 yr BP (maxima seasonal insolation) occurred at 20?N which allows dust generation in the Sahel region. In the suggested model, the high seasonality typical during minima in the precessional index, may have contributed in establishing suitable conditions, first for weathering in summer and second for deflation by the Saharan winds in winter. Thus, the Sahel region can be considered a permanent source of dust.

Therefore, the record of dust supply into the NBC can be interpreted as the result of combining two meteorological scenarios, a winter and a summer one, both linked to minima in the precessional index. The summer scenario of enhanced Trade winds explains the productivity variations and may also account for part of the dust signal while the winter scenario can explain most of the variation in dust supply. However, by means of frequency analysis we have found that some of the studies proxies (Si/Al ratio and grain-size parameters) have a clear response to the eccentricity cycle (100-kyr). In addition, productivity results in several cores from the NCB also display this glacial-interglacial signal (Freudenthal *et al*., 2002; Moreno *et al*., 2002). Productivity signal in this area is linked to the Trade wind system, by means of upwelling intensification. Therefore, we will discuss the importance of this cyclicity in our proxy records to understand the Trade winds system variability over the last 250 kyrs.

1.6.2. Response of wind strength to the 100-kyr cycle

Grain-size parameters, Si/Al ratio and grain-size families display a clear glacial-interglacial pattern of variation. On average, maximum values of these proxies appear associated with OIS 2, 4 and 6. In addition, Si/Al ratio and the grain-size parameters present mainly a 100-kyr response. However, these proxies are not in phase with the glacial maximum. On the contrary, they appear between 3,000 and 6,000 years after maximum ice conditions in the eccentricity wheel (Figure 6). Therefore, we propose that the variation in these proxy records may be related to any change that took place at Terminations.

In principle, these grain-size variations might be coupled with changes in the sedimentation patterns during glacial-interglacial transitions. Higher rates of sea-level rise occur at Terminations (Shackleton, 1987). Besides the common turbidite deposition during sea-level

lowstands, turbidite systems are observed to occur during sea-level rise (Prins and Postma, 2000). Therefore, we may consider that coarse particles deposited at the shelf edge may have advected via turbidites to the NCB at Terminations. However, the fact that both cores record the same events and Core GeoB 5559-2 is located in the slope of a seamount, any influence from the shelf in the core records seems unlikely.

Arguably, the observed grain-size variations can be interpreted as related to changes in the energy of the transporting wind (Rea, 1994). Sarnthein *et al*., (1981) and Grousset *et al*., (1998) found glacial-interglacial patterns of variation in their records, south of the Canary Islands. They concluded that the increase in the particles grain-size during full glacial conditions was related to higher Trade wind intensities. However, the coarsest grain-sizes and the higher values in the Si/Al ratio are recorded at Terminations and not at glacial maxima in the studied cores from the NCB (Figure 4). Although the overall pattern is an increase in the dust proxies during glacial stages, superimposed to this signal there is a significant increment of the wind strength proxies at Terminations.

As discussed before, wind and productivity are linked to Trade wind strength. In Figure 7 the TOC record from Core GeoB 4216-1 is represented and compared with dust proxies and summer insolation at 30?N. The %TOC record contains an intermediate mixture of the 23-kyr proxies (%Al, Fe/Al ratio) and the 100-kyr proxies (grain-size parameters and Si/Al ratio). This may indicate that, although the precessional pattern is evident, the glacial-interglacial signal is influencing Trade winds variations. Consequently, a good correlation between grain-size and Si/Al ratio and peaks in the TOC record is shown (Figure 7). Therefore, the Trade winds in this region were strongly intensified at the Terminations. This conclusion is strengthened by the results from different authors around this area. Thus, Lézine and Denèfle (1997) produced a detailed pollen records for Termination I from a core from offshore Portugal and concluded that anticyclonic circulation was strengthened over the Northeastern Atlantic. They further stated that cooler Sea Surface Temperatures (SST) were coeval with stronger Trade winds. After a palynological study from a core located offshore Morocco, Marret and Turon (1994) postulated an enhancement in Trade winds strength during last deglaciation. South of the Canary Islands Martinez *et al*. (1999) and Ternois *et al*. (2000) also found an increase in grain-size and productivity proxies at Termination I, which they related to Trade wind intensity (Figure 8a).

Terminations are unique intervals of climate change, in which climate switches from a glacial to an interglacial mode. In these intervals, maxima in boreal summer insolation, rapid ice-sheet melting and fast rates of sea-level rise concur. Hughen *et al*. (1996) and Overpeck *et al*. (1989) proposed that under this scenario the North Atlantic SST lowered by the melt water, may have strengthened the high-pressure system over the North Atlantic. Therefore, SST variations in the North Atlantic provide a mechanism to explain changes in Trade wind intensity. Moreover, this conclusion reinforces previous ideas on how SST changes in North Atlantic have influence upon the African climate (deMenocal, 1995).

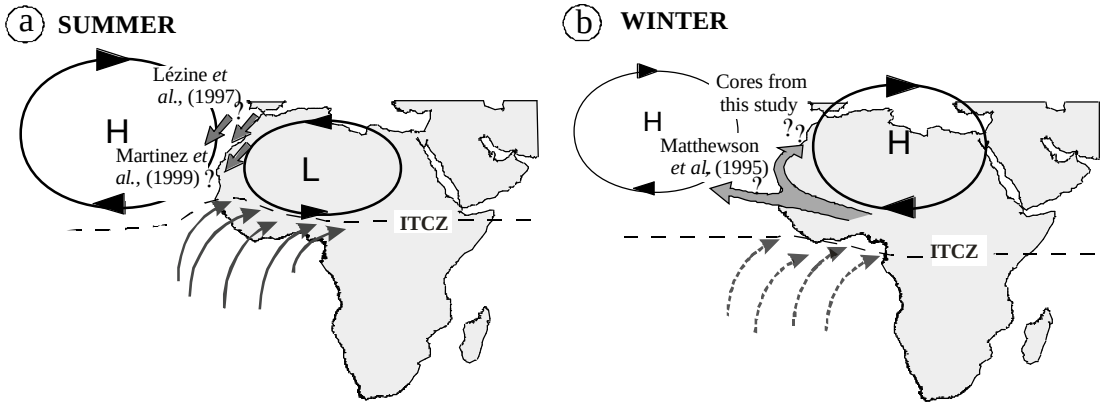

Figure 8.- Inferred climate scenarios at precession minimum (see text for explanation). a) Summer. b) Winter. Grey arrows represent dust-bearing wind systems: the Trade winds and the SAL; black arrows represent the monsoon winds; weaker winds are shown by dashed arrows.

Figura 8.- *Escenarios climáticos inferidos para los periodos de mínimos valores en el índice de precesión (ver texto para explicación). A) Verano. B) Invierno. Las flechas grises representan los sistemas de vientos que transportan polvo: los vientos alisios y la Capa de Aire Sahariano; las flechas negras representan los monzones; los vientos más débiles se muestran con flechas punteadas*.

1.7. Conclusion

This paper shows that precession and eccentricity cycles play a role in driving changes in dust input to the North Canary Basin. The record of dust can be interpreted in terms of a summer and a winter scenarios during a minimum in the precessional index. During summers, Trade winds were intensified which resulted in higher productivity and the transport of coarser grains from a Northwest African source. Meanwhile, in the Sahel area conditions were suitable for increased dust generation. During winter, the Saharan Air Layer could transport this dust to the NCB.

Superimposed to the overall pattern of a Trade winds enhancement during glacial periods, maxima in productivity and grain-size both appear at Terminations I, II and III. At these periods of higher insolation but lower SST over the North Atlantic, the subtropical anticyclonic circulation may have intensified. Then, the strengthened Trade winds forced upwelling and had the ability to carry coarser particles at Terminations.

Acknowledgements

We gratefully acknowledge the officers and crew of the R/V Meteor for technical support during the CANIGO cruises (December 1996 and October 1998) and people from Bremen University, Geological Institute of Lisbon and Geological Institute of Zurich for their help in sampling and description of sediment cores. We thank E. Segui, J. M. Socias (XRF laboratory), P. Hortolà and M. Guart (sedimentological laboratory) for laboratory analyses. We sincerely thank I. Cacho and J. Villanueva (Institute of Chemical and Environmental Research, CSIC, Barcelona), L. Dupont

(University of Bremen), P. Bertrand, P. Martinez and F. Grousset (University of Bordeaux) for useful comments on an earlier version of the manuscript. Prof. J. Rose and B. Ruddiman reviewed the manuscript and provided helpful suggestions. The present study was supported by the CANIGO project (MAS3-CT9-0060) and a Comissionat d'Universitats i Recerca fellowship (Ana Moreno).

1.8. References

Anderson, T. F. and Steinmetz, J. C. (1981) Isotopic and biostratigraphical records of calcareous nannofossils in a Pleistocene core. *Nature*, **294,** 741-744.

Arimoto, R., Duce, R. A., Ray, B. J., Ellis, W., Cullen, J. D. and Merrill, J. T. (1995) Trace elements in the atmosphere over the North Atlantic. *Journal of Geophysical Research*, **100,** 1199-1213.

Balsam, W. L., Otto-Bliesner, B. L. and Deaton, B. C. (1995) Modern and last glacial maximum eolian sedimentation patterns in the Atlantic Ocean interpreted from sediment iron oxide content. *Paleoceanography*, **10,** 493-507.

Beltagy, A. I., Chester, R. and Padgham, R. C. (1972) The particle-size distribution of quartz in some North Atlantic deep-sea sediments. *Marine Geology*, **13,** 297-310.

Bergametti, G., Gomes, L., Coudé-Gaussen, G., Rognon, P. and Le Coustumer, M. N. (1989) African dust observed over Canary Islands: source-regions identification and transport pattern for some summer situations. *Journal of Geophysical Research*, **94,** 14.855-14.864.

Berger, A. (1978) Long-term variations of caloric insolation resulting from the Earth's orbital elements. *Quaternary Research*, **9,** 139-167.

Bertrand, P., Shimmield, G. B., Martinez, P., Grousset, F. E., Jorissen, F., Paterne, M., Pujol, C., Bouloubassi, I., Buat-Menard, P., Peypouquet, J.-P., Beaufort, L., Sicre, M.-A., Lallier-Verges. E., Foster, J. M. and Ternois, Y. (1996) The glacial ocean productivity hypothesis: the importance of regional temporal and spatial studies. *Marine Geology*, **130**, 1-9.

Boyle, E. (1983) Chemical accumulation variations under the Peru current during the past 130.000 years. *Journal of Geophysical Research*, **88,** 7667-7680.

Bustos, J. J., Cuevas, E., Marrero, C. and Afonso, S. (1998) Fenómenos y sistemas meteorológicos: caracterización de masas de aire en la troposfera libre y en la capa de mezcla en Canarias. *In*: *IX Asamblea Nacional de Geodesia y Geofísica*, Aguadulce (Almería).

Chiapello, I., Bergametti, G. and Chatenet, B. (1997) Origins of African dust transported over the northeastern tropical Atlantic. *Journal of Geophysical Research*, **102,** 13.701-13.709.

Clemens, C. and Prell, W. (1990) Late Pleistocene variability of Arabian Sea summer monsoon winds and continental aridity: eolian records from the lithogenic component of deep-sea sediments. *Paleoceanography*, **5,** 109-145.

Clemens, C. (1998) Dust response to seasonal atmospheric forcing: proxy evaluation and calibration. *Paleoceanography*, **13,** 471-490.

Davenport, R., Neuer, S., Hernández-Guerra, A., Ruedas, M. J., Llinas, O., Fischer, G. and Wefer, G. (1999) Seasonal and interannual pigment concentration in the Canary Islands region from CZCS data and comparison with observations from the ESTOC. *International Journal of Remote Sensing*, **20,** 1419-1433.

deMenocal, P. and Rind, D. (1993a) Senstivity of asian and african climate to variations in seasonal insolation, glacial ice cover, sea surface temperature and asian orography. *Journal of Geophysical Research*, **98,** 7265-7287.

deMenocal, P., Ruddiman, W. and Pokras, E. M. (1993b) Influences of high-and low- latitude processes on African terrestrial climate: Pleistocene eolian records from equatorial Atlantic Ocean Drilling Program site 663. *Paleoceanography*, **8**, 209-242.

deMenocal, P. (1995) Plio-Pleistocene African Climate. *Science*, **270,** 53-59.

Flores, J. A., Bárcena, M. A. and Sierro, F. J. (2000) Ocean-surface and wind dynamics in the Atlantic Ocean off Northwest Africa during the last 140,000 years. *Palaeogeography, Palaeoclimatology, Palaeoecology*, **161**, 3-4, 459-478.

Freudenthal, T., Meggers, H., Henderiks, J., Kuhlmann, H., Moreno, A. and Wefer, G. (2002) Variability of upwelling instensity and filament activity off Morocco during the last 250,000 years. *Deep Sea Research II*, **in press**.

Fütterer, D. K. (1983) The modern upwelling record off NW Africa. *In*: Thiede, J. and Suess, E. (eds.), *Coastal upwelling; its sediment record*, 105-121, NATO Advanced Research Institute, Plenum Press, New York.

Gabric, A. J., García, L., Van Camp, L., Nykjaer, L., Eifler, W. and Schrimpf, W. (1993) Offshore export of shelf production in the Cape Blanc (Mauritania) giant filament as derived from coastal zone color scanner imagery. *Journal of Geophysical Research*, **98,** 4697-4712.

Game, P. M. (1962) Observations on a dustfall in the Eastern Atlantic. *Journal of Sedimentary Petrology*, **34,** 355-359.

Gasse, F., Stabell, B., Fourtanier, E. and Van Iperen, Y. (1989) Freshwater diatom influx in Intertropical Atlantic: relationships with continental records from Africa. *Quaternary Research*, **32,** 229-243.

Gasse, F., Tehet, R., Durand, A., Gibert, E. and Fontes, J.-C. (1990) The arid-humid transition in the Sahara and the Sahel during the last deglaciation. *Nature*, **346,** 141-146.

Gasse, F. and Fontes, J. C. (1992) Climatic changes in northwest Africa during the last deglaciation (16-7 ka BP). *In*: Bard, E. and Broecker, W. S. (eds.), *The Last Deglaciation: absolute and radiocarbon chronologies*, **12**, 295-325, Springer-Verlag.

Grousset, F. E., Parra, M., Bory, A., Martinez, P., Bertrand, P., Shimmield, G. B. and Ellam, R. M. (1998) Saharan wind regimes traced by the Sr-Nd isotopic composition of subtropical Atlantic sediments: last Glacial maximum vs today. *Quaternary Science Reviews*, **17,** 395-409.

Guieu, C. and Thomas, J. (1996) Saharan aerosols: from the soil to the ocean. *In*: Guerzoni, S. and Chester, R. (eds.), *The impact of desert dut across the Mediterranean*, 207-216, Kluwer Academic Publishers.

Hagen, E., Zülicke, C. and Feistel, R. (1996) Near-surface structures in the Cape Ghir filament off Morocco. *Oceanologica Acta*, **19,** 577-597.

Hoelzmann, P., Jolly, D., Harrison, S. P., Laarif, F., Bonnefille, R. and Pachur, H.-J. (1998) Mid-Holocene land-surface conditions in northern Africa and the Arabian peninsula: a data set for the analysis of biogeophysical feedbacks in the climate system. *Global Biochemical Cycles*, **12**, 35-51.

Hooghiemstra, H. (1989) Variations of the NW African trade wind regime during the last 140.000 years: changes in pollen flux evidenced by marine sediment records. *In*: Leinen, M. and

Sarnthein, M. (eds.), *Paleoclimatology and paleometeorology: modern and past patterns of global atmospheric transport*, 733-770, NATO ASI Series, Kluwer, Dordrecht.

Hooghiemstra, H., Stalling, H., Agwu, C. O. C. and Dupont, L. M. (1992) Vegetational and climatic changes at the northern fringe of the Sahara 250.000-5.000 years BP: evidence from 4 marine pollen records located between Portugal and the Canary Islands. *Review of Palaeobotany and Palynology*, **74,** 1-53.

Hooghiemstra, H. (1996) Aspects of Neogene-Quaternary environmental and climatic change in equatorial and Saharan Africa. *Palaeoecology of Africa*, **24,** 115-132.

Hughen, K. A., Overpeck, J. T., Peterson, L. C. and Trumbore, S. (1996) Rapid climate changes in the tropical Atlantic region during the last deglaciation. *Nature*, **380,** 51-54.

Imbrie, J., Hays, J. D., Martinson, D. G., McIntyre, A., Mix, A. C., Morley, J. J., Pisias, N. G., Prell, W. L. and Shackleton, N. J. (1984) The orbital theory of Pleistocene climate: support from a revised chronology of the marine ?^{18}O record. *In*: Berger, A. (ed.), *Milankovitch and Climate*, 269-305, Proceesing of the NATO Advanced Research Workshop on Milankovitch and Climate, D. Reidel publishing Company, Palisades, New York.

Klein, B. and Siedler, G. (1989) On the origin of the Azores current. *Journal of Geophysical Research*, **94,** 6159-6168.

Kolla, V., Biscaye, P. and Hanley, A. F. (1979) Distribution of quartz in late Quaternary Atlantic sediments in relation to climate. *Quaternary Research*, **11,** 261-277.

Kutzbach, J. E. (1981) Monsoon climate of the Early Holocene: climate experiment with the Earth's orbital parameters for 9000 years ago. *Science*, **214,** 59-61.

Kutzbach, J. E. and Street-Perrott, F. A. (1985) Milankovitch forcing of fluctuations in the level of tropical lakes from 18 to 0 kyr BP. *Nature*, **317,** 130-134.

Kutzbach, J. E. and Gallimore, R. G. (1988) Sensitivity of a coupled atmosphere/mixed layer ocean model to changes in orbital forcing at 9.000 years B.P. *Journal of Geophysical Research*, **93,** 803-821.

Lamb, H., Gasse, F., Benkaddour, A., El Hamoutl, N., Van der Kaars, S., Perkins, W. T., Pearce, N. J. and Roberts, C. N. (1995) Relation between century-scale Holocene arid intervals in tropical and temperate zones. *Nature*, **373,** 134-137.

Lézine, A. M. and Denèfle, M. (1997) Enhanced anticyclonic circulation in the eastern North Atlantic during cold intervals of the last deglaciation inferred from deep-sea pollen records. *Geology*, **25,** 119-122.

Loring, D. H. and Rantala, R. T. T. (1992) Manual for the geochemical analyses of marine sediments and suspended particulate matter. *Earth Science Reviews*, **32,** 235-283.

Marret, F. and Turon, J. L. (1994) Paleohydrology and paleoclimatology off Northwest Africa during the last glacial-interglacial transition and the Holocene: Palynological evidences. *Marine Geology*, **118,** 107-117.

Martinez, P., Bertrand, P., Shimmield, G. B., Cochrane, K., Jorissen, J., Foster, J. M. and Dignan, M. (1999) Upwelling intensity and ocean productivity changes off Cape Blanc (Northwest Africa) during the last 70.000 years: geochemical and micropalaeontological evidence. *Marine Geology*, **158,** 57-74.

Martinson, D. G., Pisias, N. G., Hays, J. D., Imbrie, J., Moore, T. C. and Shackleton, N. J. (1987) Age dating and the orbital theory of the Ice Ages: development of a high-resolution 0 to 300.000-year chronostratigraphy. *Quaternary Research*, **27,** 1-29.

Matthewson, A. P., Shimmield, G. B., Kroon, D. and Fallick, A. E. (1995) A 300 kyr high-resolution aridity record of the North African continent. *Paleoceanography*, **10,** 677-692.

McIntyre, A., Ruddiman, W., Karlin, K. and Mix, A. C. (1989) Surface water response of the equatorial Atlantic ocean to orbital forcing. *Paleoceanography*, **4,** 19-55.

Mittelstaedt, E. (1983) The upwelling area off northwest Africa - a description of phenomena related to coastal upwelling. *Progress in Oceanography*, **12,** 307-331.

Moreno, A., Nave, S., Kuhlmann, H., Canals, M., Targarona, J., Freudenthal, T. and Abrantes, F. (2002) Productivity response in the North Canary Basin to climate changes during the last 250,000 years: a multi-proxy approach, *Earth and Planetary Science Letters*, **196**, 3-4, 147-159.

Neuer, S., Ratmeyer, V., Davenport, R., Fischer, G. and Wefer, G. (1997) Deep water particle flux in the Canary Island region: a seasonal trends in relation to long-term satellite derived pigment data and lateral sources. *Deep Sea Research I*, **44,** 1451-1466.

Overpeck, J. T., Peterson, L. C., Kipp, N., Imbrie, J. and Rind, D. (1989) Climate change in the circum-north Atlantic region during the last deglaciation. *Nature*, **338,** 553-557.

Paillard, D., Labeyrie, L. and Yiou, P. (1996) Macintosh program performs time-series analysis. *Eos Transactions*, **77,** 379.

Parkin, D. W. and Shackleton, N. J. (1973) Trade wind and temperature correlations down a deep-sea core off the Saharan coast. *Nature*, **245,** 455-457.

Paull, C. K. and Thierstein, H. R. (1987) Stable isotopic fractionation among particles in Quaternary coccolith-size deep-sea sediments. *Paleoceanography*, **2,** 423-429.

Pisias, N. G., Martinson, D. G., Moore, T. C., Shackleton, N. J., Prell, W., Hays, J. D. and Boden, G. (1984) High resolution stratigraphic correlation of benthic oxigen isotopic records spanning the last 300.000 years. *Marine Geology*, **56,** 119-136.

Pokras, E. M. and Mix, A. (1985) Eolian evidence for spatial variability of Late Quaternary climates in Tropical Africa. *Quaternary Research*, **24,** 137-149.

Pokras, E. M. and Mix, A. C. (1987) Earth's precession cycle and Quaternary climatic change in tropical Africa. *Nature*, **326,** 486-487.

Pokras, E. M. (1991) Source areas and transport mechanisms for freshwater and brackish-water diatoms deposited in pelagic sediments of the Equatorial Atlantic. *Quaternary Research*, **35,** 144-156.

Prins, M. and Postma, G. (2000) Effects of climate, sea level, and tectonics unraveled for last deglaciation turbidite records of the Arabian Sea. *Geology*, 28, 375-378.

Prospero, J. M. (1996) Saharan dust transport over the North Atlantic ocean and Mediterranean: an overview. *In*: Guerzoni, S. and Chester, R. (eds.), *The impact of desert dust across the Mediterranean*, 133-151, Kluwer Academic Publisher.

Rea, D. (1994) The paleoclimatic record provided by eolian deposition in the deep sea: the geologic history of wind. *Reviews of Geophysics*, **32,** 159-195.

Reichart, G., den Dulk, M., Visser, H. J., van der Weijden, C. H. and Zachariasse, W. J. (1997) A 225 kyr record of dust supply, paleoproductivity and the oxygen minimum zone from the Murray Ridge (northern Arabian Sea). *Palaeogeography, Palaeoclimatology, Palaeoecology*, **134,** 149-169.

Ruddiman, W. (1997) Tropical Atlantic terrigenous fluxes since 25.000 yrs B.P. *Marine Geology,*

136, 189-207.

Sarnthein, M. (1978) Sand deserts during glacial maximum and climatic optimum. *Nature*, **272,** 43-46.

Sarnthein, M. and Koopmann, B. (1980) Late Quaternary deep-sea record on northwest African dust supply and wind circulation. *Palaeoecology of Africa*, **12,** 239-253.

Sarnthein, M., Tetzlaff, G., Koopmann, B., Wolter, K. and Pflaumann, U. (1981) Glacial and interglacial wind regimes ower the eastern subtropical Atlantic and North-West Africa. *Nature*, **293,** 193-196.

Sarnthein, M., Thiede, J., Pflaumann, U., Erlenkeuser, H., Fütterer, D., Koopmann, B., Lange, H. and Seibold, E. (1982) Atmospheric and oceanic circulation patterns off Northwest Africa during the past 25 million years. *In*: Rad, U., Hinz, I., Sarnthein, M. and Scibold, E. (eds.), *Geology of the Northwest Africa continental margin*, 547-604, .

Schütz, L., Jaenicke, R. and Pietrek, H. (1981) Saharan dust transport over the North Atlantic Ocean. *In*: Pèwè, T. (ed.), *Desert Dust: origin, characteristics and effect of man*, **186**, 87-100, Special Paper, Geological Society of America.

Shackleton, N. J. (1987) Oxygen isotopes, ice volume and sea level. *Quaternary Science Reviews*, **6**, 183-190.

Stein, R. (1985) Late Neogene changes of Paleoclimate and Paleoproductivity off Northwest Africa. *Palaeogeography, Palaeoclimatology, Palaeoecology*, **49,** 47-59.

Steinmetz, J. C. and Anderson, T. F. (1984) The significance of isotopic and paleontologic results on Quaternary calcareous nannofossil assemblages from Caribean core P6304-4. *Marine Micropaleontology*, **8,** 403-424.

Street-Perrot, F. A. and Perrot, R. A. (1990) Abrupt climate fluctuations in the tropics: the influence of Atlantic Ocean circulation. *Nature*, **343,** 607-612.

Ternois, Y., Sicre, M.-A. and Paterne, M. (2000) Climatic changes along the northwest African continental margin over the last 30 kyr. *Geophysical Research Letters*, **27,** 133-136.

Tetzlaff, G. and Wolter, K. (1980) Meteorological patterns and the transport of mineral dust from the north African continent. *Palaeoecology of Africa*, **12,** 31-42.

Tiedemann, R., Sarnthein, M. and Stein, R. (1989) Climatic changes in the Western Sahara: aeolo-marine sediment record of the last 8 million years (sites 657-661). *In*: Ruddiman, W. and Sarnthein, M. (eds.), *Proceedings of the Ocean Drilling Program, Scientific Results*, **108**, 241-261.

Torres-Padrón, M. E., Gelado-Caballero, M. D., Collado-Sánchez, C., Siruela-Matos, V. F., Cardona-Castellano, P. J., y Hernández-Brito, J. J. (2002). Variability of dust inputs to the CANIGO zone. *Deep Sea Research II*, **in press**.

Van Camp, L., Nykjaer, L., Mittelstaedt, E. and Schlittenhardt, P. (1991) Upwelling and boundary circulation off Northwest Africa as depicted by infrared and visible satellite observations. *Progress in Oceanography*, **26,** 357-402.

Wefer, G., Abrantes, F. and cruise participants (1997) Report and preliminary results of METEOR-Cruise M 37/1, Lisbon-Las Palmas, 04.12.-23.12.1996. Berichte, Fachbereich Geowissenschaften, Universität Bremen, Bremen, 79 p.

Wefer, G., Segl, M. and cruise participants (1998) Report and preliminary results of METEOR-Cruise M 42/4, Las Palmas-Viena do Castelo, 26.09.-26.10.1998. Berichte, Fachbereich

Geowissenschaften, Universität Bremen, Bremen, 104 p.

White, F. (1983) The vegetation of Africa. UNESCO, Paris, 356 p.

Wooster, W. S., Bakun, A. and McLain, D. R. (1976) The seasonal upwelling cycle along the eastern boundary of the North Atlantic. *Journal of Marine Research*, **34,** 131-141.

ARTÍCULO 2

Productivity response in the North Canary Basin to climate changes during the last 250,000 yr: a multi-proxy approach

Ana Moreno[1], Silvia Nave[2], Holger Kuhlmann[3], Miquel Canals[1*], Jordi Targarona[1], Tim Freudenthal[3] and Fatima Abrantes[2]

[1]*Grup de Recerca Consolidat en Geociències Marines, Departament d'Estratigrafia, Paleontologia i Geociències Marines, Universitat de Barcelona, Campus de Pedralbes, E-08028 Barcelona, Spain*

[2]*Departamento de Geologia Marinha, Instituto Geologico e Mineiro, P-2720 Alfragide, Portugal*

[3]*Universität Bremen, FB Geowissenschaften, Postfach 33 04 40, D-28359 Bremen, Germany*

Publicado en:

Earth and Planetary Science Letters, 196, 147-159 (2002)

0012-821X/02/$

PII:SO012-821X (01)00605-7

Abstract

We present results from the investigation of the primary productivity record over the last 250 kyr in the North Canary Basin (30ºN) off Northwest Africa. Two distinct productive systems interfere in this area: the oligotrophic open ocean and the upwelling filament off Cape Ghir, that occasionally carries offshore cool nutrient-rich waters. The following geochemical and micropaleontological paleoproductivity proxies have been used in our study: calcium carbonate, barium excess (Ba_{excess}), Total Organic Carbon (TOC) and diatoms.

Time series analysis of these proxies indicates that paleoproductivity in the North Canary Basin underwent important changes following precession and eccentricity cycles. While the precessional signal appears to be mainly related to Trade Wind strength, superimposed peaks in Ba_{excess}, TOC and diatom records point to large productivity events at Terminations I, II and III. Lowering of the North Atlantic sea surface temperatures by melt water discharges which in turn strengthened the Azores high-pressure centre and increased Trade Wind velocities is postulated as the mechanism to explain the enhancement of the coastal upwelling and associated filaments at Terminations. Additionally, the Canary Current may play a role in transmitting cold melt-waters and nutrients from higher latitudes to the North Canary Basin.

Keywords: Terminations, Northwest African margin, paleoproductivity, upwelling filament, Trade winds

2.1. Introduction

Upwelling is driven by the interaction of alongshore wind stress and surface current that brings cold and nutrient-rich subthermocline waters and CO_2 to the surface. This process results in high rates of primary production and carbon fixation. Thus, upwelling systems play an important role in global carbon cycle, acting as CO_2 sources and sinks [1]. Stronger upwelling and associated higher productivity were discussed as cause for variations in atmospheric CO_2 contents during the last glacial/interglacial periods [2]. Therefore, investigation of productivity gradients and patterns in upwelling areas has become a very important issue in global climate reconstructions.

Coastal upwelling is especially intense in eastern boundary currents, the most important regions being NW Africa-Iberia, SW Africa, Peru-Chile and Oregon-California, that account for the 80-90% of total new production [3]. Along the northeastern Atlantic, productivity off Iberia and the NW African coast is linked to the Trade Winds and the Canary Current (CC) systems through the outgrowth of coastal upwelling and upwelling filaments [4]. Thus, the location of the Azores high-pressure centre and its pressure gradient are the main forcings behind upwelling intensity and the resulting productivity pattern in both upwelling regions [5].

According to classical paleoproductivity studies, the NW African upwelling was considered the paradigm for glacial high productivity [6]. However, recent high-resolution studies reported a distinct paleoproductivity maximum at Terminations off Cape Blanc (20ºN) [7, 8].

These authors found that productivity was controlled by advection from the shelf and/or offshore shifts of the upwelling cells related to sea level changes. Since these study areas are under the influence of continental margin processes local oceanographic conditions will determine the productivity records [7]. Similar productivity peaks during glacial/interglacial transitions were found in the Portuguese margin at 41ºN from diatom abundance, barium and organic carbon records [9]. The mechanisms that could explain these striking productivity events are a matter of debate.

Although many paleoproductivity records have been obtained from the NW African margin, very few of them are from the region north of the Canary Islands. Within the MAST III funded CANIGO (Canary Islands Azores and Gibraltar Observations) Project, paleoproductivity response to climate changes was studied in the North Canary Basin (NCB) (Figure 1). The intermediate location of the NCB (30ºN), between the upwelling off Cape Blanc and the Portuguese margin, allows us to compare new paleoproductivity records in terms of productivity patterns and forcing mechanisms as related to atmospheric and oceanographic changes. In this study, a multi-proxy approach was carried out in two sediment cores from the hemipelagic environment that record climatically forced productivity changes beyond the direct influence of coastal processes.

2.2. Present-day situation

The NCB is located off NW Africa, between 28ºN and 32ºN (Figure 1). At present, the NCB receives dust transported from NW Africa by two wind systems: the Saharan Air Layer, with dust sources in the southern Sahara and the Sahel, and the Trade Winds that carry dust from Morocco and the eastern Sahara [10].

As a consequence of the northward displacement of the subtropical high-pressure, coastal upwelling occurs at the NCB latitude mainly during summer and fall [4]. A characteristic feature of this coastal upwelling is the presence of a prominent upwelling filament off Cape Ghir that was revealed by satellite imagery [11, 12] and CTD surveys [13]. The filament structure was modelled in both the temperature and velocity fields showing that it carries nutrient-rich cool water offshore out beyond 13ºW [14]. Several studies in the NCB area have shown that Cape Ghir filament growth appears to be forced by favourable high wind stress [11]. However, recent SST satellite images indicate that it may extend further offshore during winter, in coincidence with the late winter/early summer productivity bloom previously described in trap studies [15, 16]. An additional factor that might control the strength of the filament is the interaction among the CC and bottom topography [4].

The core sites GeoB 5559-2 (30º37,8’N; 12º23,7’W; 3,178 m water depth) and GeoB 4216-1 (31º38,7’N; 13º11,2’W; 2,324 m water depth) are located under the influence of the Cape Ghir upwelling filament, in a productivity gradient from the coast to the open ocean. Recent studies in the NCB have shown that the present-day productivity signal of Cape Ghir upwelling filament is transferred through the water column and preserved in surface sediments [17, 18]. Therefore, the hemipelagic setting off Cape Ghir holds a strong potential to record climatically induced productivity changes. In addition, the site locations allow us to study the extent of Cape Ghir upwelling filament through the records.

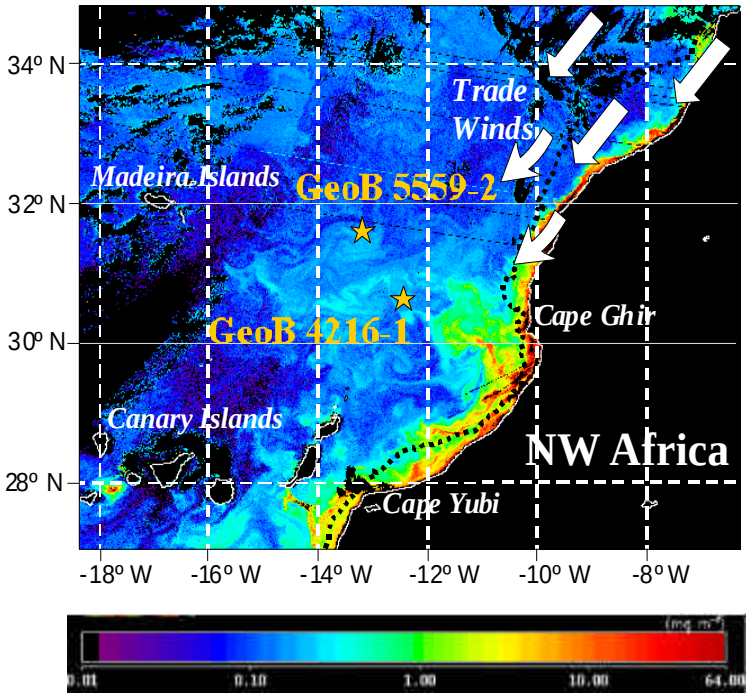

Figure 1.- Surface pigment concentration (mg m^{-3}) in the North Canary Basin as observed by SeaWiFS during an extraordinary Cape Ghir filament event on the 19th March 1998 (processed by R. Davenport). GeoB 4216-1 (30º37,8'N; 12º23,7'W; 2,324 m depth) and GeoB 5559-2 (31º38,7'N; 13º11,2'W; 3,178 m depth) core sites are marked by black stars. The shelf boundary is indicated with a black dashed line.

Figura 1.- *Concentración de pigmentos en superficie (mg m^{-3}) en la Cuenca del Norte de Canarias observada por el satélite SeaWIFs durante un extraordinario evento del filamento de aguas afloradas de Cabo Ghir el día 19 de Marzo de 1998 (imagen procesada por R. Davenport). Las localizaciones de los testigos GeoB 4216-1 (30º37,8'N; 12º23,7'W; 2.324 m depth) y GeoB 5559-2 (31º38,7'N; 13º11,2'W; 3.178 m depth) están marcadas con estrellas negras. El límite de la plataforma está indicado con una linea negra punteada.*

2.3. Methods

Opening and visual description of the sediment cores was carried out on board (see [19] for core description). Age models based on oxygen isotope stratigraphy for these cores are published [19, 20]. Mean sedimentation rates are 2.4 and 4.9 cm/kyr in cores GeoB 5559-2 and GeoB 4216-1, respectively.

2.3.1. Major and trace elements

Bulk major and trace element contents were analysed with a sample spacing of 5 cm by means of X-ray fluorescence (XRF). Samples were ground and homogenised in an agate mortar and prepared for major and trace element determination. For major element measurement, glass discs were processed by melting about 0.3 g of ground bulk sediment with a Li tetra borate flux. For trace element analysis, discs were produced by pressing about 5 g of ground bulk sediment into a briquet, with boric acid backing. Finally, XRF analyses were performed with a Philips PW

2,400 sequential wavelength dispersive X-ray spectrometer. Analytical accuracy was checked measuring international standards (GSS-1 to GSS-7) and precision was determined by replicate analyses of samples (0.8% and 4% for major and trace elements, respectively). All standard X-ray fluorescence results were corrected for the contribution and dilution effect of the sea-salt content in the dried sediment [8].

Calcium records obtained by the standard XRF technique were compared with those achieved at 1 cm interval by means of the XRF core scanner at the Geosciences Department of the University of Bremen. The central sensor unit consists of a molybdenum X-ray source (3-50kV), a Peltier-cooled PSI detector (KEVEX^{TM}) with 125 µm beryllium window and a multichannel analyser with a 20 eV spectral resolution. The system configuration (X-ray tube energy, detector sensibility) at the University of Bremen allows the analyses of elements from K (atomic nº 19) to Sr (atomic nº 38) (X-ray tube voltage: 20 kV). Each measurement took place over a 1 cm^2 area and we used 30 s count time and an X-ray current of 0.087 mA. The KEVEX software Toolbox© processes the acquired XRF spectrum for each measurement. Background substraction, sum-peak and escape-peak correction, deconvolution, and peak integration are successively applied. The resulting data are element intensities in counts per second.

Total carbonate content was calculated from the total Ca concentration using a correction for clay-derived Ca, which was established for carbonate-rich sediments:

$CaCO_3 = 2.5\ (Ca_{TOT} - (Ca/Al_{Clay}\ ?\ Al_{TOT}))$; where Ca/Al_{Clay} is 0.345 [21].

2.3.2. Organic carbon

Total carbon was analysed using a LECO CS-244 at the University of Bremen. Total Organic Carbon (TOC) was measured after removing the carbonate with 6M HCl and heating at 80?C. The loss of acid soluble organic carbon was negligible. Precision was determined by replicate analyses and it was better than 3%.

2.3.3. Diatoms

While for core GeoB 5559-2 diatoms were counted for the entire length of the core, in core GeoB 4216-1 diatoms were only studied for the two Termination intervals. Presence of diatoms was investigated by smear-slide analysis. In samples where diatoms were present, 2 cm^3 of fresh sediment were treated according to the method described in Fenner et al. [22]. Four slides were prepared from each sample using the evaporation tray method [23] and mounted with Permount medium. Diatoms were counted in three of the four prepared slides.

2.4. Results

2.4.1. Calcium carbonate

Calcium and carbonate values display the same general trends and amplitudes in both cores (Figure 2). Higher contents are recorded during the cold periods of interglacial stages and at Stage 3, and tend to correlate with lower values of summer insolation at 30ºN.

Table 1.- Correlation and phase angle of the studied proxies in cores GeoB 5559-2 and GeoB 4216-1 with respect to ETP. Maximum Ice Volume (?^{18}O) is based on the SPECMAP curve. ?^{18}O values refer to measurements in core GeoB 5559-2. Phase angle is shown for selected proxies (coherency with ETP higher than 0.6 at the 80% of confidence).

Tabla 1.- *Valores de correlación y de ángulo de fase de las proxies estudiadas en los testigos GeoB 5559-2 y GeoB 4216-1 respecto a la curva ETP. El Máximo Volumen de Hielo (?^{18}O) está basado en la curva SPECMAP. Los valores de ?^{18}O se refieren a las medidas realizadas en el testigo GeoB 5559-2. Los ángulos de fase se muestran para algunas proxies seleccionadas (las que tienen valores de coherencia con ETP mayores de 0,6 al 80% de confianza).*

Period (kyr)	SPECMAP	Ca (GeoB 5559-2)	Ca (GeoB 4216-1)	Ba_{excess}	TOC (GeoB 5559-2)	TOC (GeoB 4216-1)
Correlation						
100	0.92	0.42	0.75	0.72	0.77	0.89
41	0.86	0.60	0.74	0.48	0.46	0.75
23	0.92	0.80	0.71	0.70	0.38	0.91
Phase angle						
100	-173?10?	-	3?17?	-135?20?	-175?17?	-145?12?
41	-104?13?	68.4?27?	51?18?	-	-	-80?23?
23	-89?10?	-143?15?	162?20?	-9?21?	-	-40?11?

The cyclicity observed in the records was analysed by means of power spectra calculations (Figure 2 and Table 1). Spectral analysis and coherence with the Eccentricity-Tilt-Precession (ETP) combination curve show that both records are dominated by precession and eccentricity cyclicities. Higher values in these proxy records are found during summer insolation minima, which correspond to maxima in the precessional index (Table 1).

2.4.2. Barium excess

In order to assess the amount of barium in core GeoB 5559-2 that is present as biogenic barite, we corrected the total barium for the non-biogenic portion. In this paper, we refer to this fraction as barium excess (Ba_{excess}). As calculation of Ba_{excess} is still a matter of debate, we have compared the results from four different approaches [24-27]. Given that both barium values and trends are independent of the approach used, we selected the Ba_{excess} determined following Gingele et al. [27] calculations since this method allows to correct the barium included in carbonates, a major component in our sediments.

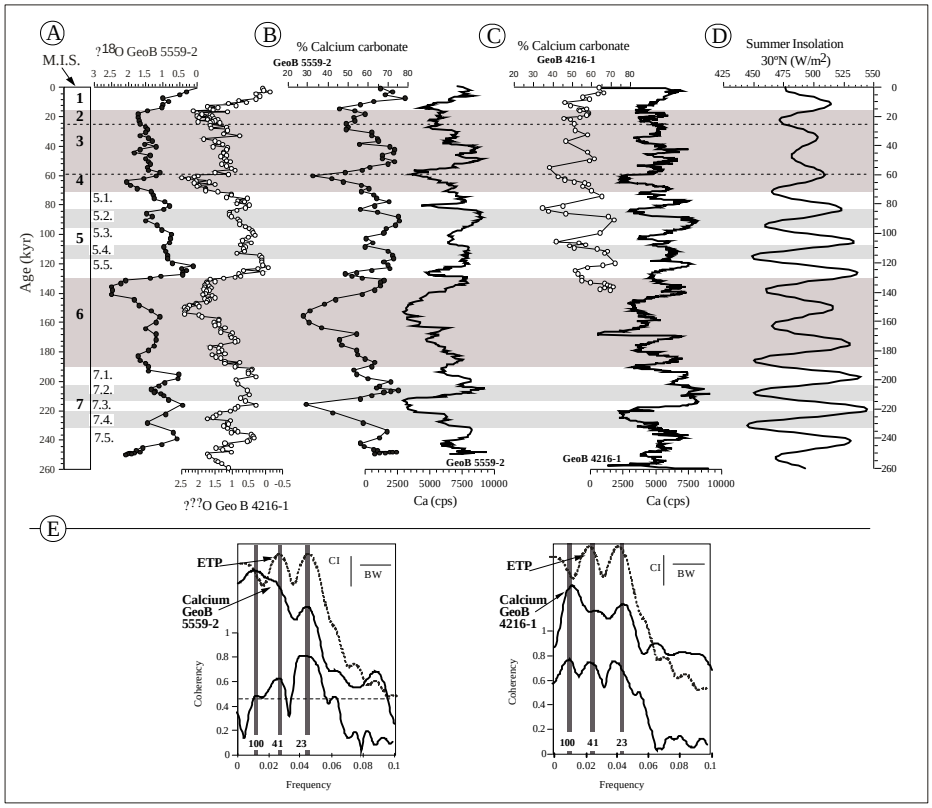

Figure 2.- (A) Oxygen isotope profiles of cores GeoB 5559-2 and GeoB 4216-1 plotted along age (kyr) axis [19, 20]. (B) Calcium carbonate (curve with symbols) and Ca-intensity from the XRF Scanner (continuous curve) in counts per second (cps), in core GeoB 5559-2 (full symbols) and (C) GeoB 4216-1 (open symbols). Glacial isotopic stages and cold substages are shaded. (D) Boreal summer insolation at 30ºN is represented for comparison. (E) Variance spectra of the previous calcium records, expressed as the logarithm of spectral power density versus frequency in cycles kyr-1 using the Blackman-Tuckey method (continuous curve) compared with the spectrum of ETP, eccentricity-tilt-precession combination curve (dashed line). The three main orbital periods of eccentricity (100 kyr), obliquity (41 kyr) and precession (23 kyr) are marked as vertical grey bands. The coherency plot (below, thicker line) indicates what frequency components are shared between the proxies and the ETP curve. An 80% confidence level is set, above which statistical significance in the coherency relationship is considered to exist (this level corresponds in this case to a coherency of 0.048). Bandwidth (BW) and 80% confidence interval (CI) are indicated with short horizontal and vertical segments, respectively.

Figura 2.- *(A) Perfiles de los isótopos de oxígeno de los testigos GeoB 5559-2 y GeoB 4216-1 representados respecto al tiempo (en miles de años) (B) Carbonato cálcico (curva con símbolos) e intensidad de Ca medida mediante el escáner de FRX (curva continua) en cuentas por segundo (cps) para los testigos GeoB 5559-2 (puntos negros) y (C) GeoB 4216-1 (puntos blancos). Los estadios isotópicos glaciales y los subestadios fríos se han sombreado. (D) Se representa la insolación de verano a 30ºN por comparación. (E) Espectros de frecuencia de la varianza de los registros previos de Calcio, expresados como el logaritmo de la densidad del poder espectral respecto a la frecuencia en ciclos de 10^{-3} usando el método de Blackman-Tuckey (curva continua) comparados con el espectro de la curva ETP, que es la combinación de los parámetros de excentricidad, oblicuidad y precesión (línea discontinua). Los tres parámetros orbitales principales de excentricidad (100.000 años), oblicuidad (41.000) y precesión (23.000) se marcan mediante líneas grises verticales. El gráfico de coherencia (abajo) indica qué frecuencias son compartidas entre las proxies y la ETP. El nivel del 80% de confianza está marcado. Por encima de dicho nivel se considera que existe una coherencia estadísticamente significativa (en este caso, corresponde con 0,048). La anchura de banda (BW) y el intervalo de confianza al 80% (CI) se indican con segmentos horizontales y verticales, respectivamente.*

Ba_{excess} estimations for core GeoB 5559-2 show a pattern marked by an increase in contents, up to three times the background values, at Terminations I, II and III (Figure 3a). Smaller peaks are also observed at 38, 60, 107 and 220 kyrs. Strong increases in the Ba/Al ratio during Terminations were also found in core GeoB 4216-1 (Kasten and Freudenthal, in preparation). In core GeoB 4216-1 Ba/Al values are higher than in core GeoB 5559-2, (i.e. 325 *versus* 180.8 at Termination I and 327.8 *versus* 211.8 at Termination II) pointing to higher productivity at site GeoB 4216-1 or/and higher degree of Barium preservation (Table 2). Ba/Al values were slightly higher in Termination II than in Termination I in both cores. The eccentricity cycle (100 kyr) dominates the spectral analysis of the Ba_{excess} record (Figure 3d). Coherence with ETP is highest at the eccentricity and precession parameters while the obliquity signal is not as significant (Table 1).

2.4.3. Total organic carbon

TOC content is low in the studied cores, ranging from 0.1% up to 0.24% in core GeoB 5559-2 and from 0.1% to 0.9% in core GeoB 4216-1 (Figures 3b and 3c). Consistent with the barium results (Table 2), highest TOC values are found at glacial-interglacial transitions in core GeoB 4216-1. However, the TOC record from site GeoB 5559-2 does not follow the Ba_{excess} trend. The spectral analysis of the TOC record does not show any significant cyclicity for core GeoB 5559-2 but reveals a clear 100-kyr and 23-kyr cyclicity in core GeoB 4216-1 (Figure 3d).

2.4.4. Diatoms

In core GeoB 5559-2 diatoms are found between 10-40 kyr while Diatom Accumulation Rate (DAR) shows three distinct peaks at 38, 28 and 18 kyr (Figure 4). One order of magnitude higher DAR is found at site GeoB 4216-1. The most common diatom is *Chaetoceros*, a genus that thrives in coastal upwelling waters.

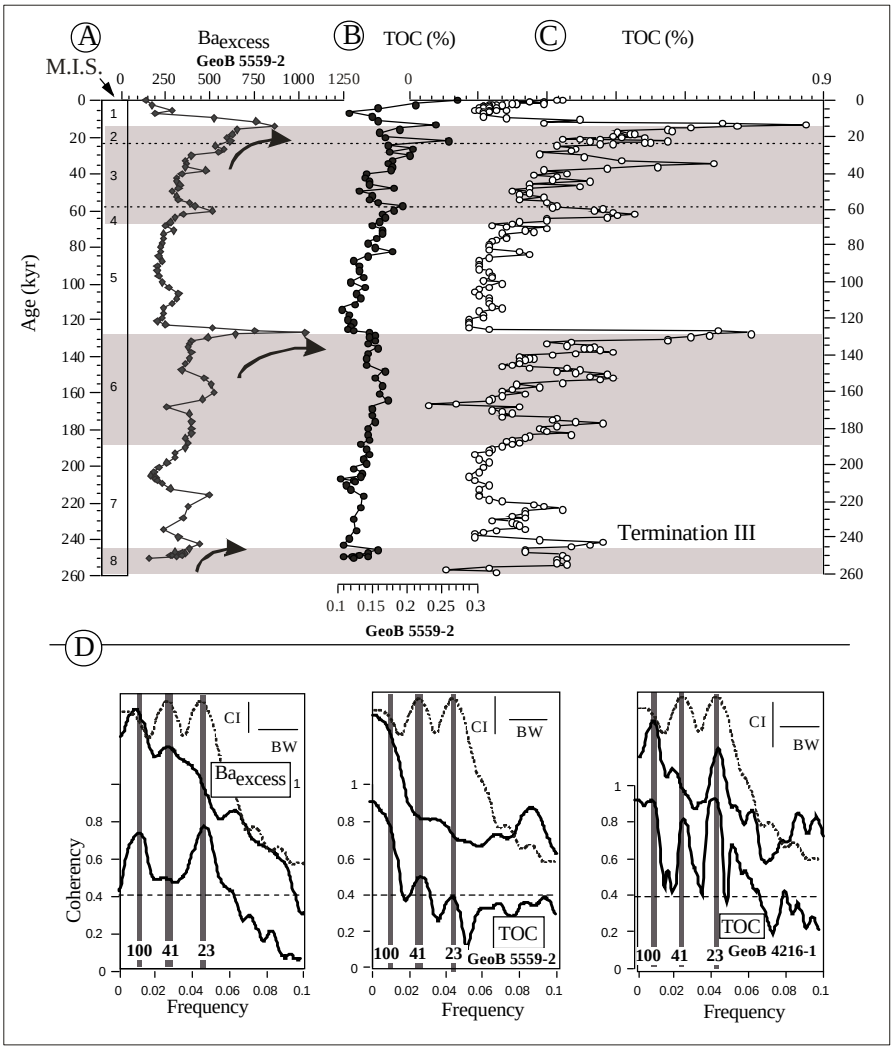

Figure 3.- (A) Ba_{excess} (ppm) record in core GeoB 5559-2 and TOC (%) records in cores GeoB 5559-2 (B) and GeoB 4216-1 (C). Note that both cores are plotted with the same horizontal scale. Glacial periods are shaded and Terminations I, II and III are indicated by arrows. (D) Variance spectra of the previous core profiles (cf. Figure 2E caption for full explanation).

Figura 3.- *(A) Registros de Ba_{exceso} (ppm) en el testigo GeoB 5559-2 y Carbono Orgánico Total (TOC) en % en los testigos GeoB 5559-2 (B) y GeoB 4216-1 (C). Nótese que los dos testigos están representados con la misma escala horizontal. Los estadios glaciales están sombreados y las terminaciones I, II y III se indican con flechas. (D) Espectro de frecuencias de la varianza de los registros anteriores (ver pie de Figura 2E para una explicación detallada).*

2.5. Discussion

2.5.1. Productivity vs. preservation

The original productivity signal might be modified by a variety of processes that include dilution by eolian dust, dissolution and diagenesis. These are considered below for the set of proxies used in the present study.

Calcium carbonate records

According to Henderiks et al. [28] dissolution should have a minor impact on carbonate variability in the NCB context and well-preserved carbonate records are expected in our cores. However, dissolution of sediment carbonate can occur even if the overlying water is saturated with respect to calcite by CO_2 release during oxic decomposition of organic matter [29]. Since carbonate values are lower during TOC peaks (Figure 2 and 3 and [20]) increased supralysoclinal dissolution could have occurred during higher TOC periods.

The lowest carbonate values are also coincident with high aluminium content and coarse grain-size [19]; therefore, dilution by an irregular supply of eolian dust should also be considered as proposed by Matthewson et al. [30] and Shimmield et al. [31] for whom dilution by aeolian dust is the dominant control on carbonate content in the NW African margin. Since our carbonate profiles mirror dust records, and after comparison with other carbonate records [30, 31] in the NW African margin, we propose that dilution by non-carbonate material is the most likely process controlling carbonate content variations in the NCB. Calculation of carbonate fluxes to avoid dilution effects has not proved to be useful in this case mainly due to the error margin inherent to the age model construction [19, 20]. As a result, we conclude that no reliable paleoproductivity signal can be inferred from the carbonate records in the two studied cores.

Barium excess record

Several studies have established a link between Ba_{excess} and high TOC contents in marine sediments underlying highly productive areas [25]. However, peaks of Ba_{excess} could result from dissolution of barite and subsequent reprecipitation as a diagenetic front under sulfate-depleted environments [32]. This would lead to the formation of Ba_{excess} peaks that are unrelated to productivity. However, according to pore water data, these conditions were not observed in this region [33]. In addition, since Ba and TOC behave differently under oxic or anoxic conditions and since their records are very similar in our cores, we therefore conclude that diagenesis had no significant effects on Ba_{excess}. Consequently, this proxy can be used as a reliable paleoproductivity indicator in the NCB.

Organic carbon records

Prior to assessing past marine carbon fluxes, the contribution of terrigenous to total organic carbon was investigated. On the basis of the C/N ratio, $?^{13}C_{org}$ and $?^{15}N$ values in cores from the NCB, Freudenthal et al. [20] concluded that marine organic matter dominates the records.

The proportion of organic matter that becomes preserved in marine sediments depends on primary production, water depth, sedimentation rate and sedimentary redox environment [34]. Differences in TOC contents in the two studied records can be attributed mainly to distinct rates of primary production at the two sites. The proximity to coastal upwelling and the fact that GeoB 4216-1 is below the direct influence of Cape Ghir upwelling filament (Figure 1) may provide a higher flux of organic matter through the water column at that site. On the contrary, GeoB 5559-2

is influenced by the upwelling filament only when it extends to the core site. The higher contents of Ba_{excess} and diatoms found in core GeoB 4216-1 support this hypothesis (Table 2).

Table 2. Comparison of Ba/Al values from GeoB 5559-2 and GeoB 4216-1 cores at Terminations I and II.

***Tabla 2**.- Comparación de los valores de Ba/Al de los testigos GeoB 5559-2 y GeoB 4216-1 en las terminaciones I y II.*

Event	Ba/Al (GeoB 4216-1)	Ba/Al (GeoB 5559-2)
Termination I	325	180.8
Termination II	327	211.8

In addition to differences in primary production, the lower sedimentation rates at site GeoB 5559-2 may contribute to reduce preservation of organic carbon by allowing a deeper oxygen penetration [34, 35]. Thus, enhanced oxidation could explain the lack of Ba_{excess} and TOC correlation in core GeoB 5559-2 at Terminations.

Kasten et al. [36] have recently proposed that in low sedimentation regimes the action of oxidation fronts induced by changes in deep-water conditions leads to a high degradation of TOC. When NADW production was restored after glacial periods aerobic degradation of the organic matter took place. These authors explain the oxidation front development in sediments of the Equatorial Atlantic Ocean in a sequence of three depositional/diagenetic stages (Figure 8 in [36]). First, there was a productivity pulse at glacial/interglacial transition indicated by the increase in Ba_{excess} and TOC. Afterwards, caused by the decreased sedimentation rates and increased oxygen concentration related to NADW production at the onset of interglacial periods, an oxidation front formed with the consequent degradation of TOC. Finally, sediments are recording the productivity event by their Ba_{excess} peak and the redistribution of redox-sensitive elements [36].

After model results, it was demonstrated that there is a correlation between sedimentation rate and TOC preservation in low sedimentation rate regimes [35]. Thus, in low sedimentation areas a higher degradation of organic matter is expected when environmental conditions change, like in a glacial/interglacial transition. The small differences of sedimentation rate between our cores could explain the lack of Ba and TOC correlation at GeoB 5559-2 core since the value of sedimentation rates above 2-3 cm/kyr seems critical in controlling TOC post-depositional oxidation [37]. Therefore, the organic carbon content initially supplied to the sediments could have been degraded at site GeoB 5559-2 by the efficient action of oxidation fronts. In contrast, the initial correlation between Ba and organic carbon in core GeoB 4216-1 still exists because the higher sedimentation rates protected the organic matter from any significant oxidation. It comes then that, while there is a good agreement between Ba_{excess} and TOC records in the relatively high sedimentation regimes, such as site GeoB 4216-1 (Kasten and Freudenthal in preparation) and the Portuguese margin [9], such a correlation is lacking in GeoB 5559-2, a low sedimentation regime.

Diatom records

Since oceans are undersaturated with respect to Si, diatoms can only be preserved in areas where surface circulation leads to significant diatom production [1]. Although the residence time in the water column or at the sediment-water interface control diatom preservation rates, the diatom abundances and assemblage composition found in the surface sediments of the NCB do reflect surface productivity conditions [18].

When compared to Ba_{excess} and TOC records, diatom maximum abundances precede these two proxies in both cores (Figure 4). This feature might be explained by any processes favouring deeper penetration of Si undersaturated waters. When surficial productivity and opal production decreased after Termination I, the Si content of sediment interstitial waters decreased concurrently, leading to opal dissolution downward. According to the estimations of Peng et al. [38] the penetration depth on these sites could reach over 8 cm in GeoB 4216-1 and 25 cm in GeoB 5559-2. The sharp and almost straight decrease of the top of the diatom record at Terminations supports this explanation. Since Ba and TOC records are not influenced by Si reduction in pore waters, the differences between the diatom, Ba_{excess} and TOC signals could be explained.

At Termination II diatoms were found only in core GeoB 4216-1. This fact could only be explained either by an enhanced primary production at this site because of the higher influence of the Cape Ghir upwelling filament, or by diatom preservation conditions. Terminations are intervals of increased meltwater discharge into the ocean. Under this scenario, the lower density of surface ocean waters would reduce NADW production. Thus, deep nutrient-rich southern ocean waters can easily spread northwards [39, 40]. However, the higher DAR recorded in the shallower core, GeoB 4216-1, from 2,324 m depth, points to primary productivity variations between the two sites, as pointed out in section 2, as the determinant factor.

We then accept Ba_{excess}, TOC and DAR records as reliable paleoproductivity proxies in the NCB and the analysis of their temporal patterns of variation must be particularly useful to infer the mechanisms that influenced paleoproductivity variations.

2.5.2. Productivity peaks at Terminations

At low latitudes paleoproductivity records are mainly dominated by the 23-kyr precession cycle [41]. In our cores, both Ba_{excess} and TOC records correlate with minima in the precessional index (Table 1). This is in agreement with the pattern of grain-size and geochemical parameters previously reported for the same cores [19, 20]. It was subsequently proposed that the Trade Wind system was stronger at times of minima in the precessional index resulting in stronger upwelling in the NCB region [19]. However, this precession-driven mechanism does not explain the large productivity peaks recorded at Terminations by Ba_{excess}, TOC and diatoms.

Several hypotheses could be then considered. The first refers to variations in NADW formation and associated penetration of southern waters to the NCB. It has been shown that

Terminations are intervals where maxima in boreal summer insolation, rapid ice-sheet melting and fast rates of sea-level rise concur. This favours both a reduction of deep water formation in the North Atlantic and a stronger northern penetration of deep nutrient-rich South Atlantic waters (AABW). However, it is improbable that this mechanism leads to stronger upwelling and higher primary production at the latitude of the NCB because deep waters are not the source of upwelling in this region [6]. Therefore, this hypothesis has to be rejected as the ultimate cause for paleoproductivity peaks at Terminations in the NCB.

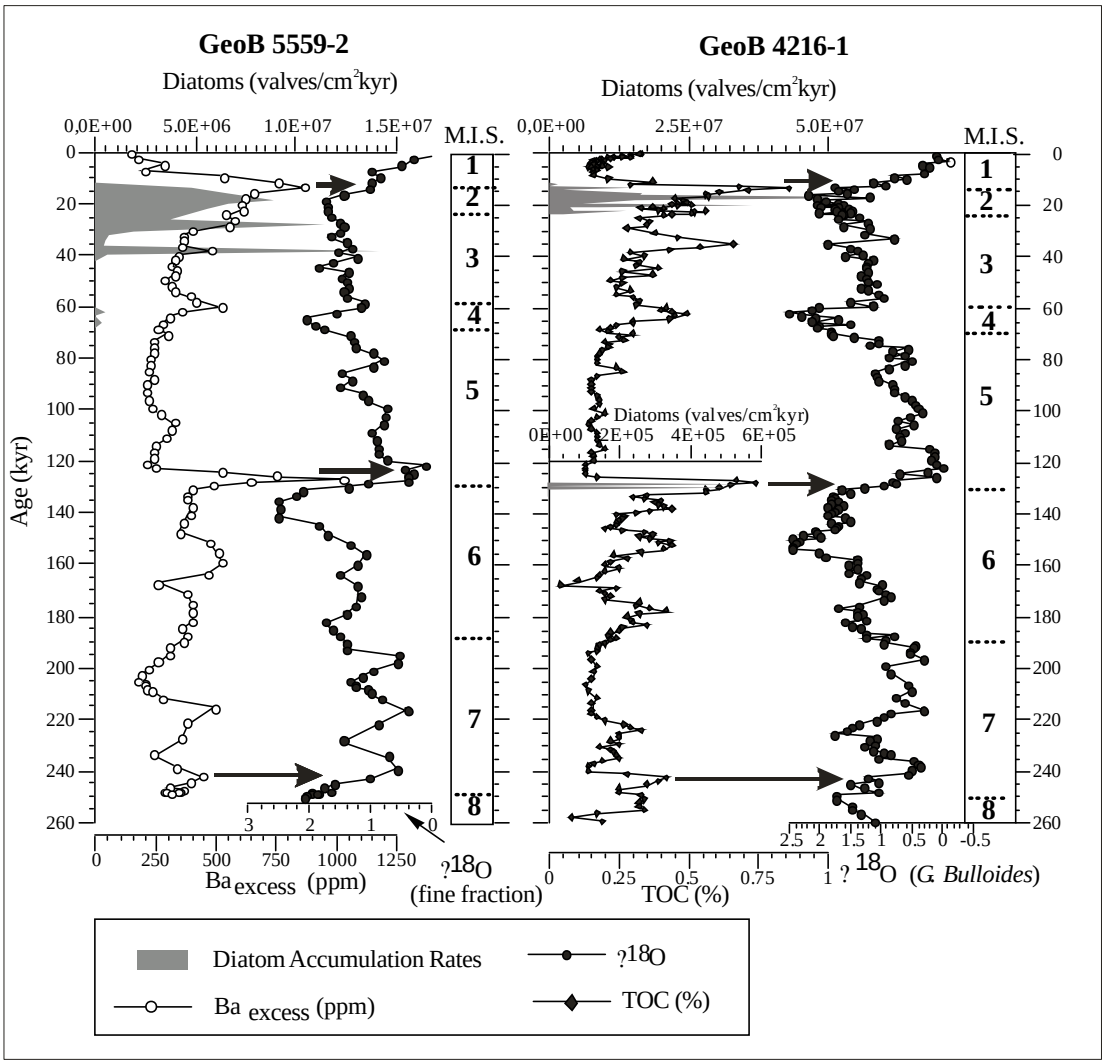

Figure 4.- Diatom Accumulation Rates (DAR), and oxygen isotope records in cores GeoB5559-2 and GeoB 4216-1. A different x-scale for DAR at Termination II in core GeoB 4216-1 is used. Ba_{excess} (ppm) and TOC (%) are plotted for comparison. Terminations are indicated with arrows.

Figura 4.- *Registros de las tasas de acumulación de diatomeas (DAR) y de los isótopos de oxígeno para los testigos GeoB 5559-2 y GeoB 4216-1. Para la DAR en la terminación II del testigo GeoB 4216-1 se usa una escala horizontal diferente. Los perfiles de* Ba_{exceso} *(ppm) y TOC (%) se muestran para comparación. Las terminaciones se indican con flechas.*

An alternative second hypothesis could be the varying influence of the Cape Ghir upwelling filament as modulated not only by Trade wind strength but also by subaerial/submarine topography and sea level. Since higher rates of sea-level rise occur at Terminations, the change in subaerial *versus* submarine topography might have been the main factor influencing in the remarkable development of the upwelling filament. However, such an explanation, which can be acceptable for local settings and coastal areas, cannot account for similar productivity records observed in far distant areas, such as the open Equatorial Atlantic Ocean [36].

A third and final hypothesis results from the combination of oceanographic and atmospheric mechanisms. Southward advection of cold surface water by the intermediation of the CC was suggested as the main pathway to transfer the high-latitude climate signal to the eastern tropical Atlantic [42]. This water mass would bring nutrients and may then increase productivity all along the NW African margin. Some authors suggested that the re-establishment of the CC system could cause the higher productivity events recorded at Terminations [9, 43]. This reasoning deserves attention when trying to explain the productivity peaks found in GeoB 5559-2 and GeoB 4216-1. Overpeck et al. [44] proposed, and tested using General Circulation Models, that the lowering of North Atlantic SST by glacial melt water releases during deglaciation strengthened the North Atlantic high-pressure system, thus favouring the enhancement of Trade Wind velocities. This ocean-wind system connection can be explained taking into account the higher thermal difference between land and sea that was reached during Terminations. This temperature contrast may modulate the Azores high pressure intensity leading to an enhancement of the Trade wind system. This hypothesis of a coupled tropical/high latitude North Atlantic climate system operating during the last deglaciation is, in addition, supported by records from various tropical records [45-47]. Therefore, high-latitude low SST anomalies at Terminations can enhance Trade Winds and thereby explain productivity events observed in the areas located under their influence.

A similar hypothesis of stronger winds at Termination has been invoked to explain the increments of *Pinus* and pollen from dry and steppe-type formations at the 2/1 oxygen isotope transition found off Northwest Africa [48, 49] and would also account for the grain-size increases at Terminations I, II and III observed in the studied cores [19]. Scanning electron microscope (SEM) observation of grains from Termination I samples shows rounded edges and impact marks in the particles surface (Figure 5), features which are common in wind-borne particles [50]. The large size of these particles (up to 600 ?m) further strengthens the hypothesis of stronger Trade Winds at Terminations.

2.6. Conclusions

Carbonate, Ba_{excess}, TOC and diatom records were produced for two NCB sediment cores in order to infer paleoproductivity variations over the last 250 kyr. After comparison with previously studied dust records [19], we conclude that calcium carbonate records are affected by dilution. In contrast, Ba_{excess}, TOC and diatom records appear as reliable indicators of paleoproductivity changes. The precessional signal found in these proxies can be related to Trade Wind variations as a response to insolation changes in tropical latitudes over the last 250 kyr. During times of maximum summer boreal insolation (minima in the precessional index) Trade Winds were more intense, enhancing water column mixing and therefore, primary productivity in the NCB.

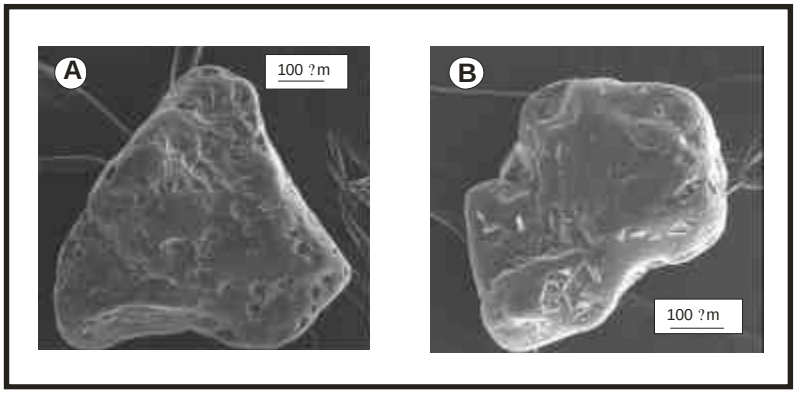

Figure 5. Scanning electron microscopy (SEM) microphotographs of eolian particles from sediments located at 28 cm depth (Termination I) in core GeoB 5559-2. Note their rounded edges and the signals of eolian impacts. (A) Dolomite, (B) Quartz.

Figura 5.- *Fotografías de partículas eólicas tomadas mediante Microscopía Electrónica de Barrido en la muestra localizada a 28 cm de profundidad (terminación I) en el testigo GeoB 5559-2. Se observan los límites redondeados y marcas de los impactos eólicos. (A) Dolomita; (B) Cuarzo.*

Large peaks of Ba_{excess}, TOC and diatoms at Terminations I, II and III suggest the operation of an additional non precessional-driven mechanism. We hypothesize that the large increase in primary productivity found at Terminations results from the intensification of the Trade Wind system. This enhancement of the atmospheric circulation is related to high-latitude processes occurring during deglaciation, that is, lowering of the North Atlantic SST by melt water discharges which in turn induced the strengthening of the Azores high-pressure centre and increased Trade Wind velocities. This mechanism may also explain the reinforcement of the coastal upwelling and associated filaments, and the productivity pulses recorded at Terminations. Additionally, the CC plays a role in transmitting cold melt-waters and nutrients from higher latitudes to the NCB.

Acknowledgements

We gratefully acknowledge the officers and crew of the R/V Meteor for technical support during the CANIGO cruises (December 1996 and October 1998) and the Scientific-Technical Services (SCT) of the University of Barcelona for their help in laboratory analyses. We thank R. Davenport for processing SeaWiFS data that were supplied by the SeaWiFS Project and the Distributed Active Archive Center, Goddard Space Flight Center, Greenbelt, MD, USA, and Isabel Cacho (University of Barcelona) and Sabine Kasten (University of Bremen) for their useful comments to an earlier version of the manuscript. We thank three anonymous reviewers who commented on a previous draft of the manuscript. The present study was supported by the CANIGO project (MAS3-CT9-0060) and a Comissionat d'Universitats i Recerca fellowship (Ana Moreno). HK acknowledges funding from "Deutsche Forschugsgemeinschaft (DF, Grant We 922/31-1). GRC Geociències Marines is funded by "Generalitat de Catalunya" through its excellency research groups programme (ref. 1999 SGR-63).

2.7. References

[1] W.S. Broecker and T.H. Peng, Tracers in the sea, Eldigio Press, 1982, 690 pp.

[2] W.S. Broecker and G.M. Henderson, The sequence of events surrounding Termination II and their implications for the cause of glacial-interglacial CO_2 changes, Paleoceanography 13(4), (1998) 352-364.

[3] W.H. Berger, V. Smetacek and G. Wefer, Productivity of the ocean: present and past, John Wiley and sons, Chichester, 1989, 471 pp.

[4] L. Nykjaer and L. Van Camp, Seasonal and interannual variability of coastal upwelling along northwest Africa and Portugal from 1981 to 1991, J. Geophys. Res. 99(C7), (1994) 14.197-14.207.

[5] E. Mittelstaedt, The upwelling area off northwest Africa - a description of phenomena related to coastal upwelling, Prog. Oceanogr 12, (1983) 307-331.

[6] M. Sarnthein, J. Thiede, U. Pflaumann, H. Erlenkeuser, D. Fütterer, B. Koopmann, H. Lange and E. Seibold, Atmospheric and oceanic circulation patterns off Northwest Africa during the past 25 million years, in: U. Rad, I. Hinz, M. Sarnthein and E. Scibold, (Eds.), Geology of the Northwest Africa continental margin, Springer-Verlag, New York, 1982, pp. 547-604.

[7] P. Bertrand, G.B. Shimmield, P. Martinez, F.E. Grousset, F. Jorissen, M. Paterne, C. Pujol, I. Bouloubassi, P. Buat-Menard, J.-P. Peypouquet, L. Beaufort, M.-A. Sicre, E. Lallier-Verges, J.M. Foster and Y. Ternois, The glacial ocean productivity hypothesis: the importance of regional temporal and spatial studies, Mar. Geol. 130, (1996) 1-9.

[8] P. Martinez, P. Bertrand, G.B. Shimmield, K. Cochrane, F. Jorissen, J.M. Foster and M. Dignan, Upwelling intensity and ocean productivity changes off Cape Blanc (northwest Africa) during the last 70.000 years: geochemical and micropalaeontological evidence, Mar. Geol. 158, (1999) 57-74.

[9] J. Thomson, S. Nixon, C. Summerhayes, E.J. Rohling, J. Schönfeld, R. Zahn, P. Grootes, F. Abrantes, L. Gaspar and S. Vaqueiro, Enhanced productivity on the Iberian margin during glacial/interglacial transitions revealed by barium and diatoms, J. Geol. Soc. London 157, (2000) 667-677.

[10] Chiapello, G. Bergametti and B. Chatenet, Origins of African dust transported over the northeastern tropical Atlantic, J. Geophys. Res. 102(D12), (1997) 13.701-13.709.

[11] L. Van Camp, L. Nykjaer, E. Mittelstaedt and P. Schlittenhardt, Upwelling and boundary circulation off Northwest Africa as depicted by infrared and visible satellite observations, Prog. Oceanogr 26, (1991) 357-402.

[12] R. Davenport, S. Neuer, A. Hernández-Guerra, M.J. Ruedas, O. Llinas, G. Fischer and G. Wefer, Seasonal and interannual pigment concentration in the Canary Islands region from CZCS data and comparison with observations from the ESTOC, Int. J. Rem. Sens. 20(7), (1999) 1419-1433.

[13] E. Hagen, C. Zülicke and R. Feistel, Near-surface structures in the Cape Ghir filament off Morocco, Oceanol. Acta 19(6), (1996) 577-597.

[14] J. Johnson and I. Stevens, A fine resolution model of the eastern North Atlantic between the Azores, the Canary Islands and the Gibraltar Strait, Deep Sea Res. 47, (2000) 875-899.

[15] S. Neuer, V. Ratmeyer, R. Davenport, G. Fischer and G. Wefer, Deep water particle flux in the Canary Island region: a seasonal trends in relation to long-term satellite derived pigment data and lateral sources, Deep Sea Research I 44(8), (1997) 1451-1466.

[16] C. Sprengel, K.-H. Baumann and S. Neuer, Seasonal and interannual variation of coccolithophore fluxes and species composition in sediment traps north of Gran Canaria (29ºN 15ºW), Mar. Micropal. 39, (2000) 157-178.

[17] H. Meggers, T. Freudenthal, S. Nave, J. Targarona, F. Abrantes, P. Helmke, R. Davenport and G. Wefer, Assessment of geochemical and micropaleontological sedimentary parameters as proxies of surface water properties in the Canary Islands region, Deep Sea Research II (CANIGO Special Issue) in press, (2002).

[18] S. Nave, P. Freitas and F. Abrantes, Coastal upwelling in the Canary Island region: spatial variability reflected by the surface sediment diatom record, Mar. Micropal. 42(1-2), (2001) 1-23.

[19] Moreno, J. Targarona, J. Henderiks, M. Canals, T. Freudenthal and H. Meggers, Orbital forcing of dust supply to the North Canary Basin over the last 250 kyrs, Quat. Sci. Rev. 20, (2001) 1327-1339.

[20] T. Freudenthal, H. Meggers, J. Henderiks, H. Kuhlmann, A. Moreno and G. Wefer, Upwelling instensity and filament activity off Morocco during the last 250,000 years, Deep Sea Research II (CANIGO Special Issue) in press, (2002).

[21] G.B. Shimmield and R. Mowbray, The inorganic geochemical record of the northwest Arabian Sea: a history of productivity variation over the last 400 kyr from sites 722 and 724, in: W. Prell and N. Niitsuma, (Eds.), Proceedings of the Ocean Drilling Program, Scientific Results 117, 1991, pp. 409-420.

[22] J. Fenner, Diatoms in the Eocene and Oligocene sediments off NW Africa, their stratigraphic and paleogeographic occurrences, University of Kiel, 1982.

[23] R. Batterbee, A new method for estimating absolute microfossil numbers with special reference to diatoms, Limn. Oceanog. 18, (1973) 647-653.

[24] H.J. Rutsch, A. Mangini, G. Bonani, B. Dittrich-Hannen, P.W. Kubik, M. Suter and M. Segl, ^{10}Be and Ba concentrations in West African sediments trace productivity in the past, Earth Planet. Sci. Lett. 133, (1995) 129-143.

[25] J. Dymond, E. Suess and M. Lyle, Barium in deep-sea sediment: a geochemical proxy for paleoproductivity, Paleoceanography 7(2), (1992) 163-181.

[26] R. Schneider, B. Price, P. Müller, D. Kroon and I. Alexander, Monsoon related variations in Zaire (Congo) sediment load and influence of fluvial silicate supply on marine productivity in the east equatorial Atlantic during the last 200.000 years, Paleoceanography 12(3), (1997) 463-481.

[27] F. Gingele and A. Dahmke, Discrete barite particles and barium as tracers of paleoproductivity in South Atlantic sediments, Paleoceanography 9(1), (1994) 151-168.

[28] J. Henderiks, T. Freudenthal, H. Meggers, S. Nave, F. Abrantes, J. Bollmann and H.R. Thierstein, Glacial-interglacial variability of particle accumulation in the Canary Basin: a time-slice approach, Deep Sea Research II (CANIGO Special Issue) in press, (2002).

[29] G. Reichart, M. den Dulk, H.J. Visser, C.H. van der Weijden and W.J. Zachariasse, A 225 kyr record of dust supply, paleoproductivity and the oxygen minimum zone from the Murray Ridge (northern Arabian Sea)., Palaeogeogr., Palaeoclimatol., Palaeocol. 134,

(1997) 149-169.

[30] A.P. Matthewson, G.B. Shimmield, D. Kroon and A.E. Fallick, A 300 kyr high-resolution aridity record of the North African continent, Paleoceanography 10(3), (1995) 677-692.

[31] G.B. Shimmield, Can sediment geochemistry record changes in coastal upwelling palaeoproductivity? Evidence from northwest Africa and the Arabian Sea, in: C.P. Summerhayes, W.L. Prell and K.C. Emeis, (Eds.), Upwelling systems: evolution since the early Miocene, Geological Society, Special Publication, 64, London, 1992, pp.

[32] S.J. Schenau, M.A. Prins, G.J. De Lange and C. Monnin, Barium accumulation in the Arabian Sea: controls on barite preservation in marine sediments, Geochim. Cosmochim. Acta 65(10), (2001) 1545-1556.

[33] G. Wefer and cruise participants, Report and preliminary results of METEOR-Cruise M 37/1, Lisbon-Las Palmas, 04.12.-23.12.1996, Berichte, Fachbereich Geowissenschaften, Universität Bremen, Bremen, 1997, 79 pp.

[34] C. Rühlemann, P. Müller and R. Schneider, Organic carbon and carbonate as paleoproductivity proxies: examples from high and low productivity areas of the tropical Atlantic, in: G. Fischer and G. Wefer, (Eds.), Use of proxies in Paleoceanography: examples from the South Atlantic, Springer-Verlag, Berlin, 1999, pp. 1-31.

[35] R.V. Tyson, Sedimentation rate, dilution, preservation and total organic carbon: some results of a modelling study, Org. Geoch. 32, (2001) 333-339.

[36] S. Kasten, R. Haese, M. Zabel, C. Rühlemann and H. Schulz, Barium peaks at glacial terminations in sediments of the equatorial Atlantic Ocean - relicts of deglacial productivity pulses?, Chem. Geol. 175, (2001) 635-651.

[37] M. Jung, J. Ilmberger, A. Mangini and K.C. Emeis, Why some Mediterranean sapropels survived burn-down (and others did not), Mar. Geol. 141, (1997) 51-60.

[38] T.H. Peng, W.S. Broecker, G. Kipphut and N.J. Shackleton, Benthic mixing in deep sea cores as determined by ^{14}C dating and its implications regarding climate stratigraphy and the fate of fossil fuel CO2, in: N. Andersen and A. Malahoff, (Eds.), The fate of fossil fuel CO_2 in the ocean, Plenum, New York, 1977, pp.

[39] J. Adkins, E. Boyle, L. Keigwin and E. Cortijo, Variability of the North Atlantic thermohaline circulation during the last interglacial period, Nature 390, (1997) 154-156.

[40] Lototskaya and G.M. Ganssen, The structure of Termination II (penultimate deglaciation and Eemian) in the North Atlantic, Quat. Sci. Rev. 18, (1999) 1641-1654.

[41] L. Beaufort, Y. Lancelot, P. Camberlin, O. Cayre, E. Vincent, F.C. Bassinot and L. Labeyrie, Insolation cycles as a major control of equatorial Indian ocean primary production, Science 278, (1997) 1451-1454.

[42] M. Zhao, N.A.S. Beveridge, N.J. Shackleton, M. Sarnthein and G. Eglinton, Molecular stratigraphy of cores off northwest Africa: sea surface temperature history over the last 80 ka, Paleoceanography 10(3), (1995) 661-675.

[43] P.G. Harris, M. Zhao, A. Rosell-Mele, R. Tiedemann, M. Sarnthein and J.R. Maxwell, Chlorin accumulation rate as a proxy for Quaternary marine primary productivity, Nature 383, (1996) 63-65.

[44] J.T. Overpeck, L.C. Peterson, N. Kipp, J. Imbrie and D. Rind, Climate change in the circum-north Atlantic region during the last deglaciation, Nature 338, (1989) 553-557.

[45] K.A. Hughen, J.T. Overpeck, L.C. Peterson and S. Trumbore, Rapid climate changes in the tropical Atlantic region during the last deglaciation, Nature 380, (1996) 51-54.

[46] F.A. Street-Perrot and R.A. Perrot, Abrupt climate fluctuations in the tropics: the influence of Atlantic Ocean circulation, Nature 343, (1990) 607-612.

[47] P. deMenocal, J. Ortiz, T.P. Guilderson and M. Sarnthein, Coherent high- and low-latitude climate variability during the Holocene warm period, Science 288, (2000) 2198-2202.

[48] A.M. Lézine and M. Denèfle, Enhanced anticyclonic circulation in the eastern North Atlantic during cold intervals of the last deglaciation inferred from deep-sea pollen records, Geology 25(2), (1997) 119-122.

[49] F. Marret and J.L. Turon, Paleohydrology and paleoclimatology off Northwest Africa during the last glacial-interglacial transition and the Holocene: Palynological evidences, Mar. Geol. 118, (1994) 107-117.

[50] K. Pye, Aeolian dust and dust deposits, Academic Press, London, 1987, 330 pp.

ARTÍCULO 3

Saharan dust transport and high-latitude glacial climatic variability: the Alboran Sea record

Ana Moreno[1], Isabel Cacho[1,2,§], Miquel Canals[1*], Maarten A. Prins[3], María-Fernanda Sánchez-Goñi[4], Joan O. Grimalt[2] and Gert Jan Weltje[5]

[1]*CRG Marine Geosciences, Department of Stratigraphy, Paleontology and Marine Geosciences, Faculty of Geology, University of Barcelona, Campus de Pedralbes, C/Marti i Franquès, s/nº, E-08028 Barcelona, Spain*

[2]*Department of Environmental Chemistry (ICER-CSIC), Jordi Girona, 18, 08034 Barcelona, Spain*

[3]*Faculty of Earth Sciences, Vrije Universiteit, De Boelelaan 1085, 1081 HV Amsterdam, The Netherlands*

[4]*EPHE, Département Géologie et Océanographie, UMR-CNRS 5805, University Bordeaux 1, France*

[5]*Department of Applied Earth Sciences, Delft University of Technology, PO Box 5028, NL-2600 GA Delft, The Netherlands*

[§]*Now at: University of Cambridge, The Godwin Laboratory, Pembroke Street, Cambridge CB2 3SA, U.K.*

En prensa en: Quaternary Research

Recibido en Diciembre 2001; Revisado y aceptado en Abril 2002

Abstract

Millennial to sub-millennial marine oscillations that are linked with the North Atlantic's Heinrich events and Dansgaard-Oeschger cycles have been reported recently from the Alboran Sea revealing a close ocean-atmosphere coupling in the Mediterranean region. We present a high-resolution record of lithogenic fraction variability along IMAGES Core MD 95-2043 from the Alboran Sea that we use to infer fluctuations of fluvial and eolian inputs to the core site during periods of rapid climate change, between 28,000-48,000 cal yr B.P. Comparison with geochemical and pollen records from the same core enables endmember compositions to be determined and to document fluctuations of fluvial and eolian inputs on millennial and faster timescales. Our data document increases in northward Saharan dust transports during periods of strengthened atmospheric circulation in high northern latitudes. From this we derive two different atmospheric scenarios which are linked with the intensity of meridional atmospheric pressure gradients in the North Atlantic region.

Keywords: Saharan dust, Dansgaard-Oeschger cycles, Heinrich Events, Mediterranean region, end-member modelling, teleconnections.

3.1. Introduction

Paleoclimatic records from a wide range of marine and terrestrial archives document rapid fluctuations during the last glacial and provide compelling evidence that the so-called Dansgaard-Oeschger (D/O) oscillations and 'Heinrich' cold events (HE) were of global significance (i.e. Leuschner and Sirocko, 2000). This millennial scale variability has been attributed to instabilities in the ocean thermohaline circulation and associated marine heat transports (Broecker, 1994; Zahn *et al*., 1997). While the driving force behind these oscillations remains unclear, evidence is mounting that sporadic meltwater injections to the Atlantic Ocean, perhaps with a stochastic component, may play a primary role in causing these ocean-climate swings (Boyle, 2000; Ganopolski and Rahmstorf, 2001).

Besides a probable ocean component, atmospheric circulation changes have also been suggested as a possible mechanism to explain the close correlation of the millennial ocean and climate signals over long distances. Indications of an intensified atmospheric circulation during cold stadial periods is contained within dust records from the Greenland ice cap (Mayewski *et al*., 1994) as well as in paleoceanographic records that document monsoonal variability (Leuschner and Sirocko, 2000; Schulz *et al*., 1998) and the Chinese loess record (An, 2000; Porter and Zhisheng, 1995). The apparent interhemispheric coupling in conjunction with the indication of rapid reorganisations of atmospheric circulation (Fuhrer *et al*., 1999) may imply a global atmospheric signal superimposed on regional climatic changes, themselves caused by thermohaline switches or ice dynamics.

In view of the increasing paleoclimatic data base and, in particular, because of their potential societal relevance it becomes increasingly important to better understand the underlying mechanisms that drove the D/O cycles and to gain better control on the timing, and potential asynchrony of these climatic oscillations between low and high latitudes (Peterson *et al*., 2000).

Because of its mid-latitude position the Mediterranean region is a key location to investigate climatic connections between high and low latitudes. In addition, its land-locked nature in conjunction with the only limited water exchange with the open ocean makes the Mediterranean Sea particularly sensitive to environmental changes. Recent studies of marine and lacustrine sediment records from the Mediterranean area have shown a strong correlation with the Greenland ice core records (Allen *et al*., 1999; Cacho *et al*., 1999; Sánchez-Goñi *et al*., 2002). For instance, the indication of rapid changes of deep-water convection in the Western Mediterranean at the pace of the North Atlantic D/O cycles has been used to infer likewise rapid changes of north-westerly winds which are the main forcing mechanism for thermohaline overturn in the region (Cacho *et al*., 2000). These studies demonstrate that Mediterranean climates and marine circulation on millennial scales were closely coupled to the North Atlantic ocean-atmosphere system.

IMAGES Core MD 95-2043 in the Alboran Sea, westernmost Mediterranean, is located at a mid-latitude position that is influenced by high-latitude and subtropical wind systems and thus provides the unique opportunity to study phase relations of millennial-scale climate variations between low and high latitudes (Figure 1). Paired records of grain-size and geochemical variability together with pollen records along this core enable temporal relations between marine and terrestrial systems to be determined without the dating uncertainties that are normally encountered in studies where such records are derived from several cores or archives. This allows a better understanding of the underlying mechanisms that drive millennial-scale climatic variability.

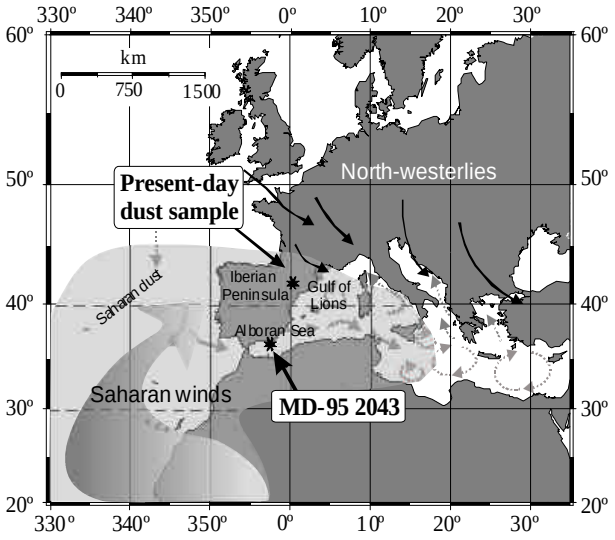

Figure 1.- Location of IMAGES core MD 95-2043 in the Alboran Sea. Black arrows indicate the mean positions of north-westerlies and thick arrow represents dust-bearing Saharan winds. Present-day oceanographic circulation is represented by dashed arrows. Also shown is the location of the station were present-day Saharan dust samples were recovered. The grey cloud represents a typical dust outbreak over the Western Mediterranean.

***Figura 1.**- Localización del testigo IMAGES MD 95-2043 en el Mar de Alborán. Las flechas negras indican la posición media de los vientos contralisios y la flecha más gruesa representa a los vientos saharianos transportando polvo de origen desértico. La circulación oceánica actual se representa mediante flechas discontinuas. También se muestra la localización de la estación donde se recuperaron muestras de polvo sahariano actual. La nube gris representa una intrusión sahariana típica sobre el Mediterráneo Occidental.*

3.2. Study area

The Mediterranean Sea acts as a concentration basin in which evaporation exceeds fresh water input through precipitation and runoff (Béthoux, 1979). The Alboran Sea constitutes the Mediterranean's westernmost basin and through the Strait of Gibraltar provides the gateway for water exchange with the Atlantic (Figure 1). Summertime climates usually are dry and hot in this region due to the influence of the atmospheric subtropical high-pressure belt (Sumner *et al*., 2001). During winter the subtropical high is shifted to the south allowing mid-latitude storms to enter the region from the open Atlantic bringing enhanced amounts of rainfall to the Mediterranean. Anomalous torrential rainfalls occur during this season in response to severe storms that are generated locally by extreme atmospheric convective overturn (Romero *et al*., 1999). Much of the present-day climate variability in this region on a decadal time-scale has been linked to a natural mode of atmospheric pressure variation, the North Atlantic Oscillation (NAO; Rodó *et al*., 1997). NAO activity is indexed as the difference between normalised winter sea-level atmospheric pressure between the Azoric high-pressure and Icelandic low-pressure cells such that a high NAO index is derived from a strong meridional pressure gradient that results in the North Atlantic depression tracks to follow a more northerly route. During low NAO index years, northwesterly winds are weaker and are guided to mid latitudes thus bringing higher precipitation to the Mediterranean and large areas of North Africa. There is increasing observational evidence for some degree of interlinking between the NAO variability and North Atlantic physical circulation so that an influence of North Atlantic thermohaline circulation on regional weather patterns cannot be ruled out (Hurrell, 1995; Dickson, 1997).

The interplay between Saharan air masses and the Azoric high pressure cell constitutes another meteorological pattern that defines Mediterranean climates. Evaluation of back trajectories and isobaric meteorological maps shows that Sahara air masses dominate the Mediterranean region whenever the Azores High is displaced westward and the North African High is strengthened and centred over Algeria (Rodriguez *et al*., 2001). The development of summer-time thermal lows over the Iberian Peninsula apparently stimulates this meteorological setting through intense heating of the land surface.

The contribution and deposition of terrigenous sediments in the Alboran Sea is closely linked with the regional meteorological patterns. Primary routes for the transportation of lithogenic particles to the Alboran Sea are through fluvial sediment transport and airborne dust. Supply of fluvial particles from the southern Iberian Peninsula is favoured by torrential local rainfalls and a scarce vegetation cover that supports surficial erosion, while fluvial sediment transport from the northern African margin seems to be negligible (Fabrés *et al*., 2002). Eolian transport of dust from the Sahara is well known as an important contributor to marine sediments and the northward and north-eastward transport of dust off North Africa seems almost as important as the dust flux into the Atlantic (Ganor and Foner, 1996). Saharan dust deposition over the Western Mediterranean has been estimated at 9-25 $t \cdot km^{-2} \cdot yr^{-1}$ which represents 10-20 % of the recent deep-sea sedimentation (Guerzoni *et al*., 1997). An eolian sedimentation rate of 23 $g \cdot m^{-2} \cdot yr^{-1}$ has been reported for continental southeastern Iberia (Díaz-Hernández and Miranda Hernández, 1997), equivalent to 12% of the lithogenic particle flux recently collected in a sediment trap experiment in the Alboran Sea (Fabrés *et al*., 2002). These results underscore the importance of eolian sediment supply as an inherent component of Alboran Sea sediments, and its value as tracer of regional climate variability during the past.

3.3. Material and methods

IMAGES Core MD 95-2043 was retrieved in 1995 in the Western Alboran Sea (36º 8.6'N; 2º 37.3'W) at a water depth of 1841 m (Figure 1). We use the age model that has been previously developed by Cacho *et al*. (1999) for this core which is derived from graphically correlating the down-core $U^{K'}_{37}$-SST record with the D/O climatic cycles displayed in the Greenland GISP2 ice core ?^{18}O record (Meese *et al*., 1997). According to this age model the records presented in this study, from 1025 to 1585 cm core depth, span the time interval from 28,000 to 48,000 cal yr B.P.

Grain-size distribution was measured at 5 cm intervals after removing organic matter from the bulk sample through oxidation with 10% H_2O_2, and leaching the carbonate fraction with an ammonium acetate solution that was buffered at a pH of 4.0. Sediment samples with and without the carbonate fraction were analysed with a Coulter LS 100 Laser Particle Size Analyser (CLS), which determines particle grain sizes between 0.4-800 ?m. CLS precision and accuracy were tested by several control runs using latex micro-spheres with a defined diameter. The high precision (reproducibility) of the measurements is demonstrated by small variations in the mean diameter (0.97% of variation) and in the standard deviation (1.37% of variation). Accuracy of the measurements as indicated by the relative departure from the nominal mean diameter is 0.30 %, corresponding to absolute deviations between 0.09-0.34 ?m. Additional test runs were performed using micro-sphere assemblages with mixed grain-sizes so as to ensure the CLS accurately determines polymodal grain-size distributions.

To aid in the interpretation of the grain-size records, we modelled end-member (EM) grain-size distributions using the down-core CLS measurements and applying the numerical-statistical algorithms developed by Weltje (1997; see also Prins and Weltje, 1999). Grain-size end-members represent a series of fixed sediment grain-size compositions that can be regarded as discrete subpopulations within the data set from all analyses. We derived grain-size end-members from data that were obtained from carbonate- and organic-fraction-free samples so as to not have our interpretations obscured by processes that are unrelated to lithogenic sediment transport and deposition.

We obtained control values for present-day eolian dust grain sizes from a sample collected by Avila (1996) during a red rainfall event (24-3-1991) at La Castanya (Montseny Mountains, 41°46'N, 2°21'E; Figure 1). The sample was filtered with Millipore 0.45-?m pore size filters, dried at 100°C, and analysed with the CLS.

Chemical analysis of the sediment samples was performed through X-ray fluorescence using a Philips PW 2,400 sequential wavelength disperse X-ray spectrometer. Prior to analysis all samples were ground and homogenised in an agate mortar. Glass discs were prepared for major element determination by fusing about 0.3 g of ground bulk sediment with a Li-tetraborate flux. Analytical accuracy was checked by measuring international standards. Precision of individual measurements was better than 0.8% as determined from replicate analyses of samples.

3.4. Results

3.4.1. Grain-size distribution

The SST record along IMAGES core MD95-2043 displays millennial-scale variability that is closely related to the Greenland ice-core D/O cycles, as has been previously reported by Cacho *et al*. (1999) (Figure 2a). The median of the two sets of samples analysed, with and without carbonate, is calculated and plotted versus age (Figures 2b,c). The median represents the grain-size distribution midpoint. The different pattern of both records prevents any common interpretation in terms of transport mechanisms. Median grain size of the carbonate-free fraction varies between 4 and 11 ?m, with maximum grain-sizes occurring during HE (Figure 2b). The correlation with the D/O cyclicity is best developed in this record in the interval between HE3 and HE4, 29-40 cal kyr B.P.

The Eolian Sortable Silt (ESS) fraction has been defined by McCave et al. (1995) as the percentage of the sediment in the 7-63 ?m size range. ESS represents the sediment fraction susceptible to be transported by wind whereas the size fraction below 7 ?m is influenced by particle scavenging through rainfall without a measurable size dependence (McCave *et al*., 1995). In our records there is no indication of a significant lithogenic component in the sand fraction, >63 µm, and thus we use the entire sediment fraction >7 ?m as representing the ESS. The results obtained show a pattern of variation similar to the previous grain-size parameters for the terrigenous fraction i.e., closest correlation with the D/O pattern in the period between HE4 and HE3 (Figure 2d).

Another grain-size parameter that we consider in this study is the sediment sorting index as defined by McManus (1988) (Figure 2e). The record reveals cyclic variations from poorly sorted sediment during colder periods to better sorting during warmer periods. Such correlation is in conflict with previously reported data that demonstrate enhanced sediment grain-size sorting during periods of increased eolian sediment contribution (i.e. Lamy *et al*., 1998).

3.4.2. Grain-size end-member model

Estimating the number of end-members

End-member modelling of grain-size distributions has been carried out to improve our interpretation of the observed grain-size variations. To estimate the minimum number of end-members required for a satisfactory approximation of our grain-size data, the coefficient of determination, r^2, was calculated. This coefficient represents the proportion of variance of each grain-size class that can be reproduced by the approximated data (Prins and Weltje, 1999; Weltje, 1997). r^2 when plotted against grain size allows for several end-member solutions to be determined (Figure 3). With the two-endmember model (r^2 mean = 0.5; Figure 3c) only the fractions between 3-5 ?m and 20-40 ?m are adequately explained (r^2 > 0.8). In the three-endmember model (r^2 mean = 0.81) the majority of grain-size fractions are well reproduced. The mean coefficient of determination increases only slightly for models with more than three end-

members. Thus, the goodness-of-fit statistics suggests that the three-end-member model provides a reasonable solution in that it also fullfills the requirement of a *minimum number of end-members* and *reproducibility* (Prins and Weltje, 1999; Weltje, 1997).

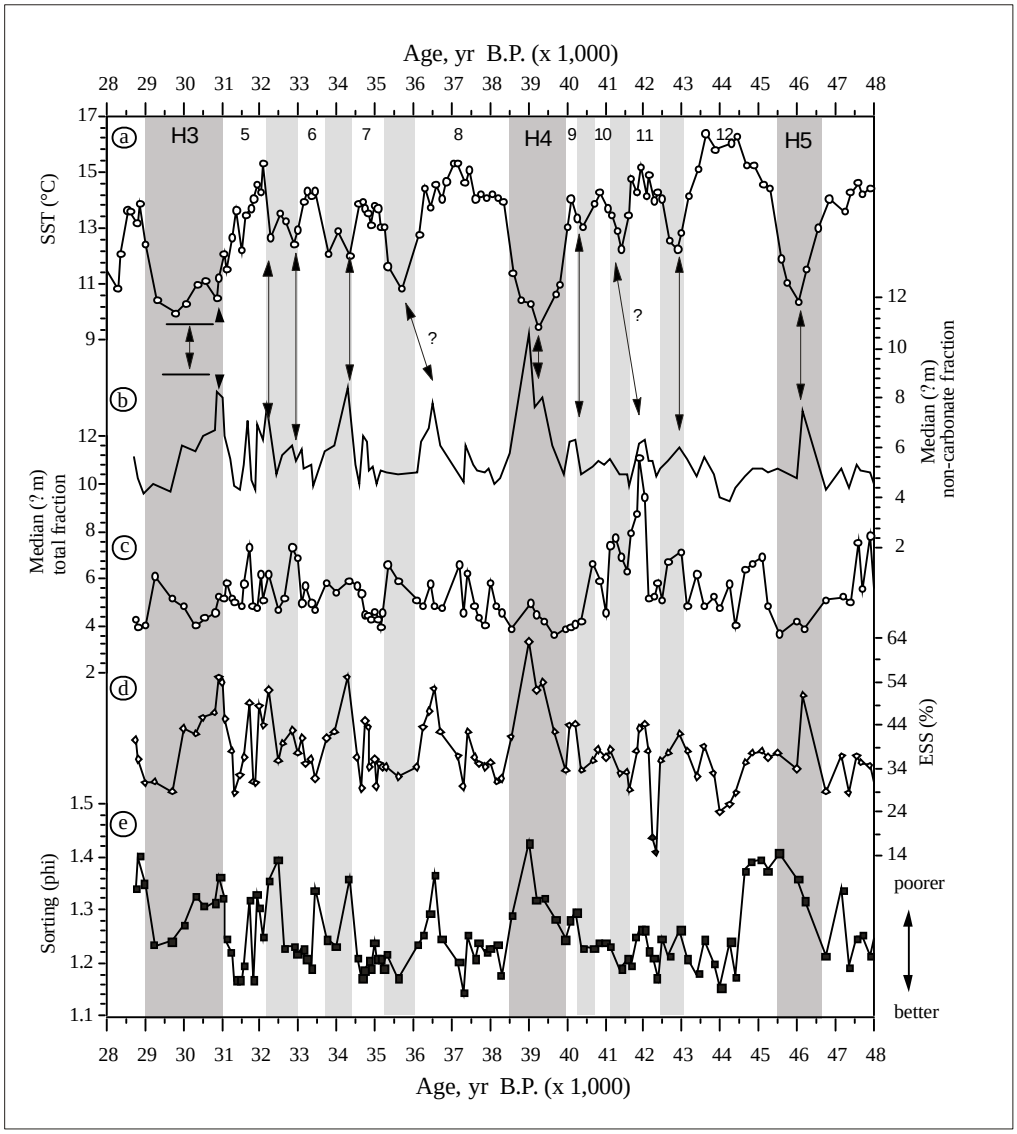

Figure 2.- Time series of (a) SST estimation based on Cacho *et al*. (1999) and grain-size parameters: (b) median (non-carbonate fraction), (c) median (total fraction), (d) "Eolian Sortable Silt" (ESS) content, and (e) sorting. HE and D/O stadial periods are indicated by shaded bars following GISP2 age model (Meese *et al*., 1997), and D/O interstadial periods are indicated by numbers. Arrows mark correlation of grain-size maxima and cold stadial periods.

Figura 2.- *Series temporales de (a) SST estimadas basándose en Cacho et al. (1999) y parámetros granulométricos: (b) mediana (fracción no carbonatada), (c) mediana (fracción total), (e) contenido de limo clasificable eólico (ESS, de sus siglas en inglés, Eolian Sortable Silt), y (e) grado de clasificación de las muestras. Los periodos de HE y los estadiales de los ciclos de D/O se indican con barras sombreadas, siguiendo el modelo de edad del testigo GISP2 (Meese et al., 1997), y los periodos interestadiales de los D/O se indican con números. Las flechas marcan la correlación entre los máximos en el tamaño de grano y los periodos fríos.*

Grain-size distribution and interpretation of end-members

The three end-members that we obtained are different such that the coarser end-members (EM1 and EM2) have a dominant mode and a well-sorted distribution whereas the mode of the finer end-member (EM3) is badly defined (from 3 to 9 ?m) which is indicative of a poorly sorted distribution (Figure 3). Interpretation of the end-members is not straightforward and needs the consideration of the most likely mechanisms that may have acted during transport and deposition of the lithogenic sediment particles, i.e. sorting by bottom currents as well as eolian and fluvial transportation processes.

Analysis of current meter data obtained in the Alboran Sea illustrates the lack of strong deep water currents in the area. According to these measurements Western Mediterranean Deep Water (WMDW) at present flows at an average of 3-4 $cm \cdot s^{-1}$, maximum flow speeds in average may reach 20 $cm \cdot s^{-1}$ (Fabrés *et al*., 2002). Following McCave *et al*. (1995) we have compared the carbonate-free grain-size record and the grain-size record of the total sediment fraction (Figure 2b,c). The very different structure of the two records excludes bottom currents as a primary sorting mechanism at the site of our sediment core during the time period considered here. We can thus safely conclude that the grain-size variations represented by the three end-members are reliable indicators of differences in origin of the terrigenous particles contributed to the core site.

Airborne dust in deep-sea sediments is generally believed to be contained in the sediment fraction >6-7 ?m (Sarnthein *et al*., 1981). We use the present-day Saharan dust grain-size distribution from the red rainfall event in 1991 (see above) as a reference for comparison with the three end-members that we infer from our down-core grain-size data (Figure 3d). The grain-size distribution of this specific Saharan dust sample is very similar to the results reported by Guerzoni *et al*. (1997) for the Mediterranean region. The mode of the sample of 10-15 ?m is very close to the mode of EM1 and quite similar to EM2. Along the core the EM2 is dominant throughout (˜ 60% average; Figure 3e). Therefore, it seems unlikely for EM2 to represent eolian dust. This interpretation can be tested by calculating the eolian flux using an average sedimentation rate of 0.034 $cm \cdot yr^{-1}$ that is implied by the age model of the core (Cacho *et al*., 1999). The resulting EM2 flux of ˜ 90 $g \cdot m^{-2} \cdot yr^{-1}$ is some four times higher than the dust flux measured by Díaz-Hernández and Miranda Hernández (1997) in southern Iberia. Therefore, EM2 is unlikely to be indicative of eolian input. EM1 much better represents the variability of eolian input as its relative contribution and flux values of 12% and 18 $g \cdot m^{-2} \cdot yr^{-1}$ respectively are in the range of modern values.

EM3, with a median size < 6 ?m, likely represents the finest sediment supplied by rivers. Irregular and intense winter precipitation events characteristic of the Alboran Sea's northern watershed, in combination with the scarce vegetation cover, mobilise large amounts of silt-sized sediments that are finally transported to and deposited in the Alboran basin. The intermediate end-member (EM2) may also result from the watershed of the Alboran Sea when rains are strong. Torrential rains could lead to the presence of coarser fluvial particles in the sediments in response to more vigorous continental runoff. Therefore, both EM2 and EM3 likely represent fluvially transported sediments, one related to the finest fraction and the other to the coarser silt particles supplied to the basin after torrential rains.

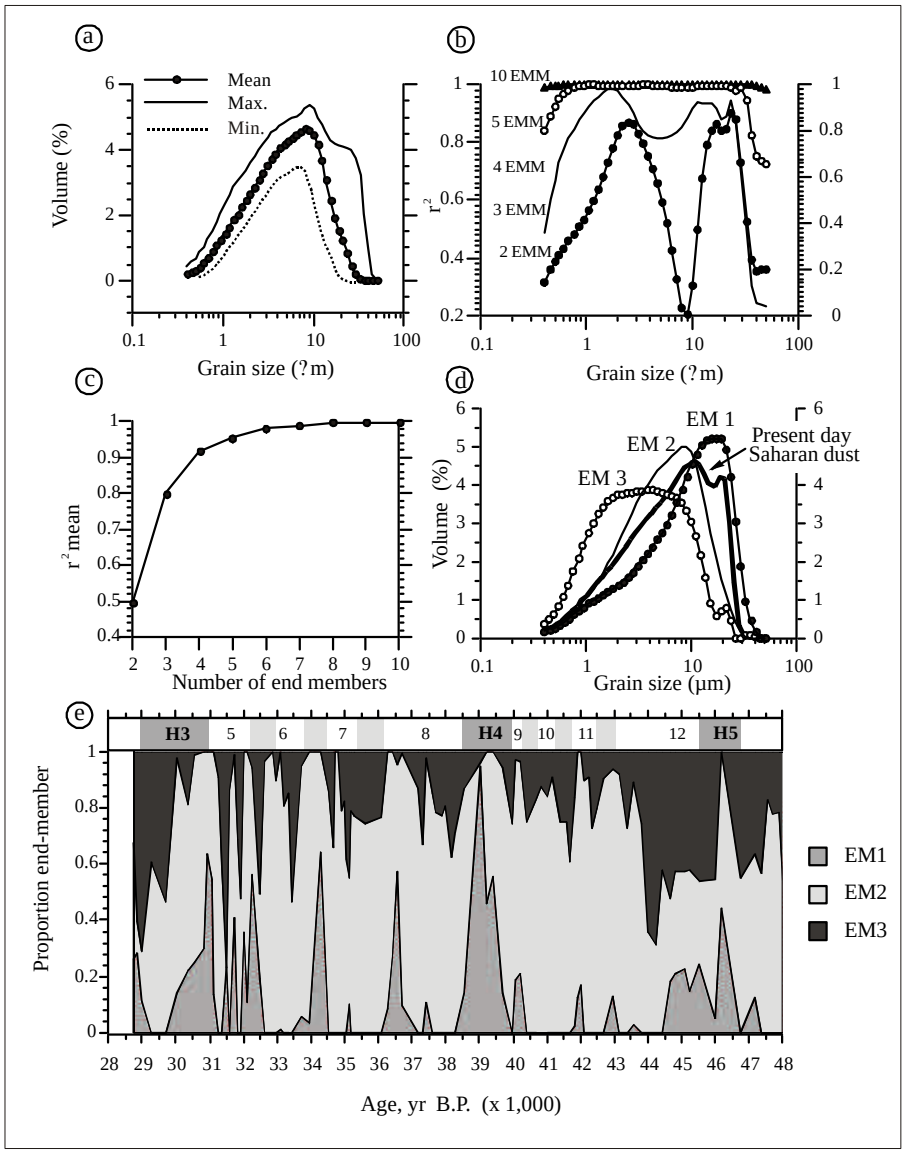

Figure 3.- End-member modelling results of grain-size data of core MD 95-2043. (a) Maximum, mean and minimum frequencies recorded in each size class; (b) coefficients of determination (r^2) plotted against grain-size for different end-member solutions (2, 3, 4, 5 and 10 EM); (c) mean coefficient of determination *versus* the number of end-members (see text for explanation); (d) grain-size distributions for the end-members of the three end-member solution. Present-day Saharan dust grain-size distribution is also shown. (e) Time series of EM1, EM2 and EM3 relative abundance.

Figura 3.- *Resultados de la modelización de los end-members de los datos granulométricos del testigo MD 95-2043. (a) Frecuencias máxima, mínima y media registras en cada clase granulométrica; (b) coeficientes de determinación (r^2) representados respecto a la granulometría obtenida para diferentes soluciones de la modelización de los end-members (EMM) (2, 3, 4, 5 y 10); (c) media del coeficiente de determinación respecto al número de end-members (ver texto para mayor explicación); (d) distribuciones granulométricas de los end-members obtenidos en la solución de 3 EM. También se muestra la distribución por tamaños de grano de una muestra de polvo de origen Sahariano actual. (e) Series temporales de la abundancia relativa de los end-members EM1, EM2 y EM3.*

Our interpretation of the three end-members is in agreement with the sorting index record (Figure 2e) in that periods with frequent eolian events are coeval with poorly sorted terrigenous sediments because of the apparent mixing between eolian and fluvial particles (clearly shown for HE4). Therefore, the down-core particle size distribution agrees well with the hypothesis of a sustained fluvial sediment input during the period 48,000-28,000 cal yr B.P. that was punctuated occasionally by pulses of enhanced eolian contributions.

3.4.3. Si/(Si+K) index for fluvial vs eolian inputs

Saharan dust is well know for its elevated quartz contents (Guieu and Thomas, 1996), thus enabling silicon (Si) abundances to be used as an indicator of dust input. Since biogenic opal contents are very low in Alboran Sea sediments (Masqué *et al*., 2002) we assume here the total Si content of the bulk sediments to represent the total terrigenous input. Fluvially delivered clays, notably illite, are potassium (K) enriched and thus we apply the Si/(Si+K) ratio as an index to assess the relation between eolian and fluvial sediment contributions. The Si/(Si+K) index is expected to be related to the mixing between the eolian and fluvial components as well as variations in the grain-size of the terrigenous material.

The Si/(Si+K) index along core MD95-2043 follows the same pattern of variation as the grain-size records in that the Si/(Si+K) maxima correlate with maximum values in the eolian end-member EM1 during the cold phases of the D/O cycles, a pattern that is particularly well developed during the time interval 28,000-40,000 cal yr B.P. (Figure 4a, b). To date there is no evidence reported of changes in the extension of the Sahara desert belt at millennial timescales. Therefore, from our data we cannot distinguish between increases of wind intensity as the ultimate cause for increased Si/(Si+K) values, or expansion and increasing proximity of Saharan dust sources during the D/O stadials. However, modelling studies consistently indicate that the changes dust deposition off Africa are primarily driven by dust transport and not so much by increased aridity in the dust source region (Mahowald *et al*., 1999). We take this as circumstantial evidence that both proxies, the EM1 and the Si/(Si+K) ratio primarily monitor changes in eolian dust transport driven by varying wind intensity.

3.5. Discussion

Past terrigenous input of lithogenic components to the Alboran Sea are the result of eolian and fluvial sediment supply. The records of both components along IMAGES Core MD-95-2043 exhibit a millennial-scale cyclicity that shows a close structural relation to D/O climatic cyclicity seen in the Greenland ice core records. Comparison of the grain-size and geochemical records from core MD95-2043 with the down-core variability of other marine and terrestrial proxies along the same core enables to investigate the timing and the mechanisms involved in these millennial climatic changes.

3.5.1. Glacial-wind regimes in the Western Mediterranean region

Abrupt changes occur within the grain size and geochemical records that suggest higher dust transports from the Saharan region to the Alboran Sea occurred during cold stadial periods of the D/O cycles (Figures 4a,b). Similar increases in dust (and salt) transport are documented in the Greenland ice records, notably the Polar Circulation Index (PCI, Figure 4c; Mayewski *et al*., 1994) which suggests an intensification of the northern hemisphere atmospheric circulation during the cold stadial phases, a contention that is further supported by coeval increases in loess deposition in Asia (An, 2000; Porter and Zhisheng, 1995) and by monsoon records (Leuschner and Sirocko, 2000; Schulz *et al*., 1998). Within the Western Mediterranean Sea, similar intensification of winter-time north-westerly winds has been inferred that resulted in an increased rate of formation of Western Mediterranean Deep Water (WMDW; Cacho *et al*., 2000; Rohling *et al*., 1998). Such changes in WMDW ventilation are particularly well documented in the down-core record of the alcohol index along core MD95-2043 (Figure 4c; Cacho *et al*. 2000). This index represents the relationship between two different molecular biomarkers (*n*-hexacosanol and *n*-noncacosane) that have the same terrestrial source but follow different pathways of degradation behaviour in the water column and sediments. Comparison of Saharan wind proxies (Figures 4a, b) with those from higher latitude wind systems (Figures 4c,e) illustrates the co-occurrence of increased wind strength during the cold phases over a wide latitudinal range. We can thus infer that both wind systems, the high-latitude north-westerlies and the low-latitude Saharan winds, display a similar pattern of variation during the last glacial period. Together with a coeval intensification of atmospheric transports over Greenland this suggests a close mechanistic linking of glacial atmospheric circulation across the latitudes.

At present, atmospheric pressure gradients over the North Atlantic region that are driving the North Atlantic Oscillation (NAO) system exert primary control on dust transports from the Saharan region with dust transports being increased during phases of increased pressure gradients (high-NAO index; Moulin *et al.* ,1997). On NAO-related time-scales, variations in Sahel rainfall over the last century are highly correlated with colder SST in the North Atlantic ocean (Folland *et al*., 1986) thus pointing to an ocean-climate teleconnection between the high and low latitudes. Similar links between North Atlantic oceanography and climatic conditions over the Sahel zone have been observed for Holocene period in paleoclimatic records. A co-existence of cold North Atlantic and warm South Atlantic SST with periods of severe drought in the Sahara zone is documented in several paleoclimatic records from continental Africa (Lamb *et al*., 1995; Street-Perrot *et al*., 2000). In addition, numerical modelling points to a close linking between cold North Atlantic SST and mean annual cooling and increased aridity in subtropical Africa (deMenocal, 1995). Cooling of North Atlantic SSTs also strengths the subtropical Atlantic high-pressure cell thus causing dust transports from the Saharan desert to be increased. Thus, a range of paleoclimatic evidence points to an increase in Sahelian aridity and meridional dust transports during periods of colder SST in the North Atlantic.

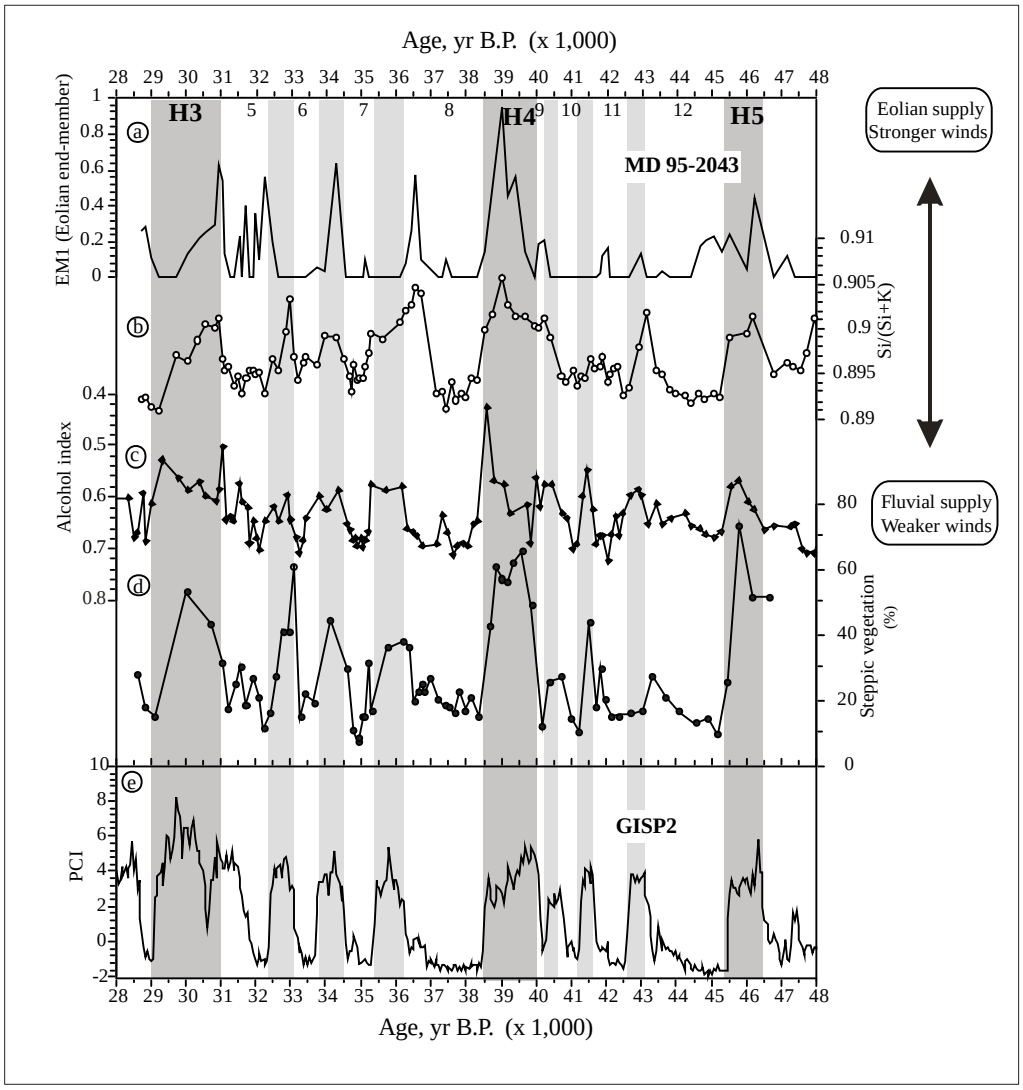

Figure 4.- MD 95-2043 time series of wind- and aridity-related proxies: (a) proportional contribution of the eolian end-member, (b) Si/(Si+K) ratio, (c) alcohol index *n*-hexacosanol/(*n*-hexacosanol+*n*-nonacosane) from Cacho *et al*., (2000), and (d) steppic vegetation abundance from Sánchez-Goñi *et al*. (2002) compared with (e) the Polar Circulation Index (PCI) calculated in GISP2 ice core (Mayewski *et al*., 1994).

Figura 4.- *Series temporales de las proxies relacionadas con la intensidad de los vientos y la aridez en el testigo MD 95-2043: (a) contribución proporcional del end-member eólico, (b) la relación Si/ (Si+K), (c) el índice alcohol n-hexacosanol/(n-hexacosanol+n-nonacosanol) de Cacho et al., (2000), y (d) abundancia de la vegetación estépica de Sánchez-Goñi et al., (2002) comparados con (e) el Índice de Circulación Polar (PCI) calculado en el testigo de hielo GISP2 (Mayewski et al., 1994).*

Our records provide compelling evidence that this cross-latitudinal teleconnection also operated during the last glacial period and that it was particularly sensitive to the D/O climatic oscillations. In fact, evidence has been presented that the decreased northward marine heat transport during HE and the cold D/O stadial periods resulted in a warming of the tropical Atlantic (Rühlemann *et al*., 1999) thereby increasing the meridional temperature gradient between the cold high-latitude and the warm tropical Atlantic. Applying the modern concepts of

atmospheric circulation and environmental controls on atmospheric pressure gradients, this should have resulted in an increased intensity of the north-westerly wind system (Schiller *et al*., 1997). The invasion of extremely cold surface waters during these periods into the Mediterranean Sea (Cacho *et al*., 1999) would have further enhanced the influence of the north-westerlies on western Mediterranean climates. These meteorological conditions would have caused both enhanced aridity (Street-Perrot *et al*., 2000) and more intense Saharan winds (Moulin *et al*., 1997) and, ultimately, increased meridional transport of Saharan dust to the Alboran Sea. The potential role of such a mechanism for driving glacial climatic variability at millennial time scales has been postulated in several studies (i.e. Sánchez-Goñi *et al*., 2002) but the details remain unclear because the influence of the large glacial ice caps over North America and Europe also play a part in modifying the atmospheric dynamics over the North Atlantic region. Nevertheless, the sedimentological and geochemical records of core MD95-2043, notably their linking with atmospheric circulation patterns, suggest that NAO-type atmospheric patterns may have caused the down-core pattern of variability of eolian sediment transports to the Alboran Sea.

3.5.2. Glacial-precipitation patterns in the Western Mediterranean Sea

Climatic conditions in the Alboran borderlands during the last glacial period have been studied previously using pollen records from core MD95-2043 (Sánchez-Goñi *et al*., 2002). Oscillations of atmospheric moisture contents between more arid and more humid conditions have been inferred from alternating dominance of steppic pollen taxa during the cold D/O stadial periods and deciduous and evergreen *Quercus* pollen during the warmer D/O interstadial periods. Arid conditions were especially extreme during the HE that constitute the most extreme cold events, as is illustrated by the maximum abundance of steppic or semi-desert vegetation pollen (*Artemisia, Chenopodiaceae, Ephedra*) (Figure 4d). These vegetation changes occurred rapidly, within 150 yr or less, and occurred in parallel with sever cooling of Alboran SST. Sánchez-Goñi *et al*. (2002) have proposed that a glacial atmospheric oscillation similar to the present-day NAO system was the primary driving force behind pluvial conditions on the Iberian Peninsula. It thus appears conceivable to infer that arid and cold climatic conditions that are documented in our records during the D/O stadial periods were caused by a rapid and prolonged change in atmospheric patterns that were similar to today's high-NAO index patterns. Such inferences are further supported by pollen records from terrestrial sequences in Italy and Greece that show a dominance of dry conditions during D/O stadial periods over the entire Mediterranean region (Allen *et al*., 1999; Tzedakis, 1999). The correlation of our proxies of wind intensity and pollen data points to southern Iberia aridity variations in association with transport intensity changes as the most viable candidates to explain the D/O variability in our record (Figure 5).

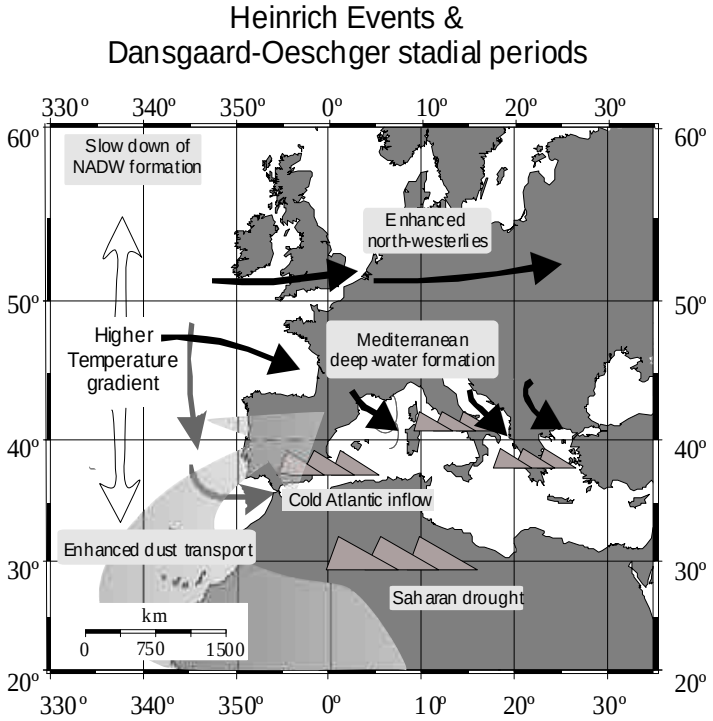

Figure 5.- Synoptic model that summarises the main processes and features that controlled the Alboran record during HE and D/O stadial periods.

Figura 5*.- Modelo sinóptico que resume los principales procesos que controlan el registro de Alboran durante los HE y los periodos estadiales de los ciclos de D/O.*

3.6. Conclusions

Geochemical records of terrigenous contributions to the Alboran Sea sediments have been established along IMAGES Core MD95-2043 to evaluate the variation of fluvial *versus* eolian inputs during the last 28,000-48,000 cal yr B.P. The records display a down-core variability that is similar in structure to the D/O climatic variability seen in the Greenland ice-core records. The data indicate an increase of Saharan wind intensity during D/O stadial periods and the Heinrich events. Existing pollen records along the same core, notably increased abundances of steppic pollen taxa indicate enhanced aridity on the southern Iberian Peninsula during these periods. This combined proxy pattern provides compelling evidence for a highly sensitive response of the low-latitude atmospheric system to the D/O climatic cycles.

We suggest that the observed proxy pattern is best explained by variability in wind systems and precipitation patterns over the Mediterranean region that was driven by rapid switches between two modes of atmosphere circulation over the North Atlantic region. In one mode atmospheric pressure gradients in the North Atlantic region were high so that north-westerly wind intensity over the Mediterranean area was increased. This mode would arise in response to decreased North Atlantic SST that was driven by a slow-down thermohaline overturn and decreased northward marine heat transport during D/O stadial periods and the Heinrich events. This would have favoured both drier conditions and more intense Saharan winds which ultimately resulted in increased meridional transport of Saharan dust. We therefore suggest that records of eolian and fluvial sediment supply that we generated for the Alboran Sea are best explained by an atmospheric pressure gradient seesaw similar to today's North Atlantic Oscillation system. This glacial atmospheric oscillator operated on a millennial time scale causing prolonged states of climate that are very similar to the much shorter periods of today's NAO extremes.

Acknowledgements

We thank Anna Avila (CREAF, Barcelona) for providing present-day aerosol samples to carry out grain-size analyses and E. Segui (XRF laboratory) and M. Guart (Sedimentological laboratory) for their help in laboratory analyses. We also thank Paul Mayewski for providing the PCI data from core GISP2. Dr. E. J. Rohling and J. R. M. Allen reviewed the manuscript and provided helpful suggestions. We are likewise grateful to Dr. R. Zahn for his discussion and help with improving the English. This study was supported by the IMAGES programme and a Comissionat d'Universitats i Recerca fellowship (Ana Moreno). I.C. also thanks funding from EC (contract: HPMF-CT-1999-00402). GRC Geociencies Marines is funded by Generalitat de Catalunya through its excellency research groups programme.

3.7. References

Allen, J. R. M., Brandt, U., Brauer, A., Hubberten, H. W., Huntley, B., Keller, J., Kraml, M., Mackensen, A., Mingram, J., Negendank, J. F. W., Nowaczyk, N. R., Oberhänsli, H., Watts, W. A., Wulf, S., and Zolitschka, B. (1999). Rapid environmental changes in southern Europe during the last glacial period. *Nature* **400,** 740-743.

An, Z. (2000). The history and variability of the East Asian paleomonsoon climate. *Quaternary Science Reviews* **19,** 171-187.

Avila, A. (1996). Time trends in the precipitation chemistry at a montane site in Northeastern Spain for the period 1983-1994. *Atmospheric Environment* **30,** 1363-1373.

Béthoux, J. P. (1979). Budgets of the Mediterranean Sea. Their dependance on the local climate and on the characteristics of the Atlantic waters. *Oceanologica Acta* **2,** 157-163.

Boyle, E. (2000). Is ocean thermohaline circulation linked to abrupt stadial/interstadial transitions? *Quaternary Science Reviews* **19,** 255-272.

Broecker, W. S. (1994). Massive iceberg discharges as triggers for global climate change. *Nature* **372,** 421-424.

Cacho, I., Grimalt, J. O., Pelejero, C., Canals, M., Sierro, F. J., Flores, J. A., and Shackleton, N. J. (1999). Dansgaard-Oeschger and Heinrich event imprints in Alboran Sea temperatures. *Paleoceanography* **14,** 698-705.

Cacho, I., Grimalt, J. O., Sierro, F. J., Shackleton, N. J., and Canals, M. (2000). Evidence for enhanced Mediterranean thermohaline circulation during rapid climatic coolings. *Earth and Planetary Science Letters* **183,** 417-429.

deMenocal, P. (1995). Plio-Pleistocene African Climate. *Science* **270,** 53-59.

Díaz-Hernández, J. L., and Miranda Hernández, J. M. (1997). Tasas de deposición de polvo atmosférico en un área semiárida del entorno Mediterráneo occidental. *Estudios Geológicos* **53,** 211-220 (In Spanish).

Dickson, B. (1997). From the Labrador Sea to global change. *Nature* **386**, 649-650.

Ditlevsen, P. D., Svensmark, H., and Johnsen, S. J. (1996). Contrasting atmospheric and climate dynamics of the last-glacial and Holocene periods. *Nature* **379,** 810-812.

Fabrés, J., Calafat, A., Sánchez-Vidal, A., Canals, M., and Heussner, S. (2002). Composition and spatio-temporal variability of particle fluxes in the Western Alboran Gyre, Mediterranean Sea. *Journal of Marine Systems,* **33-34,** 431-456.

Folland, C. K., Palmer, T. N., and Parker, D. E. (1986). Sahel rainfall and worlwide sea temperatures, 1901-85. *Nature* **320,** 602-607.

Fuhrer, K., Wolff, E. W., and Johnsen, S. J. (1999). Timescales for dust variability in the Greenland Ice Core Project (GRIP) ice core in the last 100,000 years. *Journal of Geophysical Research* **104,** 31,043-31,052.

Ganopolski, A., and Rahmstorf, E. (2001). Rapid changes of glacial climate simulated in a coupled climate model. *Nature* **409**, 153-158.

Ganor, E., and Foner, H. A. (1996). The mineralogical and chemical properties and the behaviour of aeolian Saharan dust over Israel. *In* "The impact of desert dust across the Mediterranean." (S. Guerzoni, and R. Chester, Eds.), pp. 163-172. Kluwer Academic Publishers, The Netherlands.

Guerzoni, S., Molinaroli, E., and Chester, R. (1997). Saharan dust inputs to the western Mediterranean Sea: depositional patterns, geochemistry and sedimentological implications. *Deep Sea Research II* **44,** 631-654.

Guieu, C., and Thomas, J. (1996). Saharan aerosols: from the soil to the ocean. *In* "The impact of desert dust across the Mediterranean." (S. Guerzoni, and R. Chester, Eds.), pp. 207-216. Kluwer Academic Publishers.

Hurrell, J. W. (1995). Decadal trends in the North Atlantic Oscillation: regional temperatures and precipitation. *Science* **269,** 676-679.

Lamb, H., Gasse, F., Benkaddour, A., El Hamoutl, N., Van der Kaars, S., Perkins, W. T., Pearce, N. J., and Roberts, C. N. (1995). Relation between century-scale Holocene arid intervals in tropical and temperate zones. *Nature* **373,** 134-137.

Lamy, F., Hebbeln, D., and Wefer, G. (1998). Late Quaternary precessional cycles of terrigenous sediment input off the Norte Chico, Chile (27.5S) and palaeoclimatic implications. *Palaeogeography, Palaeoclimatology, Palaeoecology* **141,** 233-251.

Leuschner, D. C., and Sirocko, F. (2000). The low-latitude monsoon climate during Dansgaard-Oeschger cycles and Heinrich Events. *Quaternary Science Reviews* **19,** 243-254.

Mahowald, N., Kohfeld, K., Hansson, M., Balkanski, Y., Harrison, S. P., Prentice, I. C., Schulz, M., and Rodhe, H. (1999). Dust sources and deposition during the last glacial maximum and current climate: a comparison of model results with paleodata from ice cores and marine sediments. *Journal of Geophysical Research* **104,** 15,895-15,916.

Masqué, P., Fabrés, J., Calafat, A., Sánchez-Cabeza, J. A., Sánchez-Vidal, A., Bruach, J. M., Cacho, I., and Canals, M. (2002). Sediment accumulation rates and main sedimentologycal patterns of recent sediments (100 y) from the Alboran Sea. *Marine Geology***, in press.**

Mayewski, P. A., Meeker, L. D., Whitlow, S., Twickler, M. S., Morrison, M. C., Bloomfield, P., Bond, G., Alley, R. B., Gow, A. J., Grootes, P., Meese, D. A., Ram, M., Taylor, K. C., and Wumkes, W. (1994). Changes in atmospheric circulation and ocean ice cover over the North Atlantic during the last 41.000 years. *Science* **263,** 1747-1751.

McCave, I. N., Manighetti, B., and Robinson, S. G. (1995). Sortable silt and fine sediment size/composition slicing: parameters for palaeocurrent speed and palaeoceanography. *Paleoceanography* **10,** 593-610.

McManus, J. (1988). Grain size determination and interpretation. *In* "Techniques in sedimentology." (M. E. Tucker, Ed.), pp. 63-85. Blackwell, Oxford.

Meese, D. A., Gow, A. J., Alley, R. B., Zielinski, G. A., Grootes, P., Ram, M., Taylor, K. C., Mayewski, P. A., and Bolzan, J. F. (1997). The Greenland Ice Sheet Project 2 depth-age scale: Methods and results. *Journal of Geophysical Research* **102,** 26411-26423.

Moulin, C., Lambert, C. E., Dulac, F., and Dayan, U. (1997). Control of atmospheric export of dust from North Africa by the North Atlantic Oscillation. *Nature* **387,** 691-694.

Peterson, L. C., Haug, G. H., Hughen, K. A., and Röhl, U. (2000). Rapid changes in the hydrologic cycle of the tropical Atlantic during the Last Glacial. *Science* **290,** 19471951.

Porter, S. C., and Zhisheng, A. (1995). Correlation between climate events in the North Atlantic and China during the last glaciation. *Nature* **375,** 305-308.

Prins, M., and Weltje, G. J. (1999). End-member modeling of siliciclastic grain-size distributions: the late Quaternary record of eolian and fluvial sediment supply to the Arabian Sea and its paleoclimatic significance. *In* "Numerical experiments in stratigraphy: recent advances in stratigraphic and ssedimentologic computer simulations.", pp. 91-111. SEPM Special Publications.

Rodó, X., Baert, E., and Comin, F. A. (1997). Variations in seasonal rainfall in Southern Europe during the present century: relationships with the North Atlantic Oscillation and the El Niño-Southern Oscillation. *Climate Dynamics* **13,** 275-284.

Rodriguez, S., Querol, X., Alastuey, A., Kallos, G., and Kakaliagou, O. (2001). Saharan dust contributions to PM10 and TSP levels in Southern and Eastern Spain. *Atmospheric Environment* **35,** 2433-2447.

Rohling, E. J., Hayes, A., Rijk, D., Kroon, D., Zachariasse, W. J., and Eisma, D. (1998). Abrupt cold spells in the northwest Mediterranean. *Paleoceanography* **13,** 316-322.

Romero, R., Sunner, G., Ramis, C., and Genovés, A. (1999). A classification of the atmospheric circulation patterns producing significant daily rainfall in the Spanish Mediterranean area. *International Journal of Climatology* **19,** 765-785.

Rühlemann, C., Mulitza, S., Müller, P., Wefer, G., and Zahn, R. (1999). Warming of the tropical Atlantic Ocean and slowdown of thermohaline circulation during the last deglaciation. *Nature* **402,** 511-514.

Sánchez-Goñi, M. F., Cacho, I., Turon, J. L., Guiot, J., Sierro, F. J., Peypouquet, J.-P., Grimalt, J. O., and Shackleton, N. J. (2002). Synchroneity between marine and terrestrial responses to millennial scale climatic variability during the last glacial period in the Mediterranean region. *Climate Dynamics* **19**, 95-105.

Sarnthein, M., Tetzlaff, G., Koopmann, B., Wolter, K., and Pflaumann, U. (1981). Glacial and interglacial wind regimes over the eastern subtropical Atlantic and North-West Africa. *Nature* **293,** 193-196.

Schiller, A., Mikolajewicz, U., and Voss, R. (1997). The stability of the North Atlantic thermohaline circulation in a coupled ocean-atmosphere general circulation model. *Climate Dynamics* **13,** 325-347.

Schulz, H., von Rad, U., and Erlenkeuser, H. (1998). Correlation between Arabian Sea and Greenland climate oscillations of the past 110,000 years. *Nature* **393,** 54-57.

Street-Perrot, F. A., Holmes, J. A., Waller, M. P., Allen, M. J., Barber, N. G. H., Fothergill, P. A., Harkness, D. D., Ivanovich, M., Kroon, D., and Perrot, R. A. (2000). Drought and dust

deposition in the west African Sahel: a 5500-year record from Kakemarum Oasis, northeastern Nigeria. *The Holocene* **10,** 293-302.

Sumner, G., Homar, V., and Ramis, C. (2001). Precipitation seasonality in Eastern and Southern coastal Spain. *International Journal of Climatology* **21,** 219-247.

Tzedakis, C. (1999). The last climatic cycle at Kopais, central Greece. *Journal of Geological Society of London* **156,** 425-434.

Weltje, G. J. (1997). End-member modeling of compositional data: numerical-statistical algorithms for solving the explicit mixing problem. *Journal of Mathematical Geology* **29,** 503-549.

Zahn, R., Schönfeld, J., Kudrass, H. R., Park, M. H., Erlenkeuser, H., and Grootes, P. (1997). Thermohaline instability in the North Atlantic during meltwater events: stable isotope and ice-rafted detritus records from core S075-26KL, Portuguese margin. *Paleoceanography* **12,** 696-710.

ARTÍCULO 4

Glacial millennial-scale variability in the Alboran Sea: productivity signal and phase relationship between marine and atmospheric processes

Ana Moreno[1], Isabel Cacho[2] , Miquel Canals[1*], Joan Grimalt[3] and María Fernanda Sánchez-Goñi[4]

[1]CRG Marine Geosciences, Department of Stratigraphy, Paleontology and Marine Geosciences, Faculty of Geology, University of Barcelona, Campus de Pedralbes, C/Martí i Franqués, s/nº, E-08028 Barcelona, Spain

[2]University of Cambridge, The Godwin Laboratory, Pembroke Street, Cambridge CB2 3SA, U.K.

[3]Department of Environmental Chemistry (ICER-CSIC), Jordi Girona, 18, 08034 Barcelona, Spain

[4]EPHE, Département Géologie et Océanographie, UMR-CNRS 5805, University Bordeaux 1, France

Enviado a: Paleoceanography

Abstract

Primary productivity of the Alboran Sea (Western Mediterranean) is reconstructed for the time interval between 48,000 and 28,000 years BP using a multi-proxy approach. All considered records show a consistent pattern that indicates enhanced primary productivity during Dansgaard/Oeschger (D/O) warm periods coherently with favourable organic matter preservation conditions. In addition, redox-sensitive elements are studied to infer bottom-water conditions. Both processes are explained by the combination of latitudinal shifts of the westerly wind system and fluvial-related inputs. These new results are integrated with several other proxies obtained in the same sediment core (MD 95-2043) to analyse frequencies and phases between different processes sensitive to the D-O climatic variability. Five spectral bands are discriminated and correlated with periodicities found in both Greenland ice cores and monsoon records. Phase analyses allow to establish the evolution of the oceanographic and atmospheric mechanisms described in the Alboran core along a D/O cycle. The fact that Saharan dust supply from Northern Africa leads high-latitude climatic changes may suggest that low-latitude feedback processes were involved in the forcing and transfer of millennial climatic variability.

INDEX TERMS: 4267: Oceanography: General: Paleoceanography; 4825: Oceanography: Biological and Chemical: Geochemistry; 1620: Global Change: Climate dynamics (3309)
KEYWORDS: paleoproductivity, Mediterranean Sea, deep-water, D/O variability, geochemistry.

4.1. Introduction

Paleoclimate studies have revealed the extreme high-frequency instability of Late Pleistocene climate on century and millennial time-scales which includes Heinrich Events (HE) and Dansgaard/Oeschger cycles (D/O) [*Bond et al.*, 1993; *Dansgaard et al.*, 1993]. Although these climate fluctuations are present in numerous marine and continental records from all over the world (see compilations in *Leuschner and Sirocko* [2000] and *Voelker*, [2002]), thus demonstrating the existence of a global climatic signal, the causes behind this variability are not fully understood [*Labeyrie and Elliot*, 1999; *Sarnthein et al.*, 2002]. Consequently, it becomes increasingly important to better constrain the underlying mechanisms that drove the D/O cycles and to figure out the connections between distinct processes at different latitudes. Dating uncertainties prevent this approach when records are derived from different cores or archives. Therefore, high-resolution cores recording both marine and atmospheric processes that operate at different latitudes are necessary to accomplish this purpose.

In the last few years, several high-frequency paleoceanographic studies have been carried out in the Western Mediterranean Sea, since its latitudinal position and hydrographic characteristics lead to an amplification of climate signals recorded in the sediments. In particular, the long IMAGES (International Marine Global Change Studies) core MD 95-2043 from the Alboran Sea has been intensively studied providing evidence for significant surface polar water invasions from the Atlantic Ocean during HE [*Cacho et al.*, 1999]. An atmospheric mechanism is invoked to explain both Sea Surface Temperature (SST) and Mediterranean deep-water formation with a D/O climate variability [*Cacho et al.*, 2000]. In addition, pollen records in the core showing significant vegetation shifts and strong changes in fluvial and aeolian inputs were observed, implying increased aridity in southeastern Iberia and stronger Saharan winds during

cold periods [*Moreno et al*., 2002; *Sánchez-Goñi et al*., 2002]. Therefore, a rapid coupling of the atmosphere-ocean systems was postulated for the Western Mediterranean region.

The response of the marine productive system to climate and hydrological changes inferred from the Alboran core has not been studied in detail. Marine productivity is believed to have the capacity to influence climate change through the regulation of atmospheric greenhouse gases. Particularly, the study of paleoproductivity variations at millennial time-scales deserves special attention because of its potential effect in the generation of abrupt climate change [*Schulz et al.*, 1998; *Vink et al.*, 2001; *Altabet et al.*, 2002]. In addition, paleoproductivity records may provide valuable information about the variability in the regional wind pattern and strength at a regional scale, when primary productivity relies on the supply by wind-driven upwelling processes.

Total Organic Carbon (TOC) and long chain alkenones were presented in a previous study from the IMAGES core MD 95-2043 [*Cacho et al*., 2000] but their interpretation in terms of paleoproductivity was prevented due to the coeval changes in deep water ventilation and thus in preservation conditions. This new study combines paleoproductivity proxies whose preservation is controlled by different deep water conditions and redox-sensitive elements for the time interval between 28 and 48 kyr BP in the same core from the Alboran Sea. This multi-proxy approach allows to separate the actual paleoproductivity signal from its diagenetic modifications. Therefore, through this productivity signal we gain, first, a better understanding of the environment conditions over the last glacial cycle in the Alboran Sea and, second, new data to inquire into the potential role played for the biological productivity in millennial-scale climatic variations. These new data are integrated in a wide data set obtained from the same core thus recording a large diversity of processes. Periodicities corresponding to the different atmospheric and oceanographic climatic mechanisms described in the Alboran core can be extracted and compared without dating uncertainties. Phase analyses have been carried out to clarify leads and lags between the studied proxies and to interpret their different patterns of variation in a global climate context at millennial time-scale.

4.2. Core location and present-day oceanography

Core MD 95-2043 was retrieved in the Alboran Sea (36º 8.6'N; 2º 37.3'W; 1,841 m water depth) during the 1995 IMAGES cruise onboard *R/V Marion Dufresne* (Figure 1). Three water masses fill this basin. The surface layer is formed by Modified Atlantic Water (MAW) and describes two quasi-permanent anticyclonic gyres, the Western and the Eastern Alboran Gyres (WAG and EAG) [*Perkins et al.*, 1990]. The second water layer is the Levantine Intermediate Water (LIW) and the deeper layer is filled by Western Mediterranean Deep Water (WMDW). WMDW is produced in the Gulf of Lions (Figure 1) where north-westerly winds evaporate and cool surface water until it sinks to the deep basin [*Millot*, 1999].

In contrast with the rest of the Mediterranean Sea which is generally oligotrophic, the Alboran Sea has high surface productivity (Figure 1). Both wind-induced upwelling, located in the northernmost part of the Western Basin and gyre-induced upwelling along the edges of the anticyclonic gyres [*Sarhan et al*., 2000; *Garcia-Gorriz and Carr*, 2001] occur in the Alboran Sea. Therefore, two main factors influence surface productivity: (i) the speed of the inflowing jet of

cold and less-saline surface waters from the Atlantic Ocean that intereacts with saltier and warmer waters from the Mediterranean [*Perkins et al.*, 1990], and (ii) westerly winds (called *Poniente*) associated with the progress of low-pressure centres into the Mediterranean region through the Strait of Gibraltar [*Parrilla and Kinder*, 1987]. Both processes enhance the development of the anticyclonic gyres thus increasing upwelling and primary productivity. In addition, seasonal fluvial nutrient discharge may contribute to phytoplancton blooms [*Fabrés et al.*, 2002].

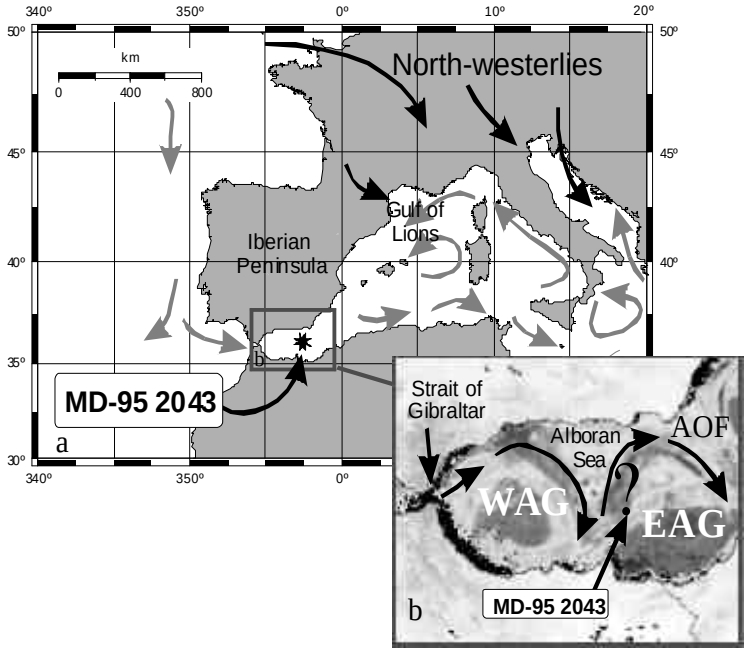

Figure 1.- (a) Location of IMAGES core MD 95-2043 in the Alboran Sea. Present-day dominant oceanographic and atmospheric circulation is represented by grey and black arrows, respectively. (b) Surface pigment concentration (mg m^{-3}) in the Alboran basin as observed by SeaWiFS in May 1999. Both antyciclonic gyres (WAG and EAG) and the position of the Almeria-Oran Front (AOF) are indicated.

Figura 1.- *(a) Situación del testigo IMAGES MD 95-2043 en el Mar de Alborán. Se representa mediante flechas grises la circulación oceanográfica dominante y con flechas negras los vientos del noroeste. (b) Concentración superficial de pigmentos (mg m^{-3}) en la cuenca de Alborán obtenida por el satélite SeaWiFS en Mayo de 1999. Se indican los giros anticiclónicos, WAG y EAG, respectivamente (de sus siglas en inglés, Western and Eastern Alboran Gyre) y la posición del Frente de Almería-Orán (AOF, de sus siglas en inglés, Almeria-Oran Front).*

4.3. Material and methods

4.3.1. Chronoestratigraphy

The chronological framework of the studied core is described and discussed in *Cacho et al.* [1999] by the construction of two different age models that demonstrate a high correspondence between the D/O climatic variability over Greenland and the SST variability in the Alboran Sea. In this study, we use the second age model, which for the core section older than 21,000 yr B.P. is based on the graphical tunning between the $U^{K'}_{37}$-SST profile from the MD 95-2043 and the

GISP2 ice core ?^{18}O curve [*Meese et al.*, 1997]. According to this age model the section presented in this study, from 1,025 to 1,585 cm depth, covers an interval of 20,000 yr, between 28,000 and 48,000 cal yr B.P with 27 cm/kyr as mean sedimentation rate and 185 years as mean temporal resolution (Figure 2).

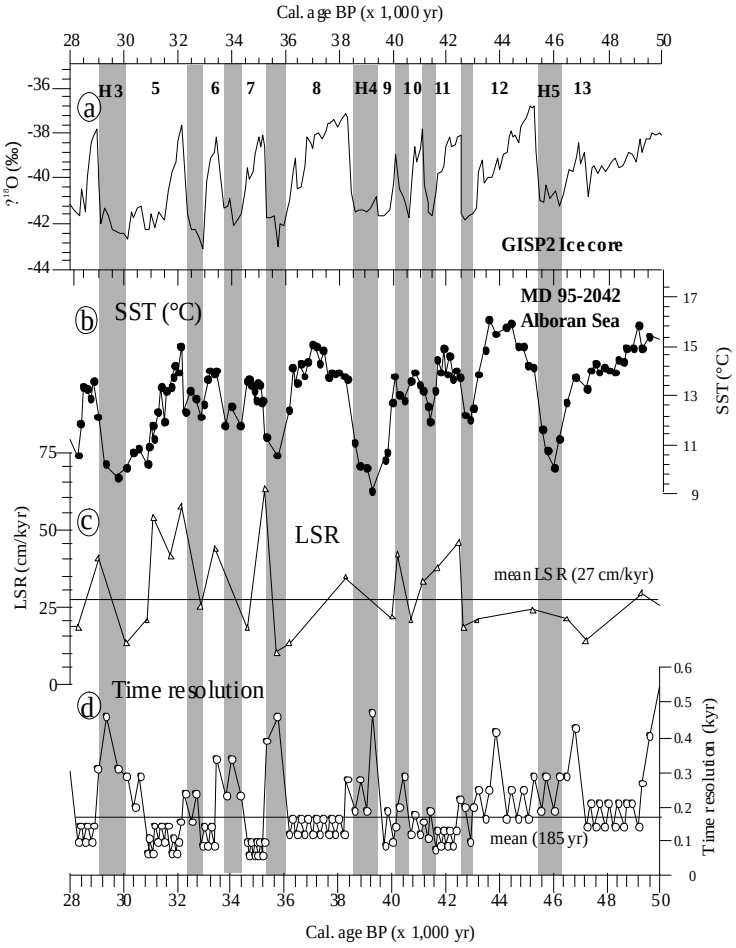

Figure 2.- Records of (a) ?^{18}O from GISP2 core [*Meese et al.*, 1997] and (b) $U^{k'}_{37}$-SST [*Cacho et al.*, 1999], (c) Linear Sedimentation Rates (LSR) and (d) time resolution for the sampling interval from MD 95-2043 core. Note that each data point in the LSR record represents an age control point in the age model constructed by *Cacho et al.* [1999] based on peak to peak correlation of the MD 95-2043 SST record with the GISP2 ?^{18}O profile (correlation coefficient r^2= 0.92). HE and D/O stadials are indicated by shaded bars following GISP2 age model [*Meese et al.*, 1997]. D/O interstadials are indicated by numbers.

Figura 2.- *Registros de (a) ?^{18}O del testigo GISP2 [Meese et al., 1997] y (b) $U^{k'}_{37}$-SST [Cacho et al., 1999], (c) tasas de sedimentación lineal (LSR, de sus siglas en inglés, Linear Sedimentation Rates) y (d) resolución temporal del intervalo de muestro del testigo MD 95-2043. Nótese que cada punto del registro de LSR representa un punto de control temporal en el modelo de edad construído por Cacho et al. [1999] y basado en la correlación pico a pico del registro de SST del testigo MD 95-2043 con el perfil de ?^{18}O de GISP2 (coeficiente de correlación r^2=0,92). Los HE y los estadiales de los ciclos de D/O se indican con barras sombreadas, siguiendo el modelo de edad del testigo GISP2 [Meese et al., 1997]. Los interestadiales de los ciclos de D/O se indican con números.*

4.3.2. Geochemical analyses

Bulk major and trace element contents were analysed with a sample spacing of 5 cm by means of X-ray fluorescence (XRF). Samples were ground and homogenised in an agate mortar and prepared for major and trace element determination. For major element measurement, glass discs were processed by melting about 0.3 g of ground bulk sediment with a Li tetra borate flux. For trace element analysis, discs were produced by pressing about 5 g of ground bulk sediment into a briquet, with boric acid backing. Finally, XRF analyses were performed with a Philips PW 2,400 sequential wavelength dispersive X-ray spectrometer. Analytical accuracy was checked measuring international standards (GSS-1 to GSS-7) and precision was determined by replicate analyses of samples (0.8% and 4% for major and trace elements, respectively).

Total Carbonate content ($CaCO_3$) was calculated from the total Ca concentration (Ca_{TOT}) obtained by XRF analyses by means of two different approaches (Figure 3b). First, we make use of a formula that corrects the clay-derived Ca, which was established for carbonate-rich sediments (1). Second, we calculated the carbonate content from the percentage of volatiles lost on ignition (% LOI) using a correction for dolomite production. Both methods lead to slightly different values within a very similar pattern (r^2 = 0.97) (Figure 3d). The offset between both methods is constant and probably related with the presence of dolomite that was not corrected in the first approach.

(1) $CaCO_3 = 2.5\ (Ca_{TOT} - (Ca/Al_{Clay}\ ?\ Al_{TOT}))$; where Ca/Al_{Clay} is 0.345 [*Turekian and Wedepohl*, 1961]

In order to assess the amount of barium in core MD 95-2043 that is present as biogenic barite, we corrected the total barium (Ba_{TOT}) obtained by XRF for the non-biogenic portion following *Dymond et al.* [1992] calculation (2). In this paper, we will refer to this fraction as barium excess (Ba_{excess}) (Figure 3i):

(2) $Ba_{excess} = Ba_{TOT} - (Ba/Al_{aluminosilicate}\ ?\ Al_{TOT})$; where $Ba/Al_{aluminosilicates}$ = 0.0075 [*Dymond et al.*, 1992]

Our approach consists of studying elemental distributions with respect to their terrigenous inventory by normalizing their concentrations to Al percentage in every sample [*Calvert and Pedersen*, 1993] (Figures 3 and 4). In addition, the values of the studied proxies are compared with values from the literature to help in detecting potential diagenetic enrichments in redox-sensitive elements (Table 1).

4.3.3. Spectral analysis

Proxy records have been resampled at an uniform 150 year interval for the studied period (28-48 kyrs), close to the mean temporal resolution of the records, before carrying out the spectral analyses (Figure 2). To extract the significant periodicities contained in the records, spectral

analysis was performed using different methods provided in the Analyseries package: Blackman-Tukey (B&T), Multi-Taper Method (MTM) and Maximum Entropy Method (MEM) [*Paillard et al.*, 1996]. The MTM method is the principal tool in spectrum estimation here since it is able to detect low-amplitude oscillations in relatively short time series, like ours, with a high degree of statistical significance [*Yiou et al.*, 1996]. In addition, the MTM has the major advantage of providing a narrow band *F-test* for the presence and significance of periodic components that does not depend on the magnitude of power [*Thomson*, 1990]. With regard to the SST spectral record, the cyclities are probably the result of the age model construction by comparing with the GISP2 ?^{18}O record [*Meese et al.*, 1997]. However, proxies that were not used for tuning the stratigraphy of this core will provide statistically independent records. Once the main frequency bands have been extracted in the studied proxies, filtering of the whole set of records has been carried out to obtain the amount of variance explained by the most significant band-pass components. Finally, we performed cross-spectral analyses using the B&T method against the SST record from the Alboran Sea. Coherence and phase results are discussed to infer the different processes influencing the proxy records and their phasing at sub-Milankovitch periodicities.

4.4. Results and discussion

4.4.1. Millennial variability in the paleoproductivity record

Paleoproductivity versus preservation

Calcium carbonate contents display a similar pattern as the $U^{k'}_{37}$-SST record in core MD 95-2043 (Figure 3a,b). However, the carbonate record is systematically delayed. Although carbonate content in oligotrophic sediments has been used as a proxy for carbonate paleoproductivity since it is recording the abundance of calcareous plankton (i.e. foraminifera and coccolithophores) [*Rühlemann et al.*, 1999], processes such as dissolution can also influence this record. A proxy to establish the importance of dissolution is the foraminifera fragmentation index. In this core, the foraminifera fragmentation ratio demonstrates that carbonate dissolution was negligible during D/O stadial periods and HE and increased during the interstadial ones [*Sierro et al.*, 2001]. Thus, the carbonate contents found during the D/O interstadial periods represent minimum values since a portion of the originally-accumulated calcite may have been dissolved within the sediment or at the water-sediment interface. However, the excellent carbonate preservation during the stadial periods indicates that other processes different than carbonate dissolution are responsible for the reduced carbonate contents at those levels.

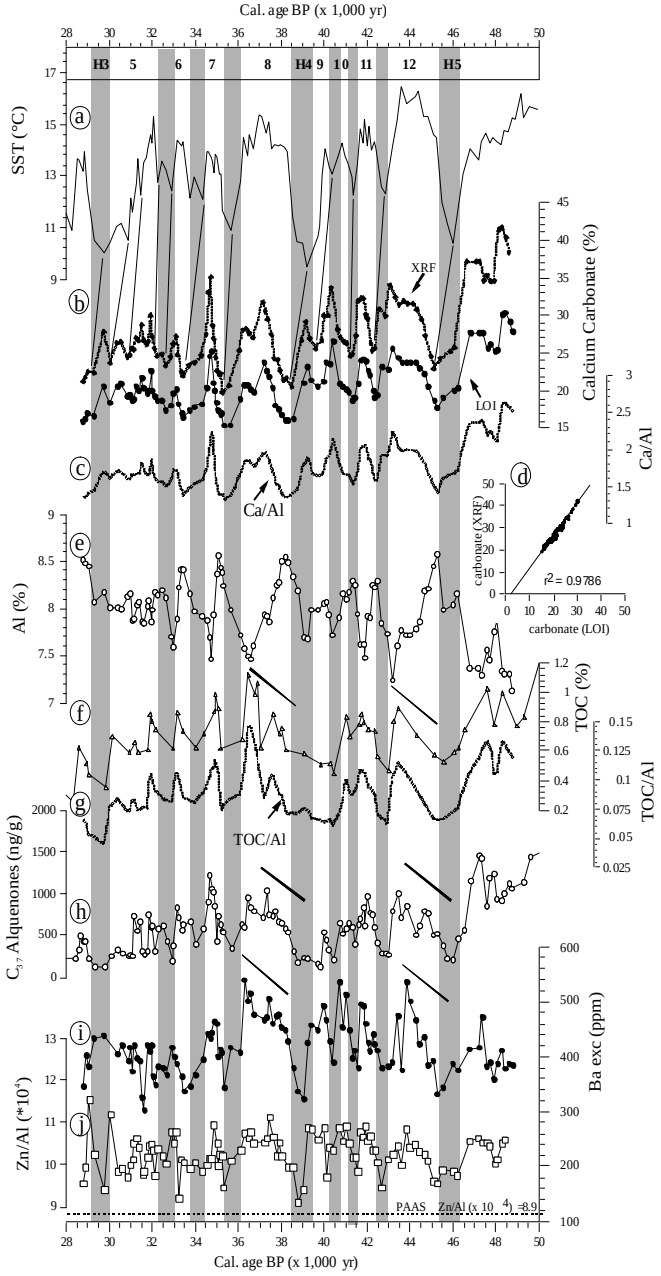

Figure 3.- MD 95-2043 age profiles of (a) $U^{k'}_{37}$-SST [*Cacho et al.*, 1999]; (b) percentage of carbonate calculated by using a formula for carbonate-rich sediments and the amount of lost volatiles (see text for explanation); (c) Ca/Al ratio; (d) comparison between both carbonate calculations (linear trend and r^2 are also indicated); (e) percentage of Al; (f) total organic carbon percentages (TOC) [*Cacho et al.*, 2000]; (g) TOC/Al ratio; (h) total C_{37} alkenone concentrations [*Cacho et al.*, 2000]; (i) Ba_{excess} concentration (ppm) and (j) Zn/Al ratio (PAAS value is indicated from *Taylor and McLennan* [1985]).

Figura 3.- *Perfiles del testigo MD 95-2043 de (a) $U^{k'}_{37}$-SST [Cacho et al., 1999]; (b) porcentaje de carbonato calculado usando una fórmula para sedimentos ricos en carbonato y a partir de la cantidad de volátiles perdidos (cf. texto para una completa explicación); (c) relación Ca/Al; (d) comparación entre los dos cálculos de carbonato (se indican la tendencia lineal y el valor de r^2); (e) porcentaje de Aluminio; (f) porcentaje de carbono orgánico (TOC) [Cacho et al., 2000]; (g) relación TOC/Al; (h) concentraciones totales de alquenonas C_{37} [Cacho et al., 2000]; (i) concentración de Ba_{exceso} (ppm) y (j) relación Zn/Al (se indican los valores del PAAS tomados de Taylor and McLennan [1985]).*

TOC, total alkenone concentration and Ba_{excess} are represented in Figure 3. These proxies have been previously used to obtain paleoproductivity variations in numerous studies where their main pitfalls and advantages are discussed [*Müller and Suess*, 1979; *Suess*, 1980; *Dymond et al.*, 1992; *Gingele and Dahmke*, 1994; *Villanueva et al.*, 1998]. In the MD 95-2043 core all the paleoproductivity proxy records show a similar pattern, thus pointing to higher productivity during D/O warmer periods (Figure 3). However, terrestrial input via rivers and wind has been proved to be important for the investigated region [*Moreno et al.*, 2002]. Thus, the influence of dilution in the productivity record may be relevant. Since lowest carbonate values parallel high aluminium content, Ca/Al ratio is plotted to infer the effect of dilution (Figure 3c,e). From comparison between carbonate records and Ca/Al ratio, we propose that this proxy is mainly controlled by productivity variations thus neglecting dilution influences. In addition, TOC/Al ratio is considered to afford the dilution influence (Figure 3g). Since this ratio correlates with the other paleoproductivity proxies, we finally reject the effect of dilution in the productivity signal.

To constrain any further preservational influence linked to deep water conditions, redox-sensitive metals have been analysed in addition to the above proxies. This adds to carbon isotope measurements in benthic foraminifera which sugested changes in deep water oxygenation in the MD 95-2043 core [*Cacho et al.*, 2000]. Higher values of $?^{13}C$ recorded in benthic foraminiferal calcareous tests have been associated in general to improved ventilation of deep water masses [*Kroopnick*, 1985]. In our core, benthic $?^{13}C$ record shows relatively high variability (0.8‰) for the study period and these oscillations occurred well coupled with the D/O cycles identified previously. Well-oxygenated conditions were recorded in the Alboran core during HE and D/O stadials and would possibly influence organic matter preservation (Figure 4a). In such scenario the paleoproductivity signal based on organic matter (TOC and alkenone concentration) may be altered. Therefore, we need to consider Barium peaks since this paleoproductivity proxy is not influenced by bottom water redox conditions in the same way than it is the TOC.

Although the production of barite is still a matter of debate, Ba_{excess} has been extensively used as a paleoproductivity proxy [*Dymond et al.*, 1992; *Dean et al.*, 1997; *Des Combes et al.*, 1999]. Under sulfate-depleted environments dissolution of barite might occur. Ba_{excess} peaks could thus result from reprecipitation processes linked to the re-establishment of oxic conditions [*De Lange et al.*, 1994; *Torres et al.*, 1996; *Kasten et al.*, 2001]. These consideration has precluded the use of Ba_{excess} as a paleoproductivity indicator in oxygen depleted environments [*Francois et al.*, 1995], such as highly productive nearshore areas [*Dymond et al.*, 1992]. The rate of burial of particulate organic matter in highly productive areas may exceed the rate of replenishment of dissolved oxygen and lead to the development of an anoxic environment where sulfate reduction is common. Therefore, Ba and TOC have a totally different behaviour during diagenetic processes. Thus, the fact that both proxies show parallel evolution in our core, lead us to propose that their signal is not mainly dominated by diagenesis. Nevertheless, we need to understand better the diagenetic processes which could have introduced an overprint signal in our different paleoproductivity proxies. The analysis of redox-sensitive elements records allows to check this interpretation.

Diagenetic enrichments can be detected by comparing redox sensitive ratios with the average composition of shales (Post-Archean Average Shale, PAAS) to characterise the composition of the aluminosilicate detritus supplied to the basin [*Turekian and Wedepohl*, 1961; *Wedepohl*, 1971] (Table 1). Data from the Cariaco Trench [*Calvert and Pedersen*, 1993] and the Eastern Mediterranean sapropels [*Wehausen and Brumsack*, 2000] are also indicated to represent

more anoxic conditions. The Mn/Al record is slightly above PAAS values in some of the D/O interstadial periods in core MD 95-2043 (Figure 4b and Table 1) indicating an enrichment of this element. Formation of diagenetic Mn-spikes has been associated to sudden increases in bottom-water oxygen content [*De Lange et al.*, 1994]. However, as we have seen previously, the $?^{13}C$ record measured in benthic foraminifers suggests that bottom water ventilation increased during D/O stadials [*Cacho et al.*, 2000] (Figure 4, plotted with reverse y axis). Clearly, interpretating Mn/Al peaks as a result of sudden increments in the oxygenation of bottom-water during D/O interstadial periods contradicts these results.

Table 1.- Trace element data in this study compared with values from the literature.

Tabla 1.- *Datos de elementos traza de este estudio comparados con valores de la literatura.*

Data	Mn/Al (10^4)	Zn/Al (10^4)	Cu/Al (10^4)	Cr/Al (10^4)	V/Al (10^4)	V/Cr	Ni/Co	Ni/Al	Co/Al
MD 95-2043	60-130	9-11.5	2.4-4.3	9-10.8	2.4-10	1-1.25	2-3.5	3.5-6.5	1.4-2.4
Shale[1]	96.2	10.8	5.1	10.2	14.8	1.4	3.5	7.7	2.15
PAAS[2]	85	8.9	5.3	11.6	15	1.36	2.4	5.5	2.3
Anoxic basin[3&4]	31.2[3]	16.2[3]	5.3[3]	13.4[3]	35.8[3]	1-4.3[4]	4.3-7[4]	5.8[3]	-
Eastern Mediterranean[5]	-	11	21	24	44	1.9	3.5	26	8

[1] Average shale, data from *Wedepohl* [1971]

[2] Post-Archean Average Shale, data from *Taylor and McLennan* [1985]

[3] Cariaco Trench, data from Table 2 in *Calvert and Pedersen* [1993]

[4] North Sea, data from *Jones and Manning* [1994]

[5] Average composition of Pliocene sediments from the eastern Mediterranean [*Wehausen and Brumsack*, 2000]. Sapropels are preserved in these sediments.

In the Alboran record, while Cu/Al, Cr/Al and V/Al values appear always below the average composition of shales, Zn/Al values lie above, yet well below anoxic basin values (Table 1). Cr and V correlate well with Al (%) ($r^2 = 0.7$), an element that does not respond to redox variations thus indicating a potential relationship of Cr and V with the detrital fraction. On the other hand, the distribution of Zn and Cu in the ocean is governed by biochemical reactions [*Calvert and Pedersen*, 1993]. In the studied core, Zn/Al and Ba_{excess} behaves similarly (Figure 3i,j). Therefore, Cr and V fluxes would be dominated by detrital input, mainly associated to Fe oxyhydroxides [*Morford and Emerson*, 1999], while Zn and Cu could be related to the flux of organic matter. Zn in particular has been linked with the presence of diatoms since it contributes to the formation of their skeleton [*Smetacek*, 1985]. The close relation of Mn/Al records to the organic matter might provide an explanation to the discrepancy among $?^{13}C$ and Mn/Al profiles. The later could be controlled by passive sinking of biogenic detritus and adsorption on $CaCO_3$ surfaces [*Boyle*, 1983; *Martin and Knauer*, 1983], thus giving higher values when the Alboran Sea was more productive (D/O interstadials).

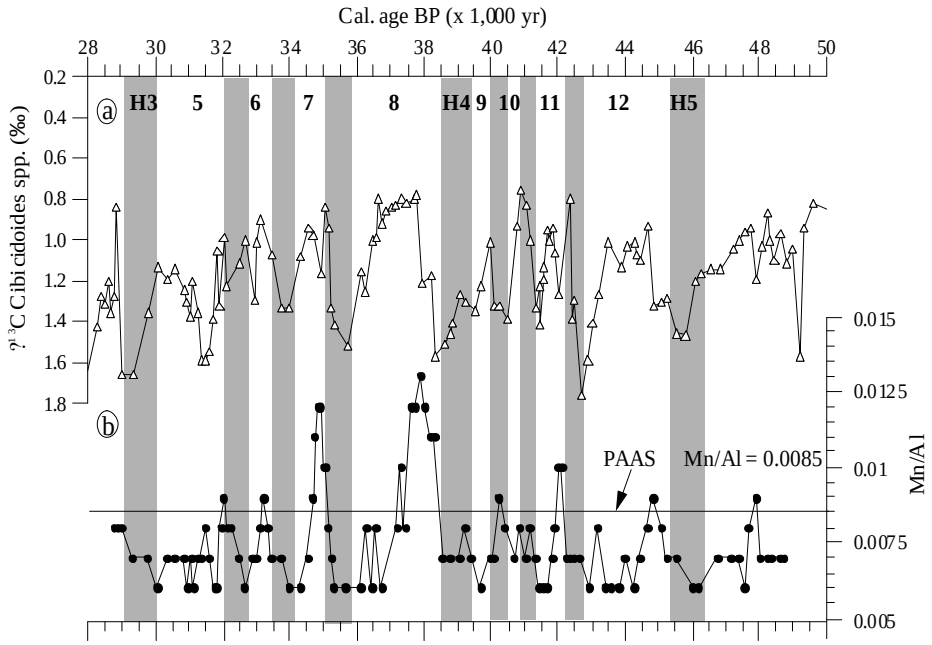

Figure 4.- MD 95-2043 age profiles of (a) ?^{13}C *Cibicidoides spp.* (reverse y axis) and (b) Mn/Al ratio records. PAAS value for Mn/Al ratio is also indicated [*Taylor and McLennan*, 1985].

Figura 4.- *Perfiles del testigo MD 95-2043 graficados respecto a la edad de los registros de (a) ?^{13}C Cibicidoides spp. (eje y invertido) y (b) de la relación Mn/Al. El valor del PAAS para la relación Mn/Al se indica igualmente [Taylor and McLennan, 1985].*

The redox-sensitive metal values tell us that bottom water oxygen concentration was high enough to prevent extensive sulfate reduction and also mobilization of Barium. Consequently, Ba_{excess} can be used as a reliable paleoproductivity proxy in the studied time interval. The productivity increments that Ba_{excess} record shows during D/O interstadials are consistent with previously published records (TOC and C_{37} alkenones) and with our carbonate record too (Figure 3). This view does not exclude the enhancement of bottom-water ventilation during cold periods (HE and D/O stadials) that could contribute to organic matter degradation. During warm intervals both higher productivity and better preservation favoured recording the observed peaks of carbonate, TOC, Ba_{excess} and alkenones.

Mechanisms involved in the D/O variability of the paleoproductivity record

The mean Atlantic-Mediterranean water exchange system has long been recognised to be density driven in response to the intensity of water overturning in the Mediterranean Sea, which is controlled by the usually negative hydrological budget in this region [*Béthoux and Gentili*, 1999]. As we described in section 2, the interaction between Atlantic and Mediterranean waters influence productivity in the Alboran Sea. However, over this control, other factors influencing productivity has been described in detailed present-day oceanographic studies. Thus, it is known that the decrease of atmospheric pressure over the Western Mediterranean produces a faster Atlantic inflow that enhances the development of the WAG with the concomitant increase in upwelling processes [*Candela and Winant*, 1989; *Vargas-Yáñez et al.*, 2002]. In addition, the availability of nutrients via fluvial input also favours high productivity in the Alboran Sea by

fertilization of surface waters: a correlation between high chlorophyll concentration and fluvial discharge from southern Iberian rivers (Guadiaro and Guadalhorce) is found in a trap study carried out in the Alboran Sea [*Fabrés et al.*, 2002]. Therefore, both decreased atmospheric pressure over the Mediterranean Sea and increased runoff mechanisms lead to the establishment of a high productivity scenario. Based on the previously presented results, we propose that those scenarios may be more frequent during D/O interstadial periods.

The SST cooling observed in many North Atlantic sediments during D/O stadial periods [*Voelker*, 2002] and the coherent SST warming in the subtropical Atlantic inferred from model simulations [*Ganopolski and Rahmstorf*, 2001] may lead to an enhancement of the north-westerly winds system, which is sensitive to the meridional SST gradients in the North Atlantic [*Kageyama et al.*, 1999]. On the contrary, in a D/O interstadial situation, the lowered pressure gradient along the North Atlantic may allow the establishment of a semi-permanent low-pressure system in the Mediterranean region thus favouring the displacement of the westerly winds to a southern location. This meteorological scenario will increase productivity in the Alboran Sea by providing (i) a faster inflow of Atlantic waters and (ii) westerly-wind-induced upwelling [*Parrilla and Kinder*, 1987; *Candela and Winant*, 1989; *Sarhan et al.*, 2000; *Garcia-Gorriz and Carr*, 2001].

An increase of precipitation during D/O interstadial periods has been previously supported in base to (i) transfer-functions applied on pollen analyses and (ii) grain-size and geochemical analyses in this core section [*Moreno et al.*, 2002; *Sánchez-Goñi et al.*, 2002]. In addition, Aluminium percentage record, represented in Figure 3e, also points to an enhancement of fluvial supply to the Alboran Basin during warm periods. Therefore, increased runoff would lead to higher nutrient input thus contributing to the enhanced paleoproductivity observed during D/O interestadials in the Alboran Sea. Coherently, wetter conditions during D/O interstadial periods were also revealed in different Mediterranean sites by *Allen et al.* [1999], *Tzedakis* [1999] and *Watts et al.* [2000]. These studies allow us to hypothesise that surface water fertilization by an enhanced runoff was a consequence of humid climatic conditions in a basin-wide context. However, further high-resolution last glacial cycle paleoproductivity studies should be carried out in other Mediterranean sub-basins to investigate the geographical extent of this hypothesis.

Finally, the coincidence during D/O interstadial periods of higher nutrient availability driven by fluvial input and the southern location of the westerly wind system would produce the observed increments in surface productivity in the Alboran Sea.

4.4.2. Frequency and phase relationships between the different proxies and their implications

In addition to the primary productivity records here presented, MD 95-2043 core has been studied for several other proxies. All these records provide a wide set of information about different atmospheric and oceanographic processes which reacted to the D/O climatic variability. Thus, MD 95-2043 core constitutes an exceptional base to perform spectral analyses over different records without dating uncertainties. In this chapter we will refer to the extracted periodicities and phase relationships between the following processes: (i) Alboran SST, inferred from the the $U^{k'}_{37}$ index and the percentage of *N. pachyderma (s.)* [*Cacho et al.*, 1999], (ii) paleoproductivity, reflected by the concentration of Ba_{excess}, TOC, alkenones, carbonate and Zn/Al

ratio (Figure 3), (iii) deep water ventilation, indicated by ?^{13}C measured in benthic foraminifera and the alcohol index, a proxy for preservation conditions [*Cacho et al.*, 2000] (Figure 4), (iv) aridity/humidity in the southern Iberian Peninsula, obtained from the abundance of steppic vegetation [*Sánchez-Goñi et al.*, 2002], and the percentage of Aluminium (Figure 3e) and (v) Saharan winds/Northern African aridity represented by the Si/(Si+K) ratio and the percentage of end-member 1 (EM1), calculated after a statistical treatment of grain-size data [*Moreno et al.*, 2002]. In addition, spectral analyses were conducted over two GISP2 records: the ?^{18}O, as an atmospheric temperature indicator over Greenland [*Meese et al.*, 1997], and the Polar Circulation Index (PCI) as a proxy for atmospheric circulation at high-latitudes obtained by the concentration in dust and sea salt particles in Greenland ice cores [*Mayewski et al.*, 1997].

Analysis in the frequency domain (sub-Milankovitch frequencies)

The results of spectral analyses obtained by using the MTM are shown in Figure 5. In Table 2 we represent the accurate times when prominent spectral peaks are attained and the value of the significance test for each of these peaks for each proxy record. The variability explained by each frequency is indicated in percentages in Table 3. This procedure permits to extract five significant cyclicities (*F-test* > 0.9): 5-10,000, 3,300, 2,400, 1,470 and 1,200 years. All these frequencies have been found previously in paleoclimatic records from high-latitudes [*Grootes and Stuiver*, 1997; *Mayewski et al.*, 1997; *Van Kreveld et al.*, 2000] and also from monsoon regimes [*Sirocko et al.*, 1996; *de Garidel-Thoron et al.*, 2001]. Although our results confirm the operation of these cyclicities at middle-latitudes, different reactions of the considered proxies are observed when the significance and variance of the obtained frequencies are analysed in detail. These findings provide a further insight in the dynamic of the associated processes.

The ˜ 8,000-yr cycle is the most significant in the abundance of *N. pachyderma (s.)*, the % of end-member 1 (EM1) and the abundance of steppic vegetation (Figure 5 and Table 2). All these proxies show an amplified signal during HE respect to the other D/O stadials. In contrast, this low-frequency cycle is not significant in the ?^{18}O from Greenland ice cores, where all the D/O stadials reached similar low values. Therefore, this spectral band can be related to the amplification of the HE which, in the context of the Alboran Sea, was particularly significant in the SST and also in the aridity conditions inferred for the nearby continent. The extreme SST HE-cooling outside the ice-rafted detritus belt has been associated to the southward displacement of polar waters [*Cacho et al.*, 1999; *Bard et al.*, 2000]. This oceanographic situation is consistent with the complete shutdown of the north Atlantic thermohaline circulation simulated by numerical models [*Ganopolski and Rahmstorf*, 2001]. The amplified HE signal of the steppic vegetation from the south of Iberia has not been observed in similar records from the Atlantic margin thus suggesting that it was an inhomogeneous process [*Sánchez-Goñi et al.*, 2002]. These authors postulated that changes in the dominance of Scandinavian or Atlantic Mobile Polar Highs between different stadials may explain the higher aridification of the Mediterranean region during the HE.

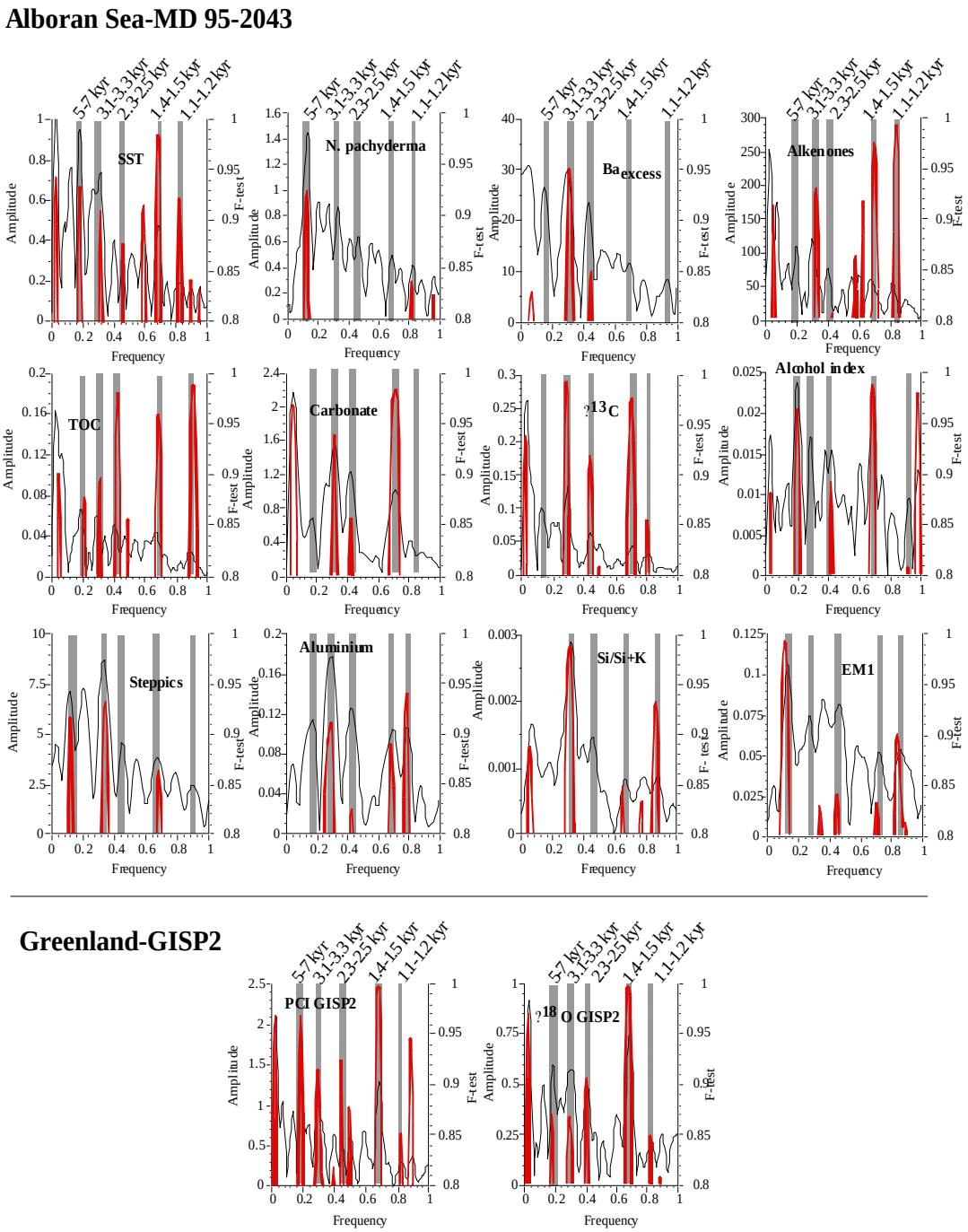

Figure 5.- Variance spectra of selected records from the IMAGES MD 95-2043 core, expressed as the line amplitude versus frequency in cycles kyr-1 using the MTM (continuous curve). *F-test* values are also plotted (thicker line). The main periods of variance are marked as vertical grey bands. See Table 2 for the accurate time when the spectral peaks occur and the value of the statistical test.

Figura 5.- *Varianza espectral de los registros seleccionados del testigo IMAGES MD 95-2043, expresada como la amplitud versus la frecuencia en ciclos de 10^{-3} años obtenida mediante el método MTM (curva continua). Los valores del F-test se grafican también (línea gruesa). Los principales periodos de varianza están marcados con líneas grises verticales. Cf. Tabla 2 para las edades exactas en las que ocurren los picos espectrales y los valores del test estadístico proporcionado.*

Most of the proxy records from the Alboran core and both records from GISP2 ice core (?^{18}O and PCI) reveal the 3,300-yr cycle in the spectral analyses (Figure 5 and Table 2). In addition, this is the frequency which explain a higher percentage of the variance for most of the considered Alboran proxies, even higher than in GISP2 records. This reveals the importance of this frequency in the reorganisation of the oceanic and atmospheric systems at this latitude. After comparison of these records with their band-pass components, we observe that the 3,300-yr cycle is related to the marked presence of the longer D/O interstadials (8 and 12) (Figure 6a). The relative long duration of these interstadial periods may had favour the reorganisation of the involved climatic systems but also it may be related to the better signal representation in the sedimentary record due to these long interstadials.

Table 2.- Results of spectral analyses carried on selected proxies from core MD 95-2043 and compared with those from GISP2 records. Frequency bands are selected from the amplitude peaks obtained from the MTM (Figure 5). The amplitude peak (in years) and the value of *F-test* (from 0 to 1) are shown. No spectral variance at a selected frequency band is indicated by (-). Intervals with *F-test* > 0.9 are considered significant (in bold type). References where the records were published are shown (Refs).

Tabla 2.- *Resultados de los análisis espectrales llevados a cabo en proxies seleccionadas del testigo MD 95-2043 y comparados con los registros del testigo GISP2. Las bandas de frecuencia se han seleccionado a partir de los picos de amplitud obtenidos por el método MTM (cf. Figura 5). Los picos de amplitud (en años) y el valor del F-test (de 0 a 1) se muestran. En los casos donde no hay varianza significativa a una frecuencia seleccionada se indica con un guión (-). Los intervalos de F-test > 0,9 se consideran significativos (en negrita). Las referencias donde los registros se publicaron se muestran (columna encabezada por Refs.).*

	Process	Variable	Frequency bands ~ 0.14	0.3	0.42	0.68	0.83	Refs.
Greenland GISP2	Temperature	?^{18}O (GISP2)	5535; 0.87	3350; 0.86	**2438; 0.9**	**1462; 0.99**	1211; 0.85	[*Meese, et al.*, 1997; *Mayewski, et al.*, 1997]
	Atmospheric circulation	PCI (GISP2)	**5250; 0.97**	**3350; 0.91**	**2226; 0.92**	**1462; 0.99**	**1125; 0.94**	
Alboran Sea MD 95-2043	SST	SST (ºC)	**5485; 0.93**	**3200; 0.91**	2194; 0.87	**1462; 0.98**	**1219; 0.92**	[*Cacho, et al.*, 1999]
		N. pachyderma	**7680; 0.93**	-	-	-	1209; 0.82	
	Productivity	Ba_{excess} (ppm)	6407; 0.83	**3334; 0.95**	2300; 0.84	1570; 0.86	**1098; 0.94**	[*Cacho, et al.*, 2000]
		Alkenones (ng/g)	-	**3350; 0.92**	-	**1484; 0.97**	**1226; 0.99**	
		TOC (%)	5250; 0.87	**3413; 0.90**	2130; 0.85	**1494; 0.96**	**1191; 0.99**	
		$CaCO_3$ (%)	-	**3200; 0.94**	2381; 0.86	**1402; 0.98**	-	
	Deep Water Conditions	?^{13}C (benthics)	-	**3470; 0.99**	**2250; 0.92**	**1412; 0.98**	1233; 0.85	[*Cacho, et al.*, 2000]
		Alcohol index	**5119; 0.96**	-	2400; 0.89	**1462; 0.98**	-	
	Aridity Iberia	Steppics (%)	**9300; 0.91**	**3011; 0.93**	-	1484; 0.86	-	[Sánchez-Goñi *et al.*, 2002]
		Aluminium (%)	-	**3413; 0.91**	2327; 0.82	1422; 0.85	**1264; 0.94**	
	Saharan winds	Si/(Si+K)	-	**3134; 0.99**	-	1505; 0.84	**1137; 0.93**	[*Moreno et al.*, 2002]
		End-member 1	**7680; 0.99**	-	2133; 0.84	1383; 0.83	**1163; 0.90**	

The 2,400-yr cycle is significant in Greenland but not in Alboran records with the exception of the $?^{13}C$ (benthics) (Table 2). This further supports a strong link between the rates of ventilation of deep water masses and the intensity of high latitude atmospheric circulation reported by the Greenland PCI index. *Cacho et al.* [2000] hypothesised that the benthic isotopic record from the Alboran core may monitor changes in the deep-water convection produced in the Gulf of Lions which in turn are strongly associated to the intensity of northwesterly winds that flow from the European continent.

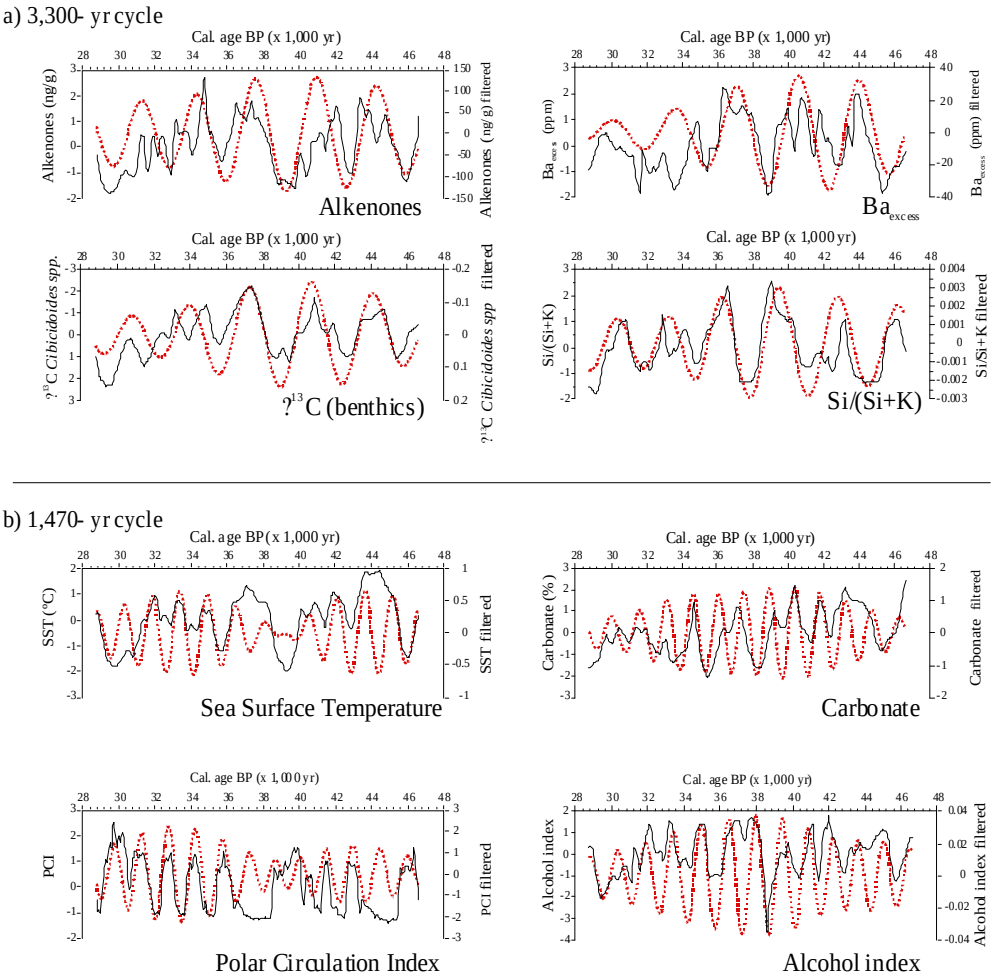

Figure 6.- Band-pass component filtered of some series from the Alboran MD 95-2043 core (dashed line) using a gaussian filter with central periods at (a) 3,300 years, and (b) 1,470 years compared with the original series (continuous line) that are normalized to the unit of variance. See Table 3 for percentage values of the variance explained by each frequency.

Figura 6.- *Componentes de algunas series del testigo de Alborán MD 95-2043 (lineas discontinuas) obtenidas mediante el filtrado usando un filtro de tipo gaussiano con periodos centrados a (a) 3.300 años y(b) 1.470 años comparados con las series originales normalizadas a la unidad de varianza (líneas continuas). Cf. Tabla 3 para los valores en porcentajes de la varianza explicada por cada frecuencia.*

The main sub-Milankovitch period described in the literature and also well represented in our records is the 1,470-yr cycle. Although both *F-test* values and the amount of variability

explained by this frequency are high for most of the proxies (Tables 2 and 3; Figure 5 and 6b), the variance that is associated with this cycle is lower than the one that is represented by the 3,300-yr cycle. Comparison among proxies points to a less significant 1,470-yr signal in the terrestrial indicators respect to SST or productivity proxies thus suggesting that changes in the terrestrial system (i.e. aridity, wind systems) were less influenced by D/O rapid climatic variations (Table 3).

Table 3.- Percentage of variance explained by the band-components of each study proxy evaluated at the most significant frequencies found for every record (periodicities with *F-test* > 0.9 in bold, see Table 2). References where the records were published are shown (Refs).

Tabla 3.- *Porcentaje de la varianza que explica cada una de las componentes filtradas a las frecuencias más significativas para cada registro (las periodicidades con F-test > 0,9 se indican en negrita, cf. Tabla 2). Las referencias donde se publicaron los registros se muestran igualmente (Refs).*

	Process	Variable	Frequency bands ~ 0.14	0.3	0.42	0.68	0.83	Refs.
Greenland GISP2	Temperature	?^{18}O (GISP2)	16.3	21.68	**16.83**	**31.87**	13.32	[*Meese, et al.*, 1997; *Mayewski, et al.*, 1997]
	Atmospheric circulation	PCI (GISP2)	**19.61**	**20.68**	**14.44**	**32.6**	**12.68**	
Alboran Sea MD 95-2043	SST	SST (ºC)	**29.68**	**31.63**	17.64	**15.64**	**5.405**	[*Cacho, et al.*, 1999]
		N. pachyderma	**25.01**	-	-	-	11.91	
	Productivity	Ba_{excess} (ppm)	22.15	**27.11**	20.34	18.39	**12**	[*Cacho, et al.*, 2000]
		Alkenones (ng/g)	-	**21.87**	-	**22**	**14.1**	
		TOC (%)	28.95	**16.9**	25.4	**19.77**	**8.99**	
		$CaCO_3$ (%)	-	**26.07**	28.31	**21.02**	-	
	Deep Water Conditions	?^{13}C (benthics)	-	**34.43**	**26.05**	**12.18**	9.591	[*Cacho, et al.*, 2000]
		Alcohol index	**13.42**	-	27.18	**29.96**	-	
	Aridity Iberia	Steppics (%)	**25.33**	**23.72**	-	15.96	-	[Sánchez-Goñi *et al.*, 2002]
		Aluminium (%)	-	**23.9**	22.43	18.65	**18.91**	
	Saharan winds	Si/(Si+K)	-	**30.85**	-	13.17	**14.26**	[*Moreno et al.*, 2002]
		End-member 1	**22.76**	-	29.32	13.91	**16.18**	

Phasing the different processes

As we discuss above, the best represented cycle by all the considered processes in these analyses is the 3,300-yr cycle corresponding to the long interstadials (8 and 12). Therefore, we select the 0.3 frequency band for phase relationship representation in order to analyse the evolution of the processes affecting the Alboran Sea. From the comparison of processes recorded in the Alboran core some differences in timing and evolution of the studied proxies are arising (Figure 7).

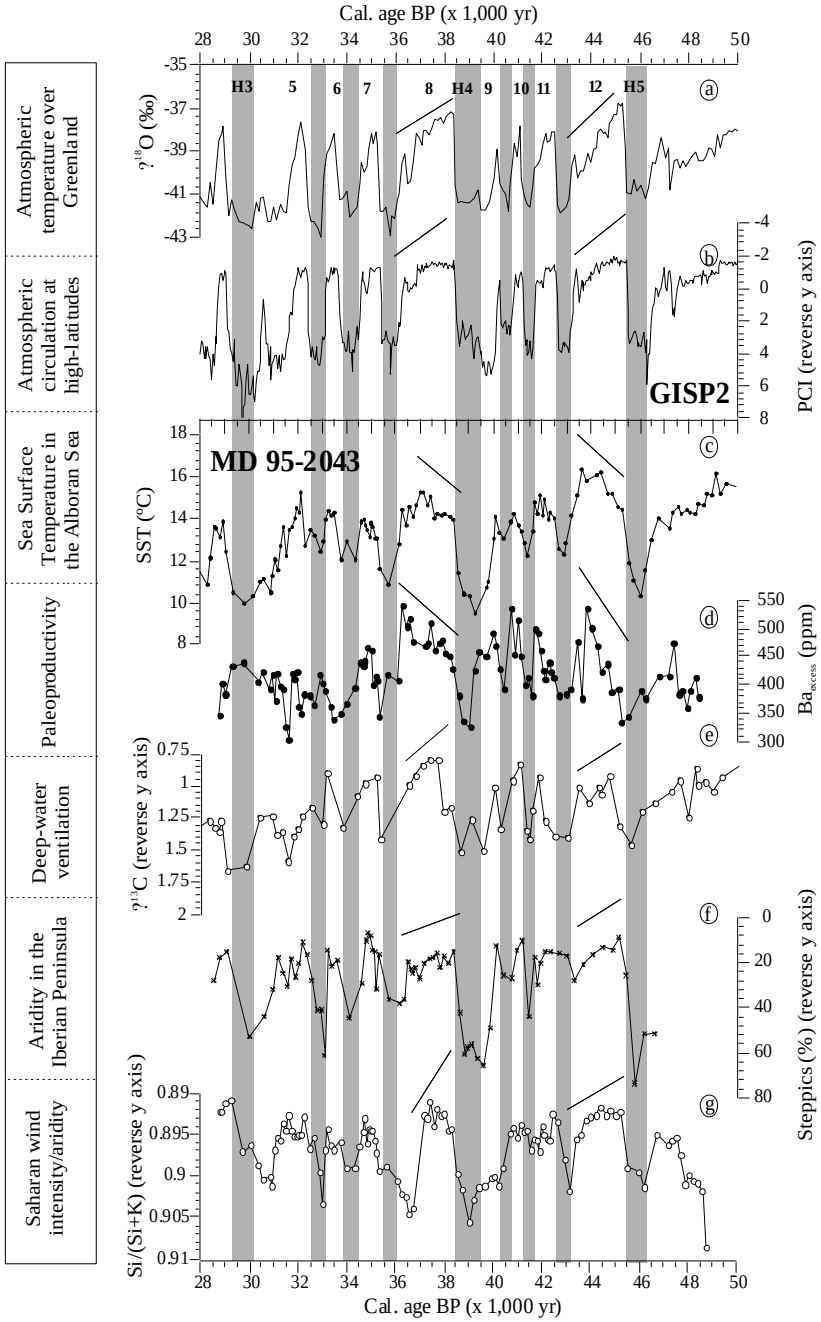

Figure 7.- Comparison of different proxies in MD 95-2043 and GISP2 cores to illustrate the differences in interstadial evolution between atmospheric and marine systems. (a) $?^{18}O$ and (b) PCI from GISP2 [*Mayewski et al.*, 1997; *Meese et al.*, 1997]; (c) $U^{k'}_{37}$-SST [*Cacho et al.*, 1999]; (d) Ba_{excess}; (e) $?^{13}C$ (benthics); (f) Steppic vegetation; and (g) Si/(Si+K) from MD 95-2043 core. Processes represented are indicated in left boxes.

Figura 7.- *Comparación de diferentes indicadores de los testigos MD 95-2043 y GISP2 para ilustrar las diferencias en la evolución de los sistemas marino y atmosférico durante los interestadiales. Registros del testigo GISP2: (a) $?^{18}O$ y (b) PCI [Mayewski et al., 1997; Meese et al., 1997] comparados con los perfiles del testigo de Alborán: (c) $U^{k'}_{37}$-SST [Cacho et al., 1999]; (d) Ba_{exceso}; (e) $?^{13}C$ (bentónicos); (f) Vegetación estépica; y (g) Si/(Si+K) del testigo MD 95-2043. Los procesos representados se indican en la izquierda.*

Particularly, the thermal evolution along D/O cycles in the Alboran and GISP2 records, mainly during 8 and 12 interstadials, is different. Alboran SST reaches the highest values towards the end of the D/O interstadials in contrast with the GISP2 ?^{18}O record [*Cacho et al.*, 1999]. In this study we provide new records that also reflect the same characteristic pattern as the $U^{k'}_{37}$-SST during interestadial periods. TOC, total alkenone concentration and Ba_{excess} records (Figure 3) show a gradual increase towards more productive conditions towards the end of D/O interstadials. On the contrary, proxies of arid and dusty conditions and deep-water ventilation are coherent with the pattern described by GISP2 records during 8 and 12 interestadials (Figure 7). We try to understand better these differences throughout analysing phase relationships between the different proxies (Figures 8 and 9; Table 4). First, cross-spectral analyses from some selected proxies were represented in Figure 8 against $U^{k'}_{37}$-SST record by using the B&T method [*Paillard et al.*, 1996]. Detailed results of the coherency values for the two most significant frequency bands are shown in Table 4. In Figure 9 phase results are represented in two ways: (i) as a phase wheel (Figure 9a) and (ii) showing the temporal sequence of processes along a D/O cycle (Figure 9b).

Table 4.- Results of cross-spectral analysis (some of these pairs of proxies are represented in Figure 8). For simplicity, only the two most significant frequency bands from those appeared in the spectral analyses with SST are represented. Negative (positive) phase angles indicate that the first variable leads (lags) the second one. Coherency at the 80% confidence level is 0.56. No phase angle is given (-) if records are not coherent at the 80% confidence level or if they are not significant at 0.3 or 0.68 frequency bands in the spectral analyses (Table 2).

Tabla 4.*- Resultados del análisis espectral cruzado (cf. Figura 8 para la representación de estas parejas de indicadores). Por simplicidad, sólo las dos bandas de frecuencia más significativas se han representado. Ángulos de fase negativos (positivos) indican que la primera variable precede (sigue) a la segunda. El valor de coherencia para un 80% de nivel de confianza es de 0,56. No se ofrecen valores del ángulo de fase si los registros no son coherentes por encima del nivel establecido o si no son significativos a las frecuencias de 0,3 y 0,68 en los análisis espectrales respectivos.*

Coherency; phase difference ± phase error (degrees); lead or lag (years)		
Variable 1 *vs* Variable 2	~ 3,300 yr (frequency band=0.3)	~ 1,470 yr (frequency band=0.68)
Ba_{excess} (ppm) *vs* SST	0.86; 41±15; 375 yr	-
Alkenones *vs* SST	0.86; 10±15; in phase	0.77; 5±19; in phase
TOC (%) *vs* SST	0.65; 20±29; in phase	0.76; 4±22; in phase
$CaCO_3$ (%) *vs* SST	0.86; 64±15; 586 yr	0.69; 54±22; 220 yr
?^{13}C (benthics) *vs* SST	0.70; -152±22; opposite	0.72; -162±25; opposite
Alcohol index *vs* SST	-	0.88; -9±14; in phase
Steppics *vs* SST	0.94; 163±10; opposite	-
Al (%)*vs* SST	0.84; -90±17; 825 yr	-
Si/Si+K *vs* SST	0.89; 149±13; 1365 yr	-
PCI *vs* SST	0.95; 149±9; opposite	0.96; 155±7; opposite
?^{18}O (GISP2) *vs* SST	-	0.96; -16±7; in phase

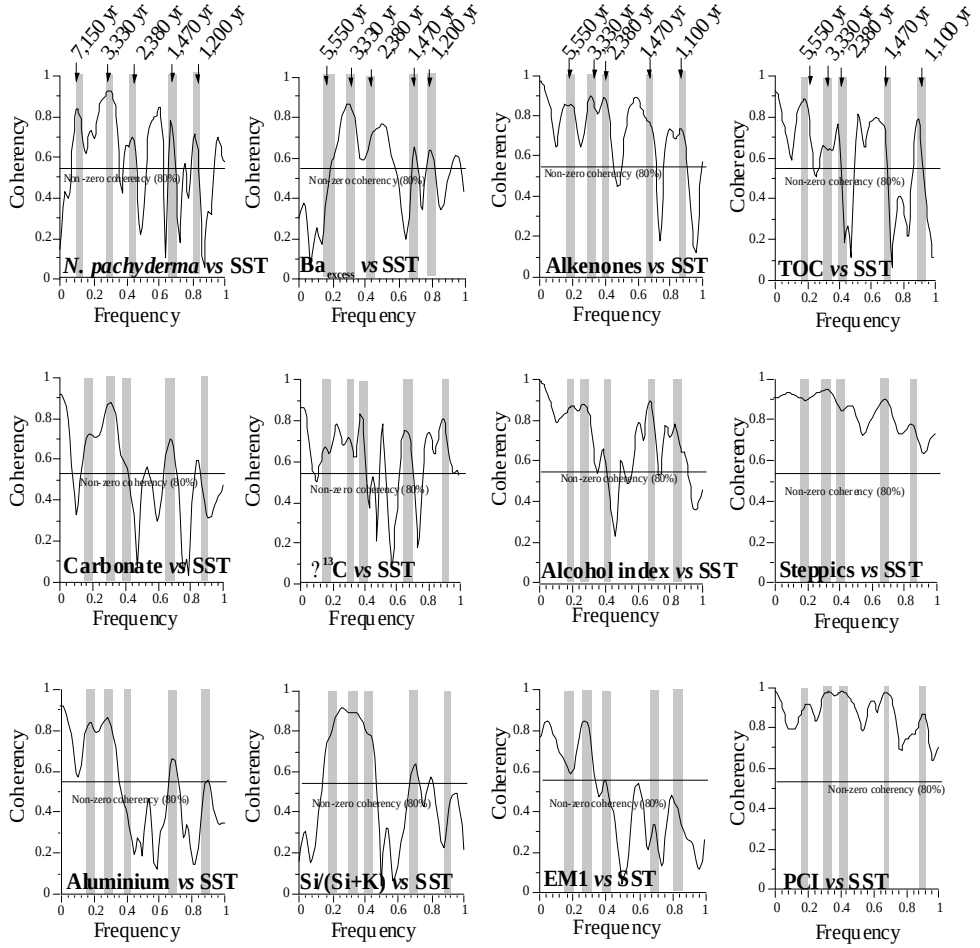

Figure 8.- Results from the cross-spectral analyses of some selected proxies from MD 95-2043 core against SST. The coherency plot indicates what frequency components are shared between the proxies and the SST record (see Table 4 for accurate coherence values). An 80% confidence level is set, above which statistical significance in the coherency relationship is considered to exist (this level corresponds to a coherency of 0.56).

Figura 8.- *Resultados del análisis espectral cruzado de algunos indicadores seleccionados del testigo MD 95-2043 respecto a las SST. El gráfico de coherencia indica qué frecuencias son compartidas entre los indicadores y las SST (cf. Tabla 4 para los valores exactos). Se especifica el nivel para el que se alcanza el 80% de confianza por encima del cual la coherencia es significativa estadísticamente (este nivel corresponde con una coherencia de 0,56 en este caso).*

Paleoproductivity proxies show a coherent phase lagging the maximum in SST by around 250 years (Fig. 9; Table 4). Nevertheless, those indicators show a wide range of phase results probably due to the noise introduced by other processes affecting each of the signals. In contrast, the maximum in fluvial input, marked by Al (%), leads productivity maxima by at least 800 years. This feature indicates that nutrient enrichment by fluvial discharges was not the critical factor limiting the productivity in the Alboran Sea during the glacial period. Therefore, the southern displacement of the westerly wind system towards the Alboran Sea latitude should have been the main controller of the paleoproductivity changes. This hypothesis is supported by the almost opposite phase angle shown by the indicators of deep water ventilation and paleoproductivity thus pointing out a tightly relationship between the location of the northern westerly wind system and

primary productivity in the Alboran Sea. Therefore, when north-westerlies were weaker on the northern basins, productivity in the Alboran Sea was maxima indicating a possible southward displacement of the wind system.

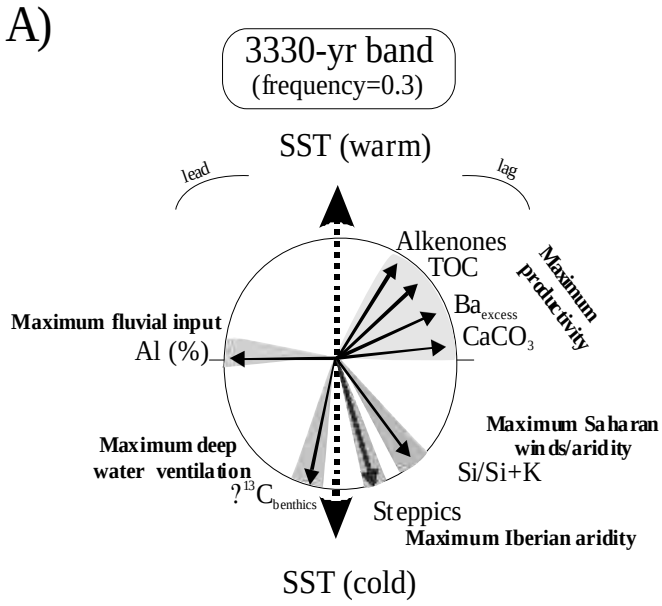

Figure 9.- (A) Phase relationships of proxy records from the IMAGES MD 95-2043 core at the 3,330-yr band. See Table 4 for accurate phase angles. (B) Temporal evolution of SST, paleoproductivity, aridity, wind intensity and deep-water ventilation processes at site MD 95-2043 in the Alboran Sea during a 3,330-yr cycle. The internal response and error range in years are shown.

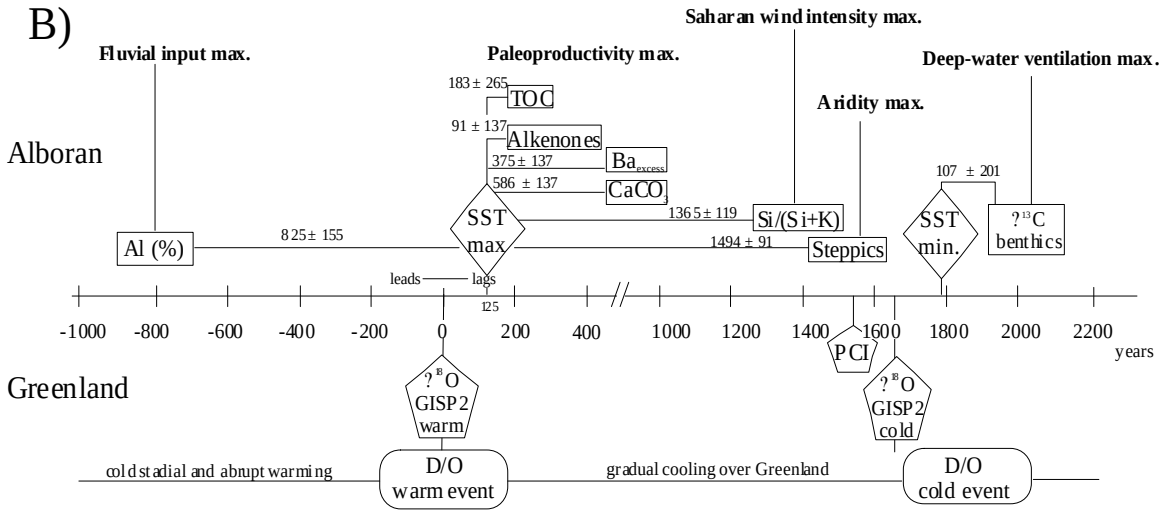

Figura 9.- *(A) Relaciones de fase entre los registros del testigo IMAGES MD 95-2043 en la banda de frecuencia de 3.330 años (cf. Tabla 4 para los valores de fase exactos). (B) Evolución temporal de las SST, la paleoproductividad, la intensidad de los vientos saharianos, la aridez de la Península Ibérica y la ventilación de las aguas profundas en el testigo MD 95-2043 del Mar de Alborán durante un ciclo de 3.330 años. Se indican el tiempo de respuesta interna y el rango de error en años.*

Among all the processes recorded during D/O stadial periods the earlier phase is shown by the transport of Saharan dust (Si/Si+K) which reached the maximum intensity around 400 yr

prior to the minimum in SST. Maximum aridity recorded by the vegetation in southern Iberia occurred next but only around 200 year prior to SST minima. Maximum values in the ventilation of the deep basin are acquired later, thus suggesting the intensification of high-latitude wind system at the very end of this evolution. This sequence suggests a lag of at least 500 yr in the maximum intensity of this high latitude wind system in relation with the Saharan wind system. This finding supports the hypothesis stated by previous studies about the influence of dust inputs in the D/O cycles [*Overpeck et al.*, 1996; *Kudrass et al.*, 2001]. In the Alboran Sea the fact that Saharan dust supply from Northern Africa leads high-latitude climate changes may suggest that low latitudes were involved in the forcing and transfer of millennial climatic variability. Further records cointaning signals from both high and low latitudes are needed to confirm such lag between the two climatic systems.

4.5. Conclusions

Paleoproductivity increments in the Alboran Sea were recorded during D/O interstadials, as it is reflected by carbonate, Ba_{excess}, TOC and total alkenone records from MD 95-2043 core. Abundances of redox-elements indicate that sulfate reduction did not occur in this deep environment and thus no Ba remobilization should be expected. In addition, trace elements expressed as Mn/Al and Zn/Al ratios, also increase coherently with the paleoproductivity indicators in agreement with enhanced production and sinking of organic matter during D/O interstadials. We interpret that during interstadials the westerly winds migrated southwards to the latitude of the Gibraltar Strait and favoured a more intense entrance of Atlantic surface waters. Consequently, both coastal upwelling and gyre-induced upwelling in the outskirts of the anticyclones experimented an effective growth. In addition, fluvial input was enhanced during these wetter periods as shown by Al (%) and pollen results. Thus, increased runoff would lead to a higher nutrient input thus contributing to the enhanced paleoproductivity observed in the Alboran Sea. Nevertheless, phase analyses indicate that surface water fertilization was not the limiting factor controlling the paleoproductivity variability in the Alboran Sea since maximum in Al% led paleoproductivity by almost 1,000 years.

The ?^{13}C record from benthic foraminifers show millennial scale changes in deep water ventilation with higher rates associated to the D/O stadials and HE. Thus, although the production of organic matter was depleted during those cold intervals, its preservation in sediments was also reduced by the predominance of more oxygenated conditions. Both processes, changes in Alboran productivity and in WMDW ventilation are consistent with the latitudinal migration of the westerly winds according to two synoptic scenarios: (i) during D/O stadials the westerly belt located in the north of the Iberian Peninsula produces an increment in deep-water formation in the Gulf of Lions and (ii) during D/O interstadials its southward location favours upwelling processes in the Alboran Sea.

Spectral and cross-spectral analyses carried out on several proxies from the same MD 95-2043 core reveal the presence of five significant frequencies: 5,000-10,000, 3,300, 2,380, 1,470 and 1,200 years. These frequencies match those obtained in several paleoclimatic records from Greenland ice cores and also in monsoon areas. This finding provides a further prove of the significant role played by these periodicities in the sub-Milankovitch climatic variability. Nevertheless, the significance and also the variance explained by the extracted frequencies differ from one process to other. The 8,000 cycle is particularly strong in records of SST, Saharan winds

and vegetation distribution in southern Iberia as a consequence of the HE amplification of those signals. The 2,400 cycle, very significant in GISP2, is only significant in the record of deep-water ventilation supporting the proposed control of this process by the atmospheric circulation in high latitudes. The 1,470 and, above all, the 3,300 frequencies are the best represented by the full group of considered processes.

Time evolution of all the studied proxies show different particularities that have been better represented by phase analyses. During the interstadials fluvial input, SST and primary productivity were all enhanced but a significant lag is observed between the maximum of each of these processes. Particularly interesting is the opposite phase between productivity and deep-water ventilation thus confirming the link of these processes by the southern displacement of the westerly winds system. Along the stadials we observe an early maximum in Saharan dust transport, followed by maximum in Iberian aridity, minimum in SST and maximum in deep water ventilation. Our results show a lag of at least 500 years between the maximum in the Saharan wind transport and maximum in the northwesterly winds. Although the leading of tropical processes respect those from higher latitudes needs to be confirmed by further studies, our results highlight the potential importance of low latitudes in the global glacial rapid climatic variability.

Acknowledgements

We gratefully acknowledge R. Zahn and J. Targarona (University of Barcelona) and F.J. Sierro and M. A. Bárcena (University of Salamanca) for their useful comments to an earlier version of the manuscript. We thank the SeaWiFs Project and the Distributed Active Archive Center, Goddard Space Flight Center, Greenbelt, MD, USA for providing the Alboran chlorophyll satellite image. This study was supported by the IMAGES programme and a Comissionat d'Universitats i Recerca fellowship (Ana Moreno). GRC Geociencies Marines is additionally funded by Generalitat de Catalunya through its excellency research groups programme. I. C. also thanks EC funding (contract HPMF-CT-1999-00402).

4.6.References

Allen, J. R. M., U. Brandt, A. Brauer, H. W. Hubberten, B. Huntley, J. Keller, M. Kraml, A. Mackensen, J. Mingram, J. F. W. Negendank, N. R. Nowaczyk, H. Oberhänsli, W. A. Watts, S. Wulf, and B. Zolitschka, Rapid environmental changes in southern Europe during the last glacial period, Nature, 400, 740-743, 1999.

Altabet, M. A., M. J. Higginson, and D. W. Murray, The effect of millennial-scale changes in Arabian Sea denitrification on atmospheric CO2, Nature, 415, 159-162, 2002.

Bard, E., F. Rostek, J. L. Turon, and S. Gendreau, Hydrological impact of Heinrich Events in the Subtropical Northeast Atlantic, Science, 289, 1321-1324, 2000.

Béthoux, J. P., and B. Gentili, Functioning of the Mediterranean Sea: past and present changes related to freshwater input and climate changes, J. Mar. Syst., 20, 33-47, 1999.

Bond, G., W. S. Broecker, S. J. Johnsen, J. McManus, L. Labeyrie, J. Jouzel, and G. Bonani, Correlations between climate records from North Atlantic sediments and Greenland ice, Nature, 365, 143-147, 1993.

Boyle, E., Chemical accumulation variations under the Peru current during the past 130.000 years, J. Geophys. Res., 88, 7667-7680, 1983.

Cacho, I., J. O. Grimalt, C. Pelejero, M. Canals, F. J. Sierro, J. A. Flores, and N. J. Shackleton, Dansgaard-Oeschger and Heinrich event imprints in Alboran Sea temperatures, Paleoceanography, 14, 698-705, 1999.

Cacho, I., J. O. Grimalt, F. J. Sierro, N. J. Shackleton, and M. Canals, Evidence for enhanced Mediterranean thermohaline circulation during rapid climatic coolings, Earth Planet. Sci. Lett., 183, 417-429, 2000.

Calvert, S. E., and T. F. Pedersen, Geochemistry of recent oxic and anoxic marine sediments: implications for the geological record, Mar. Geol., 113, 67-88, 1993.

Candela, J., and C. D. Winant, Meteorologically forced subinertial flows through the strait of Gibraltar, J. Geophys. Res., 94, 12667-12679, 1989.

Dansgaard, W., S. J. Johnsen, H. B. Clausen, D. Dahl-Jensen, N. S. Gundestrup, C. U. Hammer, C. S. Hvidberg, J. P. Steffensen, A. E. Sveinbjörnsdóttir, J. Jouzel, and G. Bond, Evidence for general instability of past climate from a 250-kyr ice-core record, Nature, 364, 218-220, 1993.

de Garidel-Thoron, T., L. Beaufort, B. K. Linsley, and S. Dannenmann, Millennial-scale dynamics of the East Asian winter monsoon during the last 200,000 years, Paleoceanography, 16, 491-502, 2001.

De Lange, G. J., B. Van Os, P. A. Pruysers, J. J. Middelburg, D. Castradori, P. Van Santvoort, P. Müller, H. Eggenkamp, and F. Prahl, Possible early diagenetic alteration of paleo proxies, in Carbon Cycling in the Glacial Ocean, edited by R. Zahn, pp. 225-257, Springer-Verlag. NATO ASI Series, 1994.

Dean, W. E., J. V. Gardner, and D. Z. Piper, Inorganic geochemical indicators of glacial-interglacial changes in productivity and anoxia on the California continental margin, Geochim. Cosmochim. Acta, 61, 4507-4518, 1997.

Des Combes, H. J., J. P. Caulet, and P. Tribovillard, Pelagic productivity changes in the equatorial area of the northwest Indian Ocean during the last 400.000 years, Mar. Geol., 158, 27-55, 1999.

Dymond, J., E. Suess, and M. Lyle, Barium in deep-sea sediment: a geochemical proxy for paleoproductivity, Paleoceanography, 7, 163-181, 1992.

Fabrés, J., A. Calafat, A. Sánchez-Vidal, M. Canals, and S. Heussner, Composition and spatio-temporal variability of particle fluxes in the Western Alboran Gyre, Mediterranean Sea, J. Mar. Syst., 33-34, 431-456, 2002.

Francois, R., S. Honjo, S. J. Manganini, and G. E. Ravizza, Biogenic barium fluxes to the deep sea: implications for paleoproductivity reconstruction, Global Biogeochem. Cycles, 9, 289-303, 1995.

Ganopolski, A., and S. Rahmstorf, Rapid changes of glacial climate simulated in a coupled climate model, Nature, 409, 153-158, 2001.

Garcia-Gorriz, E., and M.-E. Carr, Physical control of phytoplankton distributions in the Alboran Sea: a numerical and satellite approach, J. Geophys. Res., 106, 16795-16805, 2001.

Gingele, F., and A. Dahmke, Discrete barite particles and barium as tracers of paleoproductivity in South Atlantic sediments, Paleoceanography, 9, 151-168, 1994.

Grootes, P., and M. Stuiver, Oxygen 18/16 variability in Greenland snow and ice with 10^3-to 10^5-year time resolution, J. Geophys. Res., 102, 26455-26470, 1997.

Jones, B., and D. A. C. Manning, Comparison of geochemical indices used for the interpretation of palaeoredox conditions in ancient mudstones, *Chem. Geol.*, *111*, 111-129, 1994.

Kageyama, M., P. J. Valdes, G. Ramstein, C. Hewitt, and U. Wyputta, Northern hemisphere storm tracks in present day and Last Glacial Maximum climate simulations: a comparison of the european PMIP models, J. Clim., 12, 742-760, 1999.

Kasten, S., R. Haese, M. Zabel, C. Rühlemann, and H. Schulz, Barium peaks at glacial terminations in sediments of the equatorial Atlantic Ocean - relicts of deglacial productivity pulses?, Chem. Geol., 175, 635-651, 2001.

Kroopnick, P. M., The distribution of ^{13}C of ? CO_2 in the world oceans, Deep-Sea Research, 32, 57-84, 1985.

Kudrass, H. R., A. W. Hofmann, H. Doose, K. C. Emeis, and H. Erlenkeuser, Modulation and amplification of climatic changes in the Northern Hemisphere by the Indian summer monsoon during the past 80 ky, Geology, 29, 63-66, 2001.

Labeyrie, L., and M. Elliot, Abrupt climatic changes-Causes and consequences: An introduction, in Reconstructing Ocean History: A Window into the Future , edited by F. Abrantes, et al., pp. 73-82, Plenum Plublishers, New York, 1999.

Leuschner, D. C., and F. Sirocko, The low-latitude monsoon climate during Dansgaard-Oeschger cycles and Heinrich Events, Quat. Sci. Rev., 19, 243-254, 2000.

Martin, J. H., and G. A. Knauer, VERTEX: Manganese transport with $CaCO_3$, Deep Sea Res., 30, 411-425, 1983.

Mayewski, P. A., L. D. Meeker, M. S. Twickler, S. Whitlow, Q. Yang, W. B. Lyons, and M. Prentice, Major features and forcing of high-latitude northern hemisphere atmospheric circulation using a 110,000-year-long glaciochemical series, J. Geophys. Res., 102, 26,345-26,366, 1997.

Meese, D. A., A. J. Gow, R. B. Alley, G. A. Zielinski, P. Grootes, M. Ram, K. C. Taylor, P. A. Mayewski, and J. F. Bolzan, The Greenland Ice Sheet Project 2 depth-age scale: Methods and results, J. Geophys. Res., 102, 26411-26423, 1997.

Millot, C., Circulation in the Western Mediterranean Sea, J. Mar. Syst., 20, 423-442, 1999.

Moreno, A., I. Cacho, M. Canals, M. A. Prins, M. F. Sánchez-Goñi, J. O. Grimalt, and G. J. Weltje, Saharan dust transport and high latitude glacial climatic variability: the Alboran Sea record, Quat. Res., in press, 2002.

Morford, J. L., and S. R. Emerson, The geochemistry of redox sensitive trace metals in sediments, Geochim. Cosmochim. Acta, 63, 1735-1750, 1999.

Müller, P., and E. Suess, Productivity, sedimentation rate, and sedimentary organic matter in the oceans- I. Organic carbon preservation, Deep Sea Research I, 26A, 1347-1362, 1979.

Overpeck, J. T., D. Rind, A. Lacis, and R. Healy, Possible role of dust-induced regional warming in abrupt climate change during the last glacial period, Nature, 384, 447-449, 1996.

Paillard, D., L. Labeyrie, and P. Yiou, Macintosh program performs time-series analysis, Eos Transactions, 77, 379, 1996.

Parrilla, G., and T. H. Kinder, Oceanografía física del mar de Alborán, Bol. Inst. Esp. Oceanogr., 4, 133-165, 1987.

Perkins, H., T. Kinder, and P. La-Violette, The Atlantic inflow in the Western Alboran Sea, J. Phys. Oceanogr., 20, 242-263, 1990.

Rühlemann, C., P. Müller, and R. Schneider, Organic carbon and carbonate as paleoproductivity proxies: examples from high and low productivity areas of the tropical Atlantic, in Use of proxies in Paleoceanography: examples from the South Atlantic , edited by G. Fischer, et al., pp. 1-31, Springer-Verlag, Berlin, 1999.

Sánchez-Goñi, M. F., I. Cacho, J. L. Turon, J. Guiot, F. J. Sierro, J.-P. Peypouquet, J. O. Grimalt, and N. J. Shackleton, Synchroneity between marine and terrestrial responses to millennial scale climatic variability during the last glacial period in the Mediterranean region, Clim. Dynam., 19, 95-105, 2002.

Sarhan, T., J. García-Lafuente, J. M. Vargas, and F. Plaza, Upwelling mechanisms in the northwestern Alboran Sea, J. Mar. Syst., 23, 317-331, 2000.

Sarnthein, M., J. P. Kennet, J. R. M. Allen, J. Beer, P. Grootes, C. Laj, J. McManus, R. Ramesh, and S.-I. w. g. 117, Decadal-to-millennial-scale climate variability-chronology and mechanisms: summary and recommendations, Quat. Sci. Rev., 21, 1121-1128, 2002.

Schulz, H., U. von Rad, and H. Erlenkeuser, Correlation between Arabian Sea and Greenland climate oscillations of the past 110,000 years, Nature, 393, 54-57, 1998.

Sierro, F. J., M. Pérez-Folgado, J. A. Flores, M. A. Bárcena, I. Cacho, N. J. Shackleton, and J. O. Grimalt, Carbonate dissolution variations and Mediterranean thermohaline circulation, MIS3, H. Okada, Ed., 7th International Conference on Paleoceanography, Sapporo, JAPAN (2001).

Sirocko, F., D. Garbe-Schönberg, A. McIntyre, and B. Molfino, Teleconnections between the subtropical monsoons and high-latitude climates during the last deglaciation, Science, 272, 526-529, 1996.

Smetacek, V., Role of sinking in diatom life-history cycles: ecological, evolutionary and geological significance, Mar. Biol., 84, 239-251, 1985.

Suess, E., Particulate organic carbon flux in the oceans surface productivity and oxygen utilization, Nature, 288, 260-263, 1980.

Taylor, S. R., and S. M. McLennan, The continental crust: its composition and evolution. A. Hallam, Ed., Geoscience Texts (Blackwell Scientific Publications), Oxford, U.K., 1985.

Thomson, D. J., Time series analysis of Holocene climate data, Phil. Trans. R. Soc. Lond., A 330, 601-616, 1990.

Torres, M. E., H.-J. Brumsack, G. Bohrmann, and K. C. Emeis, Barite fronts in continental margin sediments: a new look at barium remobilization in the zone of sulfate reduction and formation of heavy barites in diagenetic fronts, Chem. Geol., 127, 125-139, 1996.

Turekian, K. K., and K. H. Wedepohl, Distribution of the elements in some major units of the earth's crust, Geol. Soc. Am. Bul., 72, 175-192, 1961.

Tzedakis, C., The last climatic cycle at Kopais, central Greece, J. Geol. Soc. London, 156, 425-434, 1999.

Van Kreveld, S. A., M. Sarnthein, H. Erlenkeuser, P. Grootes, S. Jung, M. J. Nadeau, U. Pflaumann, and A. Voelker, Potential links between surging ice sheets, circulation changes

and the Dansgaard-Oeschger cycles in the Irminger Sea, 60-18 kyr, Paleoceanography, 15, 425-442, 2000.

Vargas-Yáñez, M., F. Plaza, J. García-Lafuente, T. Sarhan, J. M. Vargas, and P. Vélez-Belchi, About the seasonal variability of the Alboran Sea circulation, J. Mar. Syst., in press, 2002.

Villanueva, J., J. O. Grimalt, L. Labeyrie, E. Cortijo, L. Vidal, and J. L. Turon, Precessional forcing of productivity in the North Atlantic Ocean, Paleoceanography, 13, 561-571, 1998.

Vink, A., C. Rühlemann, K. A. F. Zonneveld, S. Mulitza, M. Hüls, and H. Willems, Shifts in the position of the North Equatorial Current and rapid productivity changes in the western Tropical Atlantic during the last glacial, Paleoceanography, 16, 479-490, 2001.

Voelker, A., Global distribution of centennial-scale records for marine isotope stage (MIS) 3: a database, Quat. Sci. Rev., 21, 1185-1212, 2002.

Watts, W. A., J. R. M. Allen, and B. Huntley, Palaeoecology of three interstadial event during oxygen-isotope Stages 3 and 4: a lacustrine record from Lago Grande di Monticchio, southern Italy, Palaeogeogr., Palaeoclimatol., Palaeocol., 155, 83-93, 2000.

Wedepohl, K. H., Environmental influences on the chemical composition of shales and clays, in Physics and Chemistry of the Earth, edited by L. H. Ahrens, et al., pp. 307-331, Pergamon, Oxford, 1971.

Wehausen, R., and H.-J. Brumsack, Chemical cycles in Pliocene sapropel-bearing and sapropel-barren eastern Mediterranean sediments, Palaeogeogr., Palaeoclimatol., Palaeocol., 158, 325-352, 2000.

Yiou, P., E. Baert, and M. F. Loutre, Spectral analysis of climate data, Surv. Geophys., 17, 619-663, 1996.